STUDY OF HIGH-ALTITUDE AIRCRAFT WAKE DYNAMICS. TASK I. PROBLEM DEFINITION

H. Hoshizaki, et al

Lockheed Missiles and Space Company

Prepared for:

Department of Transportation

December 1972

Report No. DOT-TST-90-3

STUDY OF HIGH-ALTITUDE AIRCRAFT WAKE DYNAMICS

Lockheed Palo Alto Research Laboratory
Palo Alto, California 94304

DECEMBER 1972
FINAL REPORT: TASK I, PROBLEM DEFINITION

Prepared for
Office of the Secretary
U.S. DEPARTMENT OF TRANSPORTATION
Washington, D.C. 20590

The contents of this report reflect the views of the Lockheed Palo Alto Research Laboratory which is responsible for the facts and the accuracy of the data presented herein. The contents do not necessarily reflect the official views or policy of the Department of Transportation. This report does not constitute a standard, specification or regulation.

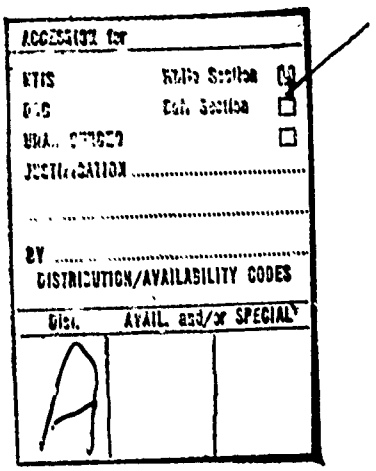

1. Report No.	2. Government Accession No.	3. Recipient's Catalog No.
DOT-TST-90-3		

4. Title and Subtitle	5. Report Date
Study of High-Altitude Aircraft Wake Dynamics Final Report: Task I, Problem Definition	December 1972
	6. Performing Organization Code

7. Author(s)	8. Performing Organization Report No.
H. Hoshizaki, R. J. Conti, L. B. Anderson, K. O. Redler, J. W. Meyer, W. J. McLean, P. E. Cassady	

9. Performing Organization Name and Address	10. Work Unit No.
Lockheed Palo Alto Research Laboratory Palo Alto, California 94304	
	11. Contract or Grant No. DOT-OS-20082
	13. Type of Report and Period Covered Final Report

12. Sponsoring Agency Name and Address	14. Sponsoring Agency Code
Office of the Secretary U.S. Department of Transportation 400 Seventh Street S.W. Washington, D.C. 20590	

15. Supplementary Notes

16. Abstract

The important features of chemically reacting aircraft wakes have been identified. The aircraft wake is modeled in terms of the jet regime (wake age $\lesssim$ 10 sec) vortex regime ($\sim$100 sec) and the wake dispersion regime ($\gtrsim$100 sec). The important thermochemical reactions were found to take place in the jet regime.

17. Key Words	18. Distribution Statement
Aircraft Wakes, Wake Dynamics, Wake Chemistry, Wake Modeling	Unlimited

19. Security Classif. (of this report)	20. Security Classif. (of this page)	21. No. of Pages	22. Price
Unclassified	Unclassified	208	$3.00/$0.95

Form DOT F 1700.7 (8-69)

TABLE OF CONTENTS

LIST OF ILLUSTRATIONS

LIST OF TABLES

Section 1

SUMMARY

The purpose of the High-Altitude Aircraft Wake Dynamics Study has been to investigate the chemically reacting wake of an aircraft flying at subsonic and supersonic velocity in the upper troposphere and stratosphere. In this study, the chemical and fluid mechanical behaviors of important emission species were traced from the time the species exited the engine exhaust nozzle to the time aircraft-induced perturbations to the atmospheric environment were no longer important. The primary result of this study will be a wake model that will predict the concentration of engine emission species at various points in the wake. The final output of the wake model will be the size and shape of the wake and the species concentrations at the time when the atmospheric environment dominates the dispersion and chemical reactions in the wake.

The High-Altitude Wake Dynamics Study has been organized into the following four major tasks:

- Task I – Problem Definition
- Task II – Model Development
- Task III – Supporting Experiments
- Task IV – Model Application and Update

This report contains the technical analyses and studies performed under Task I, Problem Definition, and the conclusions developed from these analyses. Data obtained under Task III, Supporting Experiments, are also presented, as appropriate, to support the findings of the analytical studies.

The relationship of the wake dynamics study to other modeling studies within the Climatic Impact Assessment Program (CIAP) is illustrated in Figure 1-1. The wake regime extends from the time engine exhaust emissions are deposited in the atmosphere up to an order of 10^3 sec thereafter. The wake model, which will be developed under Task II, Model Development, will describe fluid mechanical and chemical behavior of engine exhaust emission in the wake regime. It will also provide final wake

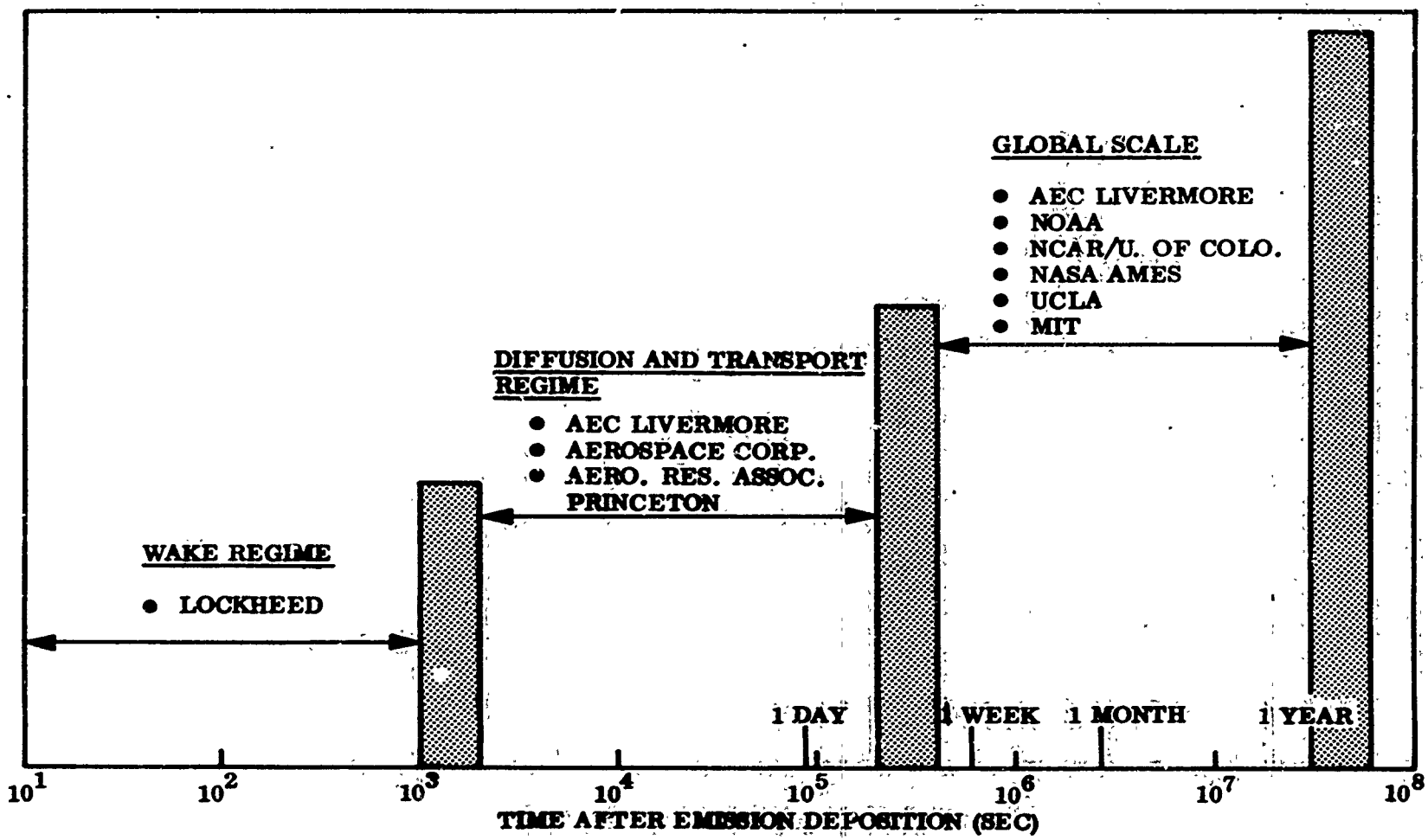

Figure 1-1 Relationship of Wake Dynamics Model to Other CIAP Models

size and shape, and species concentration input data to the diffusion and transport regime, which begins at the end of the wake regime and extends over a time interval on the order of days. The diffusion and transport regime is currently under study by other CIAP contractors. Finally, global circulation models will extend analysis of the interaction of engine exhaust emissions with the atmosphere up to a period on the order of years after their introduction into the atmosphere.

The basic objective of Task I was to examine the interaction of high-altitude aircraft engine emissions with the aircraft wake flow field and to determine the extent to which this flow regime must be considered in specifying the types and amounts of effluents entering the global circulation as a result of high-altitude aircraft operations. The general approach to Task I was to examine the fluid mechanical and chemical behavior of the engine exhaust emission to identify and evaluate, where possible, the important mechanisms by which the engine emissions can interact with the atmosphere. For those mechanisms that were deemed to be important, the dependence of parameters that control the mechanism of interest on aircraft characteristics, flight conditions, and atmospheric environment were established. In this manner, different flight conditions and differences in the atmospheric environment between the troposphere and stratosphere are taken into account.

The important features of the wake fluid mechanical model were found to be the dominance of the early wake growth (up to a few minutes) by the engine exhaust jet flow field and the rolled-up vortex pair flow. At early times, the wake growth is primarily in the vertical direction because of mass detrainment from the sinking vortex pair. The vortex pair breaks up because of pair instability at a wake age of 1 to 2 min but continues to sink for an additional 5 to 10 min. At the time of vortex pair breakup (wake age $\approx$ 1 to 2 min) the wake width is about twice the aircraft wing span and the wake height or thickness is about four times the wing span. At a wake age between 5 and 10 min, depending on the particular aircraft, the wake height reaches a maximum of about seven times the wing span. The fluid mechanical behavior beyond this point in time is not perfectly clear. However, preliminary data from contrail photographs taken in the troposphere indicate that after reaching the maximum height of about six wing spans, the wake begins to collapse – because of gravitational forces – until the wake height is about 1/3 to 1/2 the maximum height. This collapse occurs in about

5 to 10 min after the maximum height is attained. The gravitational collapse of the wake necessitates an increase in wake width by a factor of 2 to 3 to conserve mass.

Additional mechanisms for dispersing the wake at these late times are vertical wind shear, aircraft wake turbulence, and buoyant rise. The deformation of wake by vertical wind shear is directly proportional to the wake height and hence reaches a maximum and then decreases. The turbulence deposited into the wake by vortex pair breakup is expected to decay to the atmospheric level in about 2 to 3 min after deposition. The decay mechanisms are wake mass dilution by low-turbulence atmospheric air and inviscid dissipation that transfers turbulent kinetic energy from large-scale to small-scale eddies. The contribution of wake and atmospheric turbulence to the dispersion of the wake is relatively small in the wake dispersion regime.

The increase in wake width due to mass entrainment as the wake rises by buoyancy is also expected to be small. The residual temperature excess in the wake is not sufficiently large (of the order of a degree) to cause the wake to rise and entrain a significant amount of additional mass.

The above description of fluid mechanical behavior of aircraft wakes is based on observation of contrails in the troposphere. It is currently believed that, in the stratosphere, the wake would behave qualitatively in the same fashion, but the quantitative behavior will be different because of differences in wind shear, atmospheric stability, and atmospheric turbulence. The wake model under development will predict the quantitative differences in wake behavior between tropospheric and stratospheric flight altitudes.

The influence of supersonic Mach numbers on aircraft wake dynamics is poorly understood at the present time. The effects of shock waves and differences in lift distribution between subsonic and supersonic wings on vortex roll-up processes are not known. Supersonic contrail data are necessary to provide a basis for assessing the influence of Mach number on aircraft wakes. A flight program to obtain wake measurements behind a supersonic aircraft is currently being planned.

The possible effect of shock heating on the chemical dynamics is somewhat better understood. The maximum air temperatures created by shock heating by a Mach-3 aircraft are in the neighborhood of 600°K. Temperatures of this magnitude are created by normal shocks that are located very close to the aircraft surfaces. A well designed supersonic aircraft will not create large normal shocks because of the excessive drag associated with such blunt configurations. Most of the shock-heated air is probably swallowed by the boundary layer where recovery temperatures are comparable to the normal shock temperatures. The hot boundary layer shed by the aircraft is expected to cool rapidly by mixing and is not expected to have a significant influence on the chemical dynamics.

The important conclusions from the wake chemical kinetics analyses are:

- In an engine operating mode, with relatively low HC emissions, finite reaction rate effects are an important aspect of the chemistry in the engine exhaust expansion nozzle and exhaust jet regime. There is substantial oxidation of CO to CO_2 in the nozzle and jet, and the concomitant production of H atoms maintains the concentrations H, O, and OH well above their equilibrium values.
- Hydrocarbon oxidation has a profound scavenging effect on the inorganic radicals. Introduction of large HC quantities reduces the H, OH, and O levels by many orders of magnitude.
- Significant oxidation of NO to NO_2 cannot be accomplished in the exhaust regime. In the absence of HC, the NO_2/NO ratio is kept very small through reduction of NO_2 by H atoms. When HC is abundant, the effect is to freeze NO_2 in the nozzle near its initial throat value. Similarly, oxidation of SO_2 to SO_3 appears not to be significant.
- OH concentrations can be high in the jet, but under such conditions, the NO_2 would be very low – thereby precluding formation of HNO_3 from the reaction

$$NO_2 + OH \rightarrow HNO_3$$

- Even if OH and NO_2 were both initially plentiful in the hot exhaust, significant conversion to nitric acid is forestalled through rapid consumption of OH by the competing reaction

$$OH + OH + M \rightarrow H_2O_2 + M$$

The wake chemical model, which will provide inputs to the diffusion and transport regime chemistry, can be either simple or complex depending on requirements of the diffusion and transport regime model. This is an area that requires further study and coordination with other CIAP program elements.

The results of the present studies have indicated that radiative cooling of the exhaust jet and wake buoyancy due to radiative transport are not important. The transport of particulates in the wake regime was also found to be unimportant because of the small size of the emitted particulates that causes the particulate motion to coincide with the gas motion.

Section 2
FLUID MECHANICAL MODEL

2.1 OBSERVED FEATURES OF AIRCRAFT EXHAUST TRAILS

A study of the data gathered in this program under Task III and the data reported in Ref. 2-1 yields a consistent picture of the major features of aircraft exhaust trails such as shown in Figures 2-1 and 2-2.

The near trail, labeled "Jet" in these figures, lasts for times on the order of 10 sec. In this region the exhaust trail occupies a fraction of the overall aircraft wake since it is confined to turbulent jets issuing from the engines. The jet regime is characterized by rapid growth of the exhaust trail, which starts on a meter scale at the engines and grows more than an order of magnitude to become comparable to the aircraft size at the end of the jet (Point A, Figure 2-2), at which point the exhaust occupies most of the aircraft wake. The end of the jet is marked by a sharp decrease in horizontal rate of growth, as shown in Figure 2-2.

The intermediate trail is labeled "Vortex," because in this region the trailing vortex pair associated with wing lift dominates the wake. The striking feature of this regime is a horizontal growth that is practically nil, while the vertical growth proceeds at a substantial rate, as shown in the Figures 2-1 and 2-2. The vortex regime lasts for times on the order of 100 sec, corresponding to distances on the order of 20 km behind the aircraft. The end of the vortex regime (Points B and C of Figure 2-2) is marked by a reversal of the growth rate pattern; i.e., the trail grows more rapidly in the horizontal direction than it does in the vertical direction.

After the vortex pair has broken down, the exhaust trail starts dispersing in the horizontal direction by a variety of mechanisms to be discussed later and continues to grow in the vertical direction because of the downward momentum of the vortex pair. The long-term wake growth behavior is illustrated in Figure 2-3 in which preliminary wake growth data from contrail photographs of the NASA Ames CV-990 are presented. The wake height

reaches a maximum at a wake age of about 5 min and then begins to decrease. This decrease is thought to be due to gravitational collapse, which occurs when a well mixed, uniform density volume of gas is located in an atmosphere that has a finite, stable lapse rate. The wake height reaches a minimum between 15 and 20 min and then begins to increase slowly. The methods employed to obtain the data presented in Figure 2-3 are discussed in Section 2.2.4.

The gravitational collapse of the wake necessitates an increase in the wake width to conserve mass. This increase in wake width by gravitational collapse occurs primarily between 5 and 15 min. Additional mechanisms for dispersing the wake are vertical wind shear, aircraft wake turbulence, and buoyant rise. The deformation of the wake by vertical wind shear probably becomes effective right after the vortex breakdown and is directly proportional to the wake height. The turbulence deposited into the wake by vortex breakdown is initially much higher than the atmospheric level but is expected to decay to the atmospheric level in about 2 to 3 min after deposition. The decay mechanisms are wake mass dilution by low turbulence atmospheric air and inviscid dissipation, which transfers turbulent kinetic energy from large scale to small scale eddies. Wake growth by wake turbulence diffusion is therefore expected to be confined to a few minutes after vortex breakdown. Thereafter atmospheric turbulence will disperse the wake. The increase in wake width due to mass entrainment as the wake rises by buoyancy is expected to be small. The residual temperature excess in the wake are not sufficiently large (of the order of a degree) to cause the wake to rise and entrain a significant amount of additional mass.

Microdensitometer traces of the jet flow field immediately behind the aircraft are shown in Figure 2-4 where the first scan shows individual jets from the four engine pods, which later merge two by two. Additional microdensitometer traces of the wake photographs at 1.5 and 7.0 min (Figure 2-1) were made to obtain a qualitative description of the mass distribution across the wake. The traces are shown in Figures 2-5 through 2-8. In Figure 2-5 the vortex pair is clearly visible in the lower portion of the wake and the microdensitometer traces show a greater concentration of light scattering particles in the vicinity of the vortex pair. The scattering particles are probably ice crystals and if their dimensions are in the submicron range, their distribution should be a good indicator

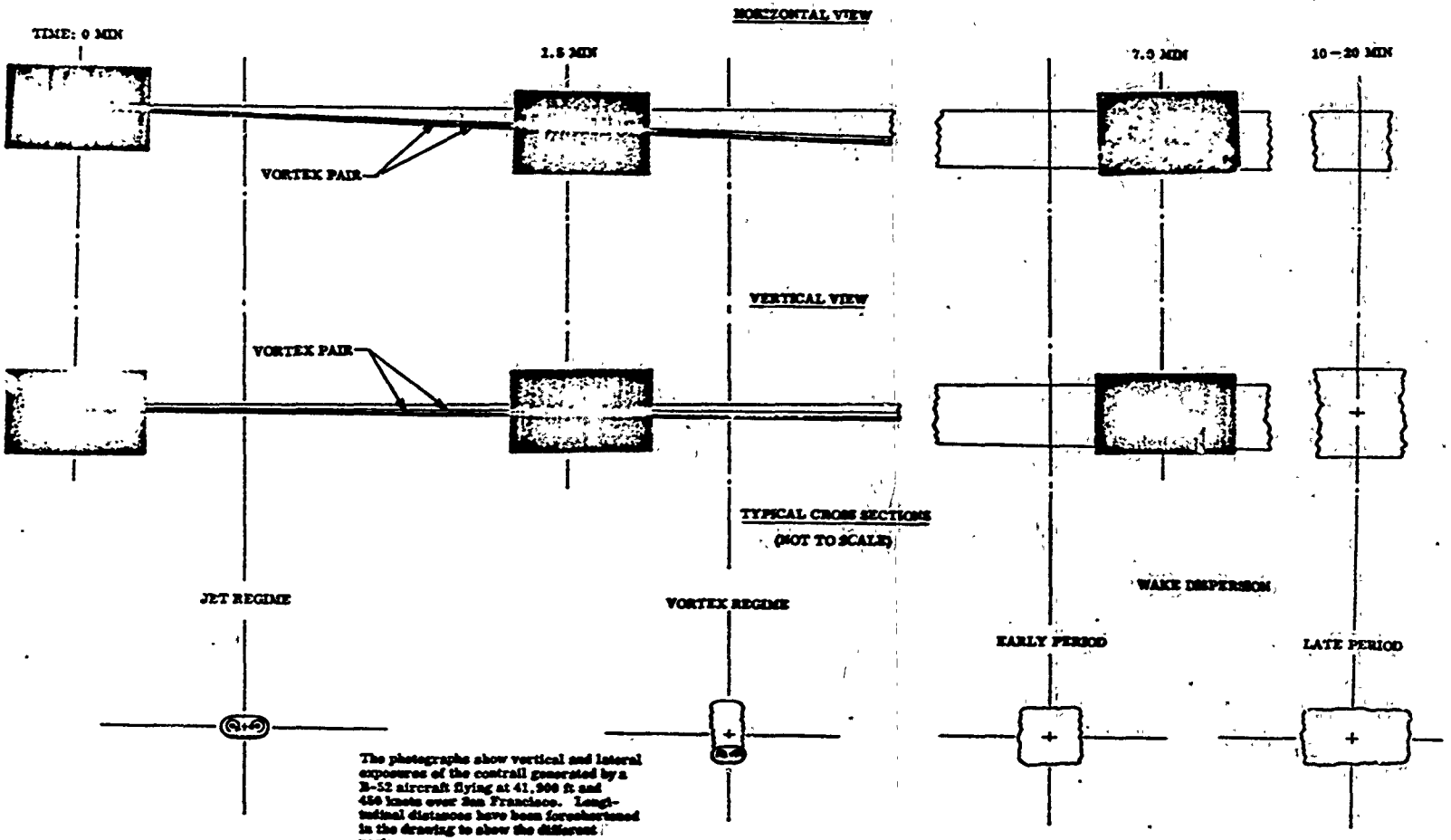

The photographs show vertical and lateral exposures of the contrail generated by a B-52 aircraft flying at 41,000 ft and 450 knots over San Francisco. Longitudinal distances have been foreshortened in the drawing to show the different regimes.

Figure 2-1 Sketch of Typical Exhaust Trail

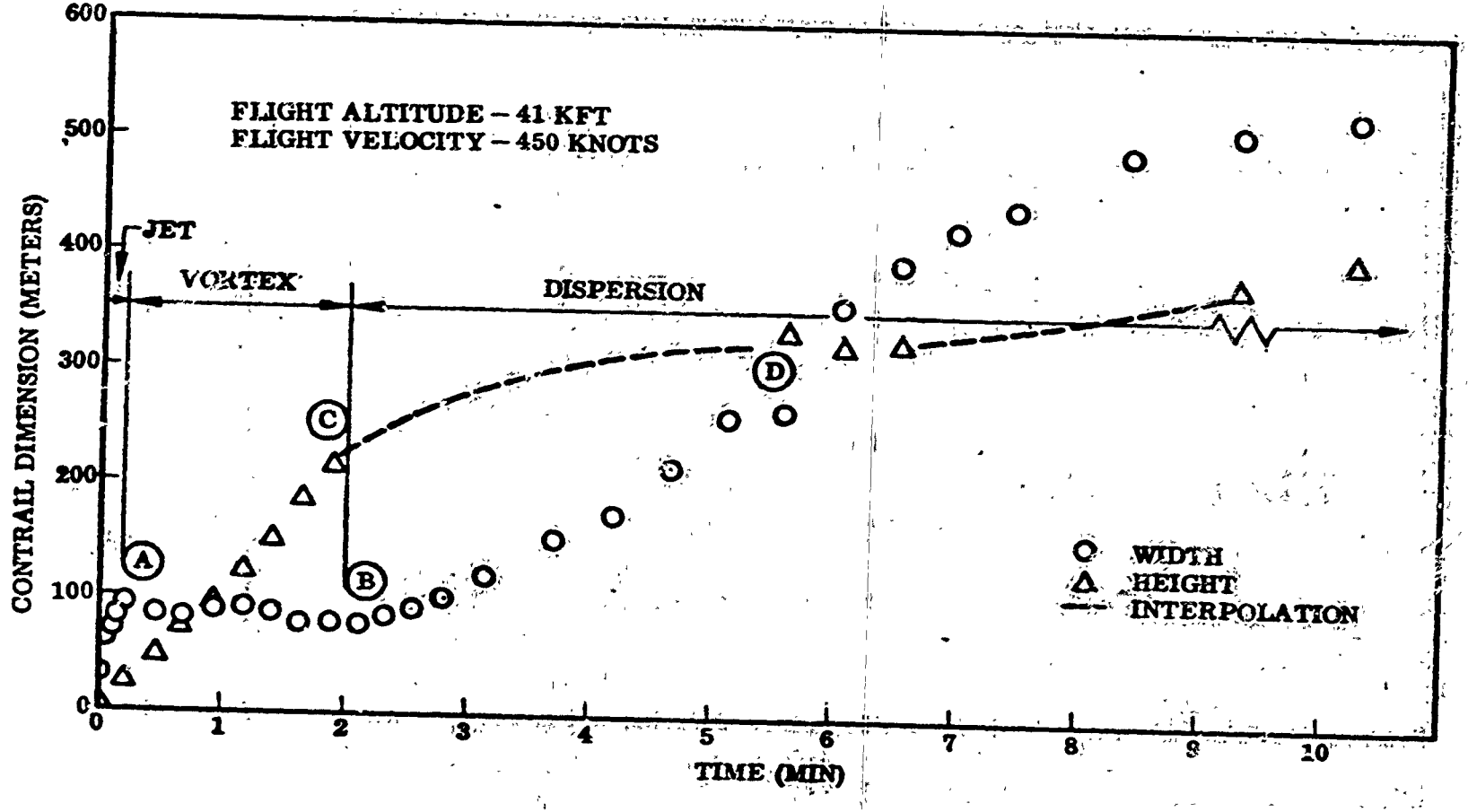

Figure 2-2 Time History of B-52 Exhaust Trail Shown in Fig. 2-1

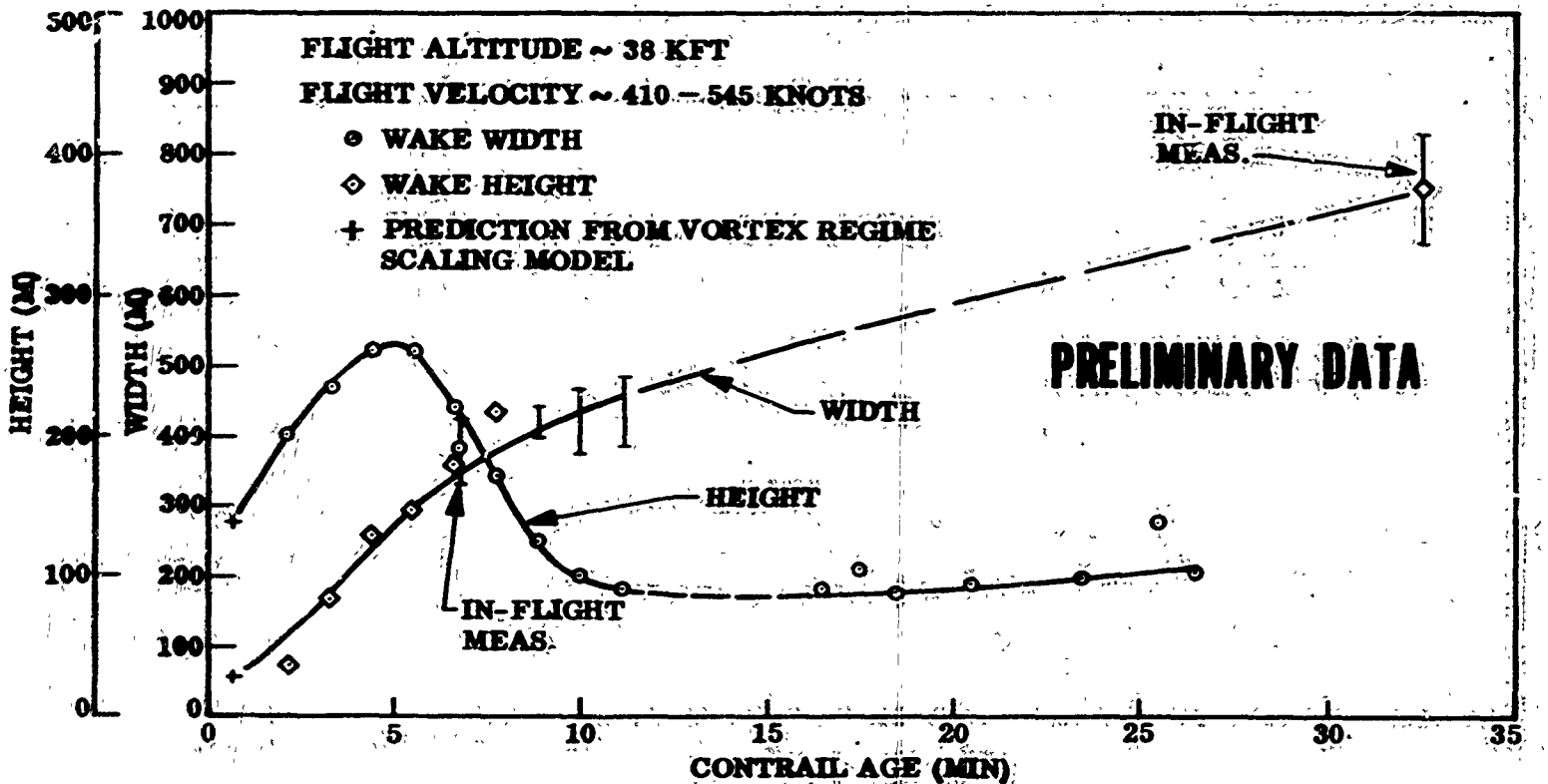

Figure 2-3 Convair 990 Contrail Dimensions, Preliminary Data

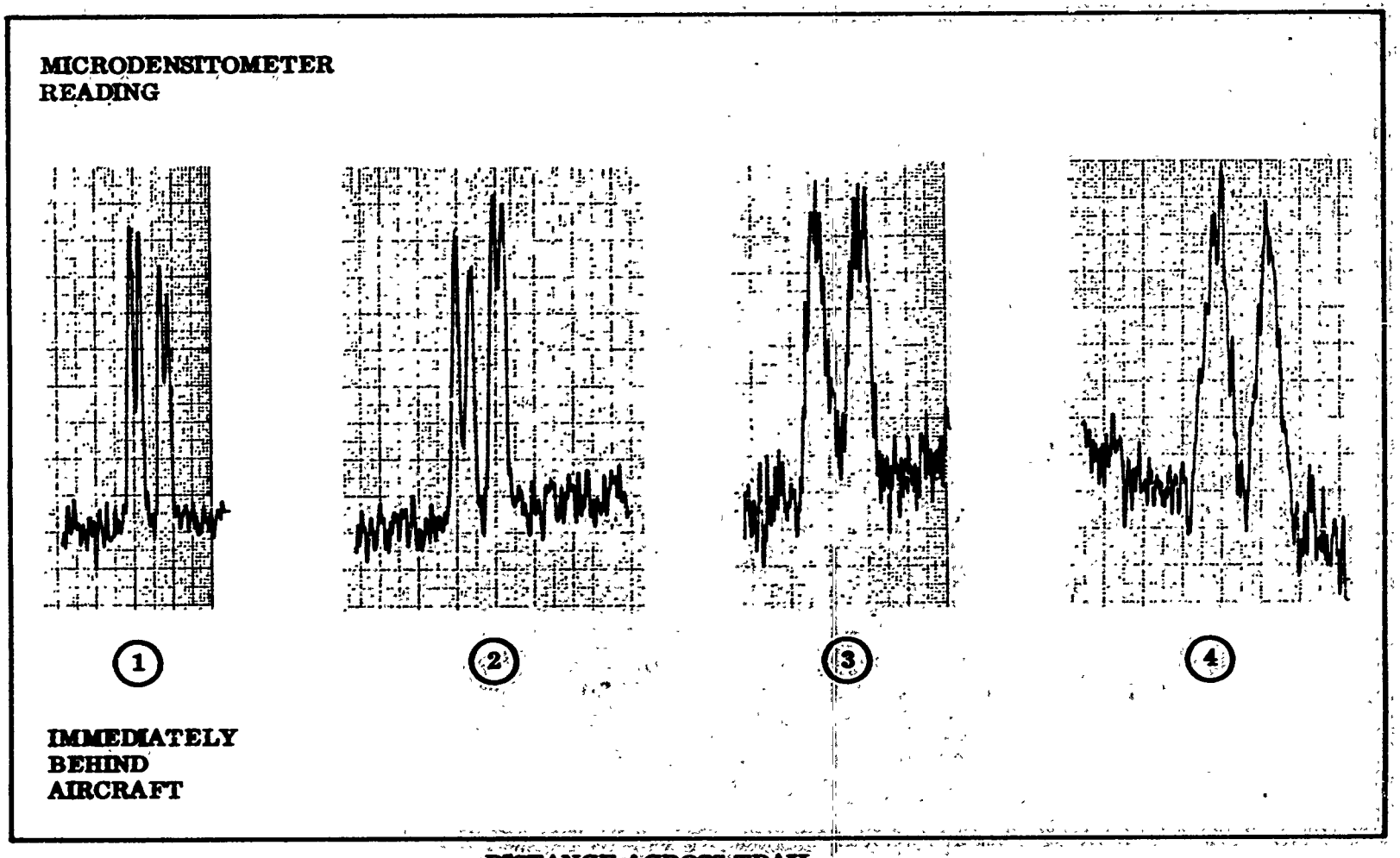

Figure 2–4 Microdensitometer Tracing for Lower Left Photograph of Fig. 2–1. Cross-cuts 1 through 4 are for increasing distance behind aircraft

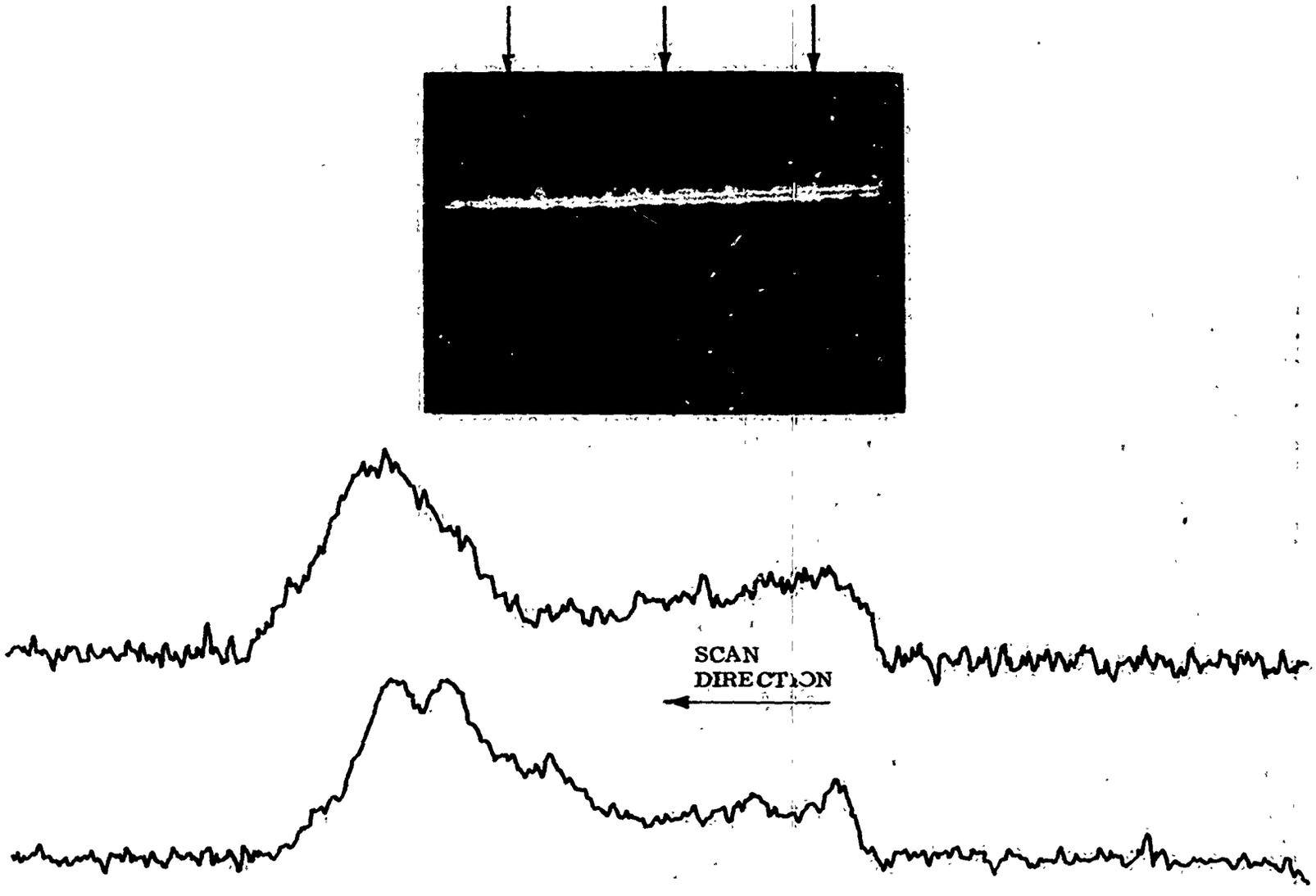

Figure 2-5 Vertical Microdensitometer Scans – B-52 at 42 kft, Wake Age = 1.5 min

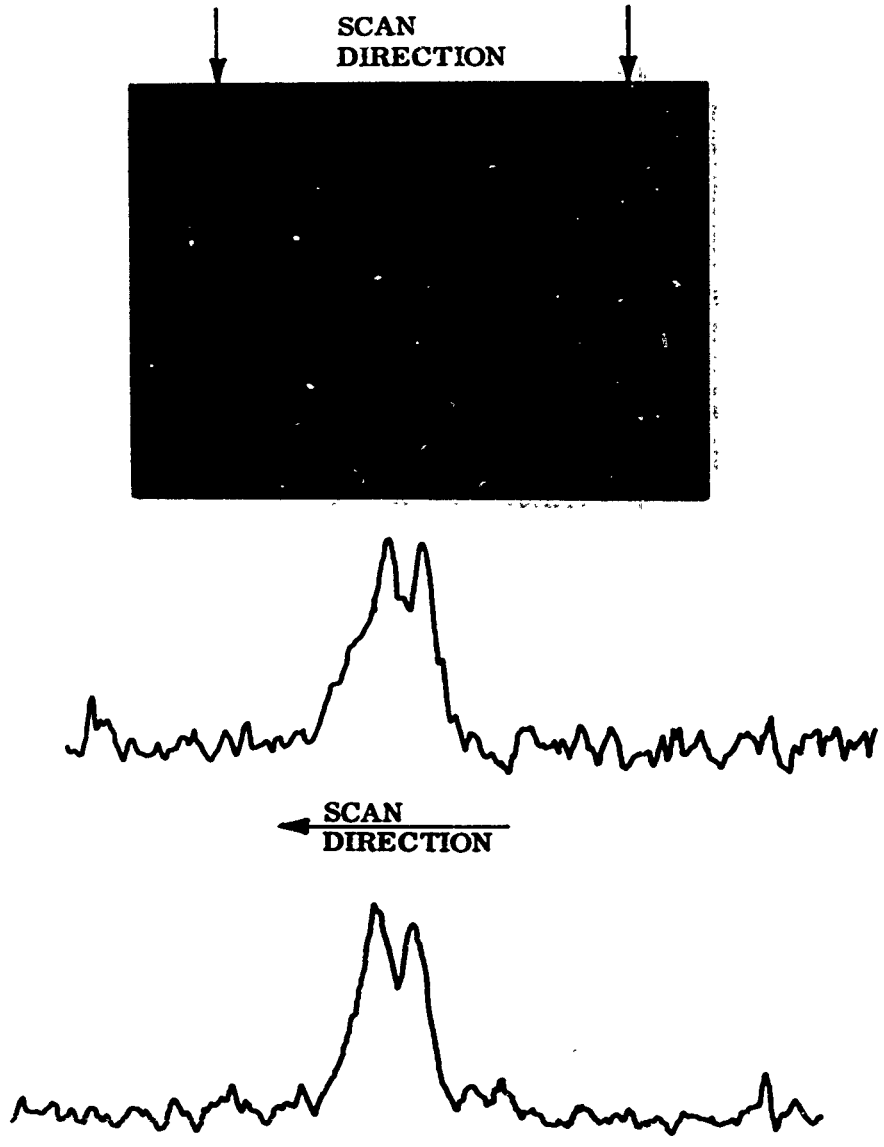

Figure 2-6 Horizontal Microdensitometer Scans – B-52 at 42 kft, Wake Age = 1.5 min

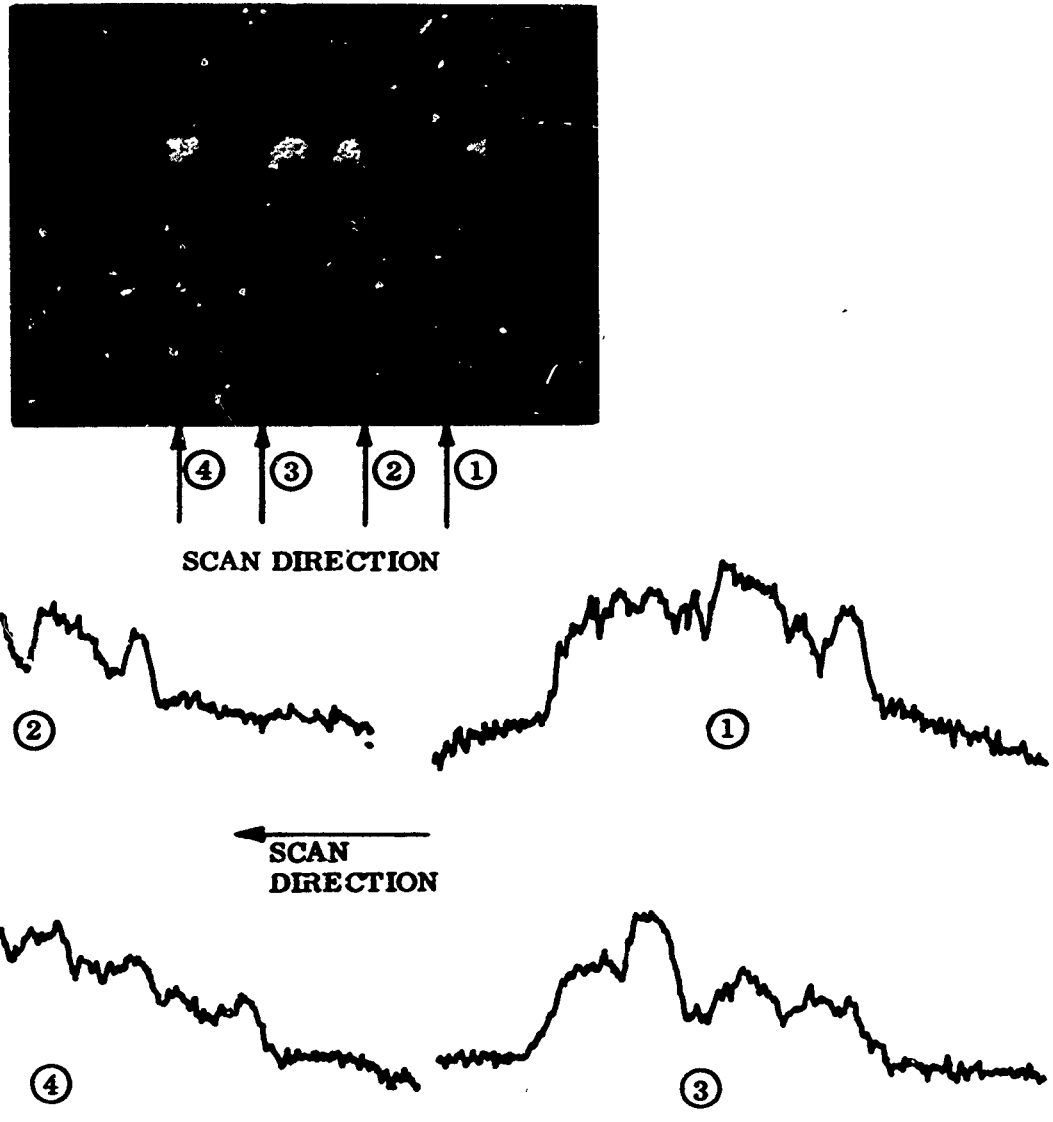

Figure 2-7 Vertical Microdensitometer Scans – B-52 at 42 kft, Wake Age = 7.0 min

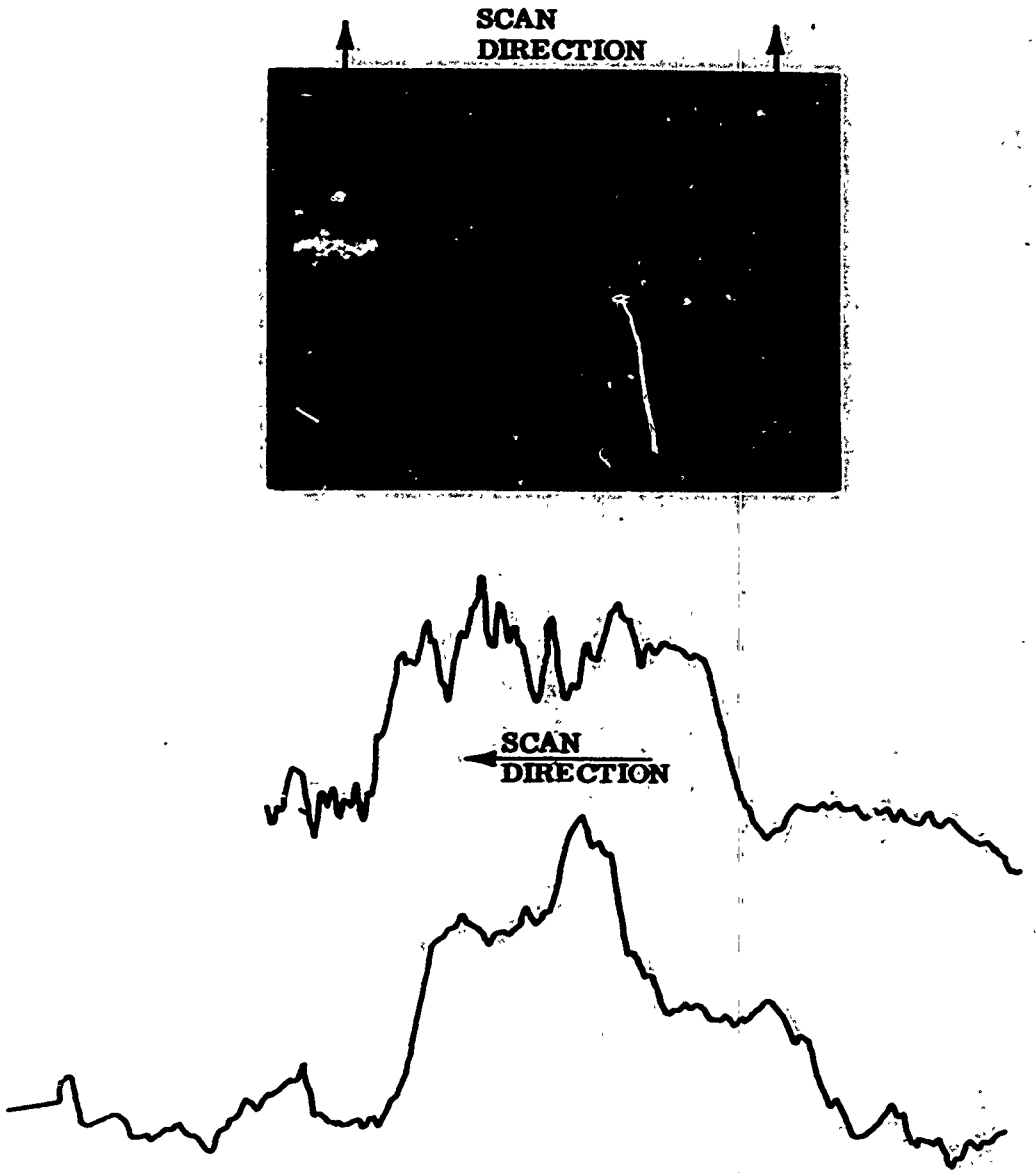

Figure 2-8 Horizontal Microdensitometer Scans — B-52 at 42 kft, Wake Age = 7 min

of the exhaust gas distribution. Figure 2-6 is the corresponding horizontal trace, which clearly shows the mass concentration due to the vortex pair.

Figures 2-7 and 2-8 are vertical and horizontal scans at 7.0 min, well into the wake dispersion regime where organized aerodynamic motion has ceased to exist. The microdensitometer traces indicate a slightly rounded distribution with a ragged top. The concentration of mass at the bottom of the wake evident in Figure 2-5 is no longer discernible. The breakup of the vortex pair evidently redistributes the mass uniformly throughout the wake cross section.

The procedure for obtaining the data shown in Figures 2-2 and 2-3 will be described in detail in future reports dealing with Task III of this program. For present purposes it is sufficient to indicate that the photography consists of still and motion pictures taken simultaneously from two locations – one directly underneath the flight path and one from the side at an elevation angle of about 10 deg. The pictures are taken in a time sequence, tracking a particular feature of the contrail. The apparent dimension of the contrail is measured with an optical comparator, and the corresponding height and width are obtained by solving a set of simultaneous equations involving the azimuth and elevation from both cameras. In a few selected cases a microdensitometer has been used to obtain accurate definition of the contrail edge. Typical traces are shown in Figure 2-4 through 2-8. The drift velocity of the contrail is obtained by geometric addition of the longitudinal drift and lateral displacement, measured from the motion picture film. Atmospheric conditions are obtained from the local sounding.

The exhaust trail is assumed to coincide with the observed condensation trail. This assumption is based on the fact that only persistent contrails are used to generate data. This type of contrail is produced at low temperatures (below -61°C) and persists for hours, which indicates that it consists of ice crystals in a supersaturated environment. Under these circumstances reevaporation would be negligible, and the condensation trail is a good indicator of the exhaust trail.

2.2 THEORETICAL MODEL OF EXHAUST TRAILS

A theoretical model for the major features of aircraft exhaust trails has been developed on the basis of data discussed in the previous section and from theoretical consideration of the physical factors affecting aircraft wakes. For present purposes the end of the wake is defined as a point where the sum of aircraft-induced effects has become negligible, and the natural atmospheric environment dominates. For modeling purposes the wake is subdivided into jet, vortex, and dispersion regimes (as illustrated in Table 2-1), corresponding to the observed behavior discussed previously. A summary of the main features of the model follows, and a more detailed description of each regime is included in subsequent subsections.

The jet regime extends from the engines to the point where the jets occupy all the recirculating region associated with the trailing vortex pair (indicated as Point A in Figure 2-2). This corresponds to a time on the order of 10 sec and a distance on the order of 2 km. In this region the exhaust gases mix with the aircraft wake according to the classical laws of turbulent jets.

In the wake model, the jet flow field is related to aircraft characteristics such as engine type, power setting, and nozzle geometry, and to flight characteristics such as flight altitude and velocity. Given the aircraft and flight characteristics for any aircraft, the jet flow field can be predicted. The atmospheric environment in this regime plays a secondary role in determining the jet flow field, with the exception of the ambient pressure. The ambient pressure, however, may be classified as a flight characteristic since it is determined by flight altitude.

The vortex regime extends from the end of the jet regime to the point where the vortex pair breaks up because of hydrodynamic instability, as described by Crow (Ref. 2-2) and others (Ref. 2-3). This regime lasts for times on the order of 100 sec and extends over distances on the order of 20 km. The unusual feature of this regime – namely, vertical growth with little or no horizontal growth – can be explained by the fact that the wake in this regime is dominated by the trailing vortex pair. The exhaust gases, which originally fill the recirculating flow associated with the sinking vortex pair,

Table 2-1

WAKE MODEL REGIMES[a]

Jet Regime	Vortex Regime	Wake Dispersion Regime
Time ≈ (10 sec)	Time ≈ 0 (10^2 sec)	Time ≈ 0 (10^3 sec)
Jet exhaust energy dominates jet flow	Horizontal wake growth restricted by vortex pair circulation	Aircraft-induced perturbations comparable to atmospheric perturbations
Jet grows symmetrically in vertical and horizontal	Vortex pair sinking causes vertical growth	Wake dispersion Mechanisms ● Wind shear ● Wake turbulence ● Gravitational collapse ● Buoyant rise
Atmospheric environment secondary	Atmospheric environment secondary	

(a) See Fig. 2-1 for physical features.

become detrained from the pair and are deposited in a region of roughly rectangular cross section, with the top at the original flight level and the bottom at the vortex pair. Thus, the vortex pair restrains the exhaust from horizontal growth and promotes vertical growth instead.

The characteristics of the vortex pair, such as circulation strength, pair separation distance, time to vortex sheet rollup, and sinking rate are related to aircraft and flight characteristics. Some of the more important parameters are aircraft weight, flight velocity, lift distribution, and wing span. Given the aircraft and flight characteristics, the major features of the vortex pair can be predicted.

In the vortex regime, atmospheric environment again plays a secondary role. The structure of the vortex pair is determined primarily by the characteristics of the aircraft and flight parameters. The rotational motion and the sinking of the vortex pair are part of the aerodynamics of the aircraft.

The wake dispersion regime lasts from vortex breakup to a time on the order of 1,000 sec, during which the exhaust changes from an aircraft-dominated condition to a mode of natural atmospheric dispersal. This regime has been generally associated with pure atmospheric dispersion, and an unexpected finding of this program is that the aircraft induced effects last for times about an order of magnitude larger than the vortex breakup time. At the beginning of the dispersion regime (Points B and C in Figure 2-2) the vortex pair breaks up, allowing the horizontal growth to resume while the vertical growth rate decreases markedly. Eventually, the horizontal spread overtakes the height (Point D) and, at very long times, the exhaust trail assumes the flattened shape characteristic of atmospheric dispersion under stable conditions.

The general approach in the wake dispersion regime is to relate the four dispersion mechanisms – i.e., wind shear, gravitational collapse, wake and atmospheric turbulence, and buoyant rise – to the appropriate aircraft parameters and the atmospheric environment. In this manner, given the aircraft and flight characteristics and the atmospheric environment, the wake growth in the wake dispersion regime for aircraft flights in the stratosphere can be estimated.

2.2.1 Jet Regime

The jet regime extends from the engines to the point at which the exhaust occupies the entire trailing vortex pair. In this region the exhaust is confined to turbulent jets issuing from the engines and submerged in the aircraft wake. As the jets become immersed in the vortex field and are attracted to the cores because of jet buoyancy, the interference to their development seems minor. Their rate of growth is still that of classical jets immersed in a uniform coflowing stream. The details of jet-vortex interaction and appearance of the exhaust trail are dependent on the detailed aircraft configuration, such as number and placement of the engines. However, by the time the end of the jet regime has been reached, the exhaust occupies the whole vortex recirculation region, and the details of entrainment into the aircraft wake become unimportant, as examination of flight data will verify. In view of the foregoing arguments, the jet regime is modeled using the classical laws of a turbulent jet in a coflowing stream and flight data. No details whose effect would not show up in the data are included in this model. The justification of this simple model lies in its ability to predict experimental results.

The jet regime is important primarily because it determines the environment in which the exhaust may still be chemically active as the result of the relatively high temperatures. As indicated in Section 3, it has been found that the important chemical reactions occur either in the engine or in its immediate vicinity, which limits the need of detailed knowledge of the jet to a region of the order of 10 exit diameters. A special study of this region has been made and is described in the following section. Although the rest of the jet regime (about 2 km in length) is not of crucial importance for pollution purposes, it also has been addressed to provide a complete description of the exhaust trail.

The Near Field – The near field of the jet regime is of special interest because it is the hottest section and closest to the engine, and therefore is a region with potential for sustaining exhaust reactions. A detailed study of the near field must take into account the differences in engine configuration, particularly with respect to whether or not the engine has a secondary nozzle. Most modern jet engines are equipped with a variable-area primary nozzle that sustains sonic flow at the exit. Thus, under most operation conditions, the exhaust is underexpanded at the exit plane and undergoes further expansion in the jet. On the other hand, some high-performance engines, such as the GE4 built for

the Boeing SST, are equipped with primary and secondary nozzles able to expand the exhaust and deliver it to the atmosphere at ambient pressure. This feature makes an important difference because it gives rise to two different cooling mechanisms: the underexpanded jet behind a primary nozzle cools rapidly by adiabatic expansion with very little mixing, whereas the ideally expanded jet behind a secondary nozzle cools by turbulent mixing with atmospheric air. Both types of jet have been calculated, and the results used as inputs for the chemical kinetics calculations described in Section 3.

For the case of primary-nozzle, underexpanded jets, calculations are carried out using the method of characteristics (Ref. 2-4). This program has the capability of accounting for external flow and internal shock-wave effects. Required by the computations are a description of the nozzle geometry, the thermodynamic properties of the exhaust at the nozzle exit plane, and the ambient conditions. Calculations for the turbulent shear layer, where mixing occurs at the edge of the inviscid jet, are carried out using the results of Ref. 2-5, which is simple to apply and sufficient to provide order-of-magnitude results. The shear layer involves a minor fraction of the exhaust up to four or five exit radii, after which there is no need to calculate the jet accurately because the temperature has decayed to values low enough to freeze the important chemical reactions. A sample calculation using the theories of Refs. 2-4 and 2-5, for an aircraft flying Mach 2.26 at 19.8 km with the J85-GE-13 engine operating at maximum afterburner setting is shown in Figures 2-9 and 2-10. For modeling purposes a few of these calculations will be made and the results correlated to provide a simple estimate of near-jet properties.

In the case of an ideally expanded (constant pressure) jet behind a secondary nozzle, the mixing layer at the edge of the jet grows until it reaches the centerline, after which the jet becomes fully developed. In the region between this point and the exit plane, there is a conical region of constant properties where mixing has not yet taken place. The theory of Abramovich (Ref. 2-6) yields the following length for the conical core:

$$\frac{x_c}{r_o} = \frac{1 + \dfrac{u_{ext}}{u_{jet}}}{0.27\left(1 - u_{ext}/u_{jet}\right)\left(0.214 + 0.144\, u_{ext}/u_{jet}\right)^{0.5}}$$

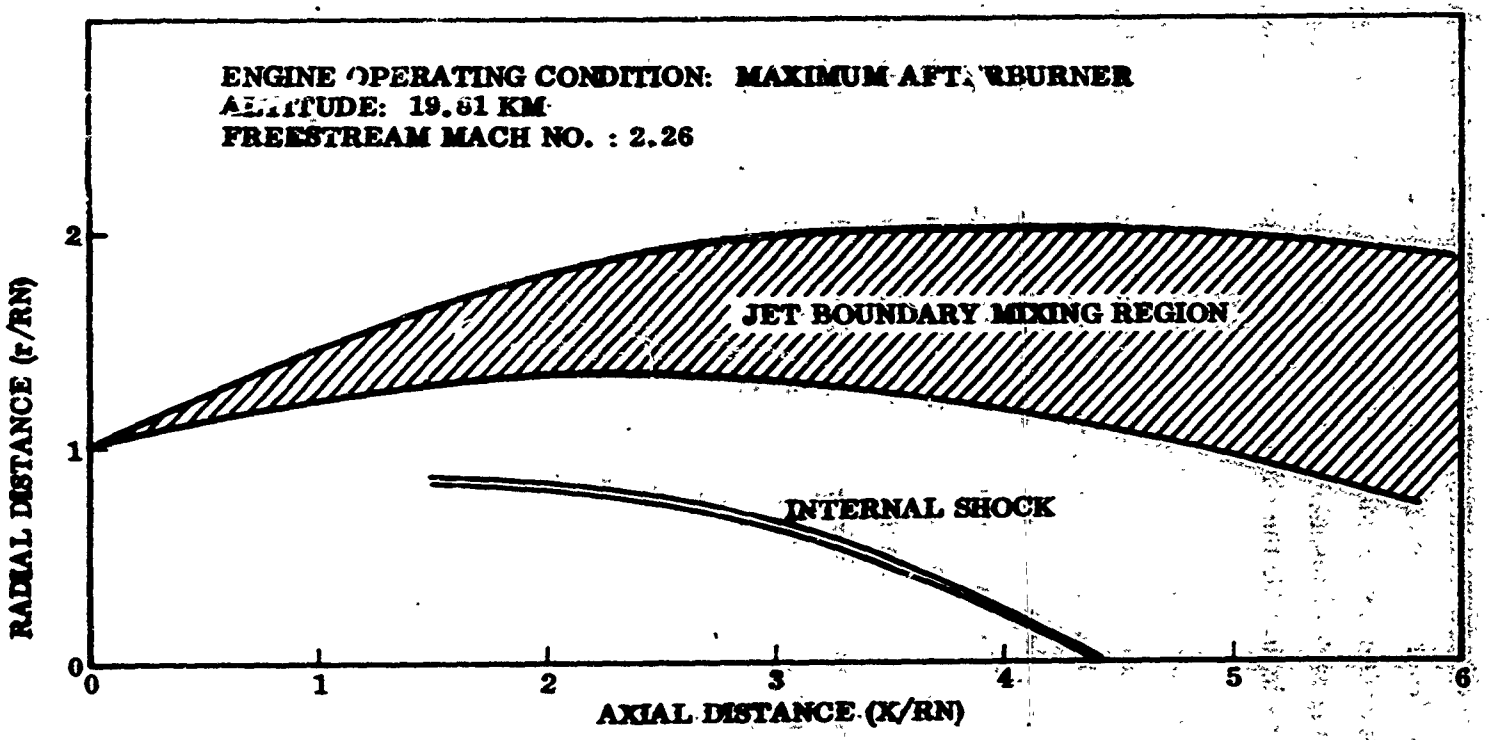

Figure 2-9 J85-GE-13 Jet Plume Properties

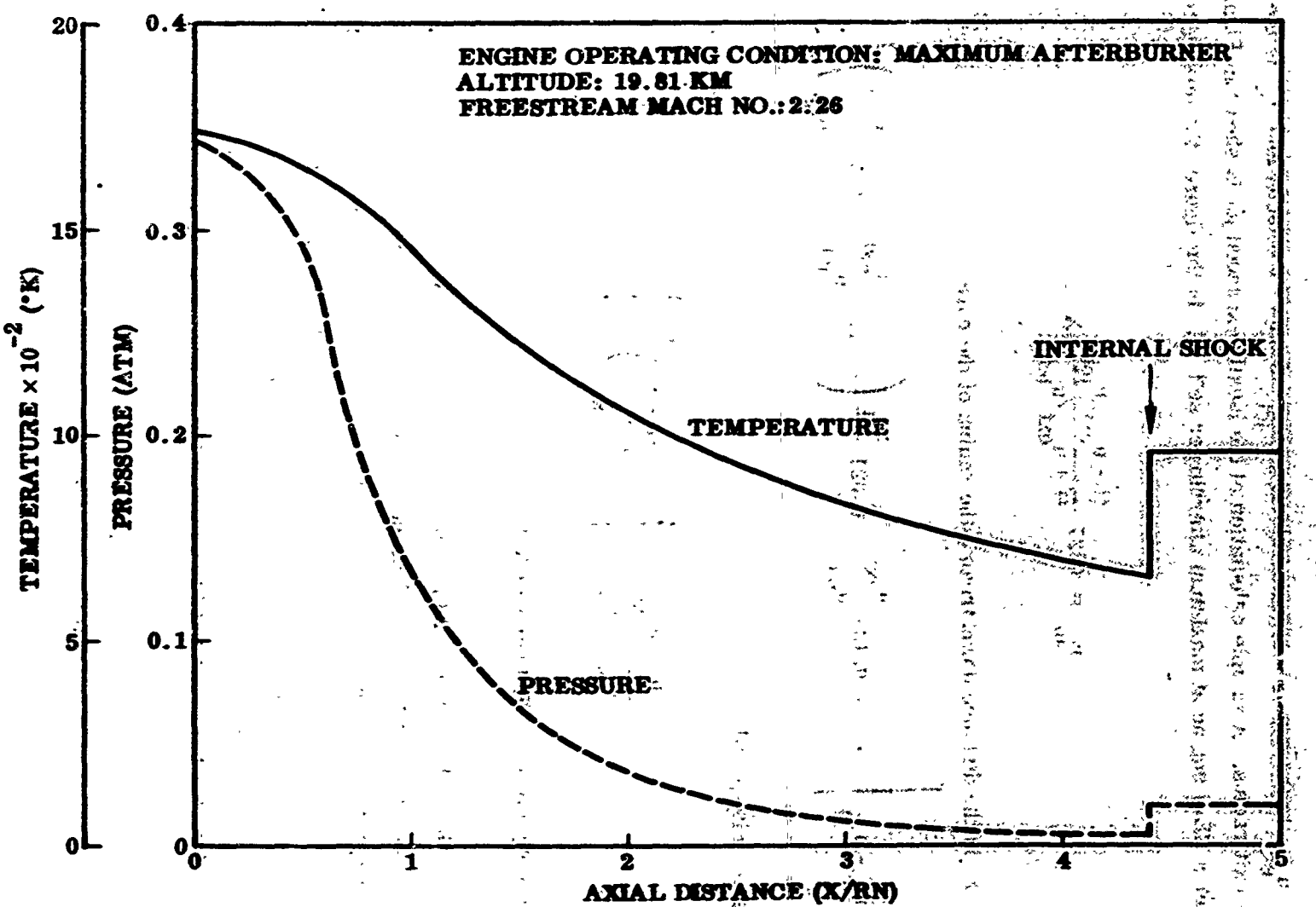

Figure 2-10 J85-GE-13 Jet Plume Centerline Properties

where u_{ext} is the external stream velocity, u_{jet} is the exit velocity and r_o is the nozzle exit radius. A sample calculation of the ideally expanded jet is shown in Figure 2-11 for a GE-4 engine at maximum afterburner setting. In the figure, the mixing region width

$$r_m = 0.27 \frac{(1 - u_{ext}/u_{jet})}{(1 + u_{ext}/u_{jet})} X$$

where X is the distance downstream, the radius of the core

$$r_c = r_o - r_m \left[0.416 + 0.134 \frac{u_{ext}}{u_{jet}} + 0.021 \frac{r_m}{r_o} \left(1 + 0.8 \frac{u_{ext}}{u_{jet}} - 0.45 \frac{u_{ext}^2}{u_{jet}^2} \right) \right]$$

and the velocity profile

$$\frac{u - u_{ext}}{u_{jet} - u_{ext}} = \left[1 - \left(\frac{r - r_c}{r_m} \right)^{1.5} \right]^2$$

are similarly given by the theory of Ref. 2-6.

The Far Field – The turbulent jets containing the exhaust grow in the developing vortex field generated by the wing. The detailed interaction between jets and aircraft wake is a complicated process, involving the buoyance of the jets and the roll-up process of the vortex sheet behind the particular type of wing of interest. For present purposes, these details are secondary; the main objective is to estimate the overall rate of jet growth and location of the point at which the exhaust fills the vortex pair. To this end the calculations of Ref. 2-7 have been used to estimate the trajectory of various points, originally on the wing trailing edge, as they proceed to roll up around the vortex core. The conclusion from this study is that, for wing-mounted engines, the jets turn about one revolution around the vortex core; at this point they can be considered as fully entrained in the vortex. This situation is confirmed by field observations and the study of photography of smoking or contrail-producing engines. The time required to turn one revolution around the core is as follows:

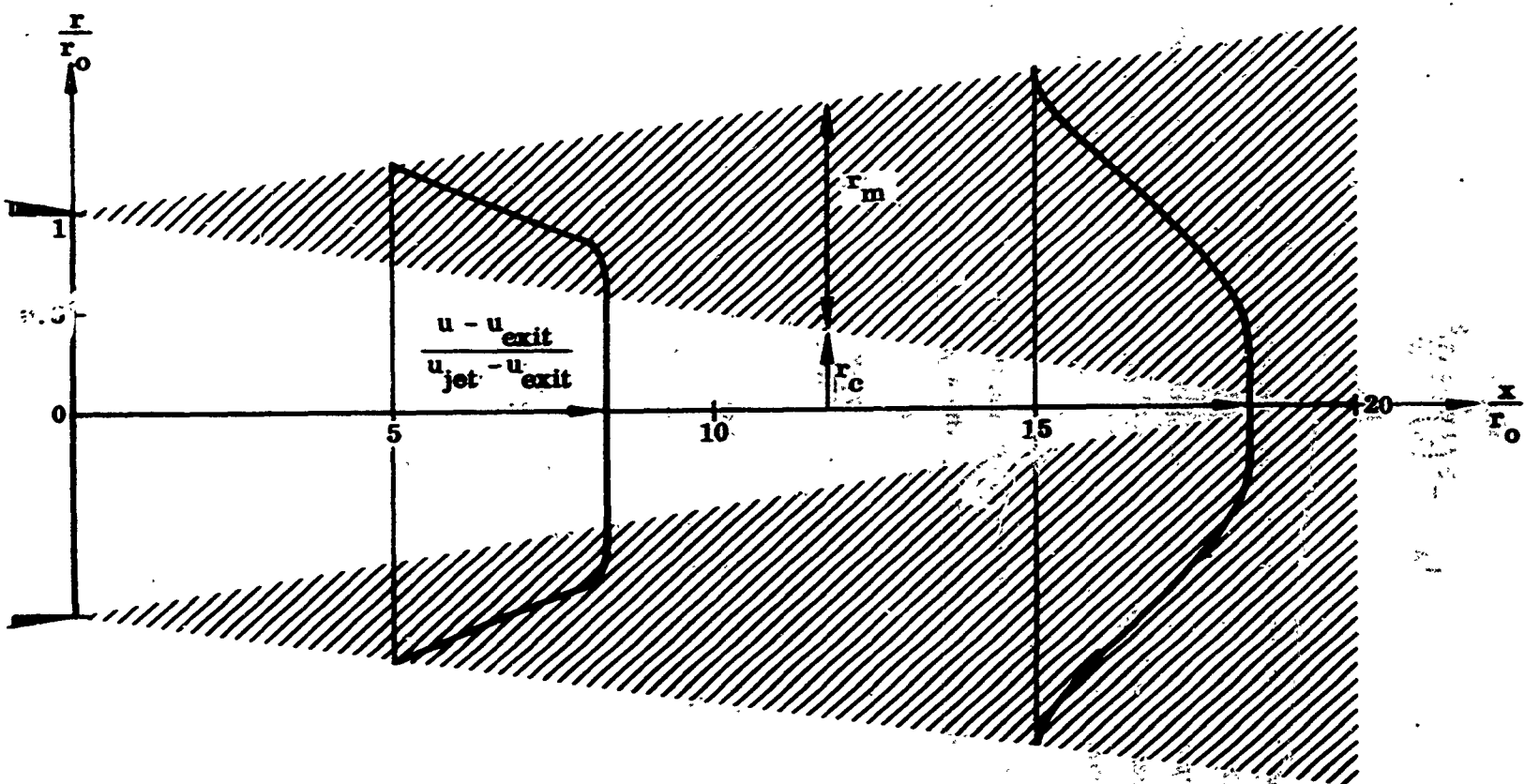

Figure 2-11 Mixing Layer in Jet of GE-4 Engine Operating at Maximum Power at Mach Number 2.7 and 20-km Altitude (Ordinate Scale Increased to Facilitate Reading Graph)

$$t_A = \pi^3 \left(\frac{\ell}{b}\right)^2 \frac{\rho V b^3}{W} \qquad (2.1)$$

where

ℓ = distance from the engine to the centerline of the vortex
b = aircraft span
V = aircraft speed
W = aircraft weight
ρ = ambient density

This time period is sensitive to aircraft configuration because of the square dependency on ℓ, but a rough average is $\ell/b \approx 0.2$, which yields

$$t_A \approx 1.5 \frac{\rho V b^3}{W} \qquad (2.2)$$

The growth of the jet up to time t_A has been calculated, using several turbulent jet theories and, in particular, that of Ref. 3-6 which gives the jet radius in the implicit form

$$\frac{x}{r_o} = 4.55 \left\{ \frac{r}{r_o} + \frac{0.69}{p^2} \left[\left(\frac{r}{r_o}\right)^2 - p^2 \right]^{1.5} + \left[\left(\frac{r}{r_o}\right)^3 - p^2 \right] \right\}$$

The parameter p is dependent upon the ratio of external velocity to jet velocity as given by

$$p = 8.04 \frac{1 - \frac{u_{ext}}{u_{jet}}}{\left(\frac{u_{ext}}{u_{jet}}\right)^2}$$

Calculations using these formulas and photographic data show that at the time t_A the jets have grown to approximately the size of the trailing vortex pair.

For modeling purposes, the time t_A is taken to be the end of the jet regime, at which time the exhaust occupies the entire vortex system and further horizontal growth is curtailed. The time

$$\tau \equiv \frac{\rho V b^3}{W} \tag{2.3}$$

is a characteristic time for the jet regime. It will be shown in Section 2.2.2 that this is also a characteristic time for the vortex regime, and therefore a convenient time-scaling parameter to reduce the data and extrapolate results.

The velocity and temperature distributions along the jet are of interest. Reference 2-8 presents results of an experimental study widely used in jet calculations. According to this study, the centerline velocity is given by

$$\frac{u_{c\ell} - u_{ext}}{u_{jet} - u_{ext}} = 8 \frac{r_o}{x} \left[1 + 3 \frac{u_{ext}}{u_{jet}} \right]$$

where u_c is the centerline velocity. According to the same study, the temperature is related to the velocity according to

$$\frac{T_{c\ell} - T_{ext}}{T_{jet} - T_{ext}} = \left[\frac{u_{c\ell} - u_{ext}}{u_{jet} - u_{ext}} \right]^{0.7}$$

The exponent 0.7 is somewhat larger than the theoretical value of 0.5 predicted by Taylor's vorticity-transport theory. The cross-sectional distribution of velocity is given by

$$\frac{u - u_{jet}}{u_{c\ell} - u_{jet}} = \left[1 - \left(\frac{y}{r} \right)^{2/3} \right]^2$$

The concentration and temperature profiles are related to the velocity profile by the 0.7 power law shown above. The preceding equations have been used to calculate temperature and velocity distributions. Examples of these are shown in Figures 2-12 and 2-13.

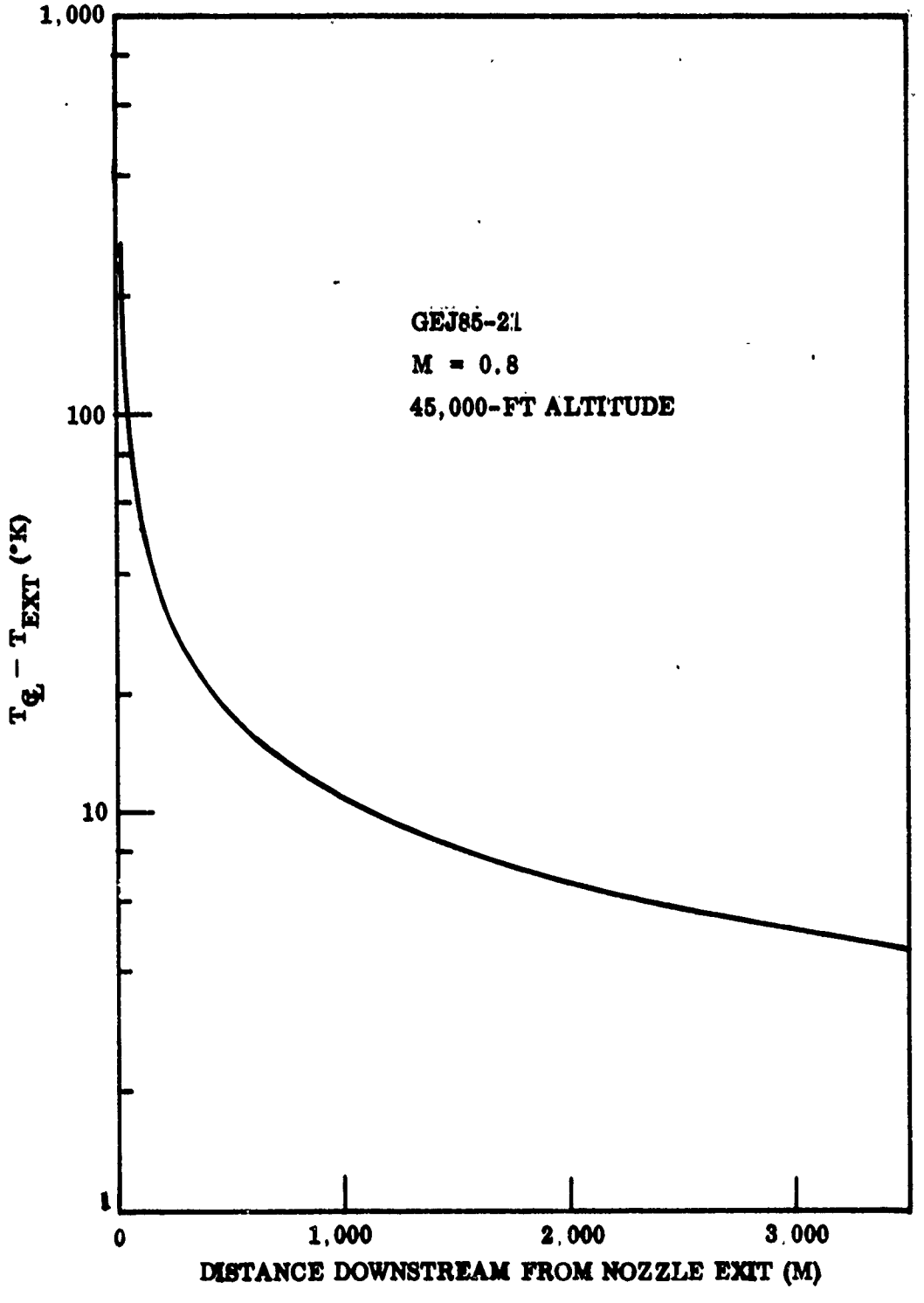

Figure 2-12 GEJ85-21 Jet Centerline Temperature Profile

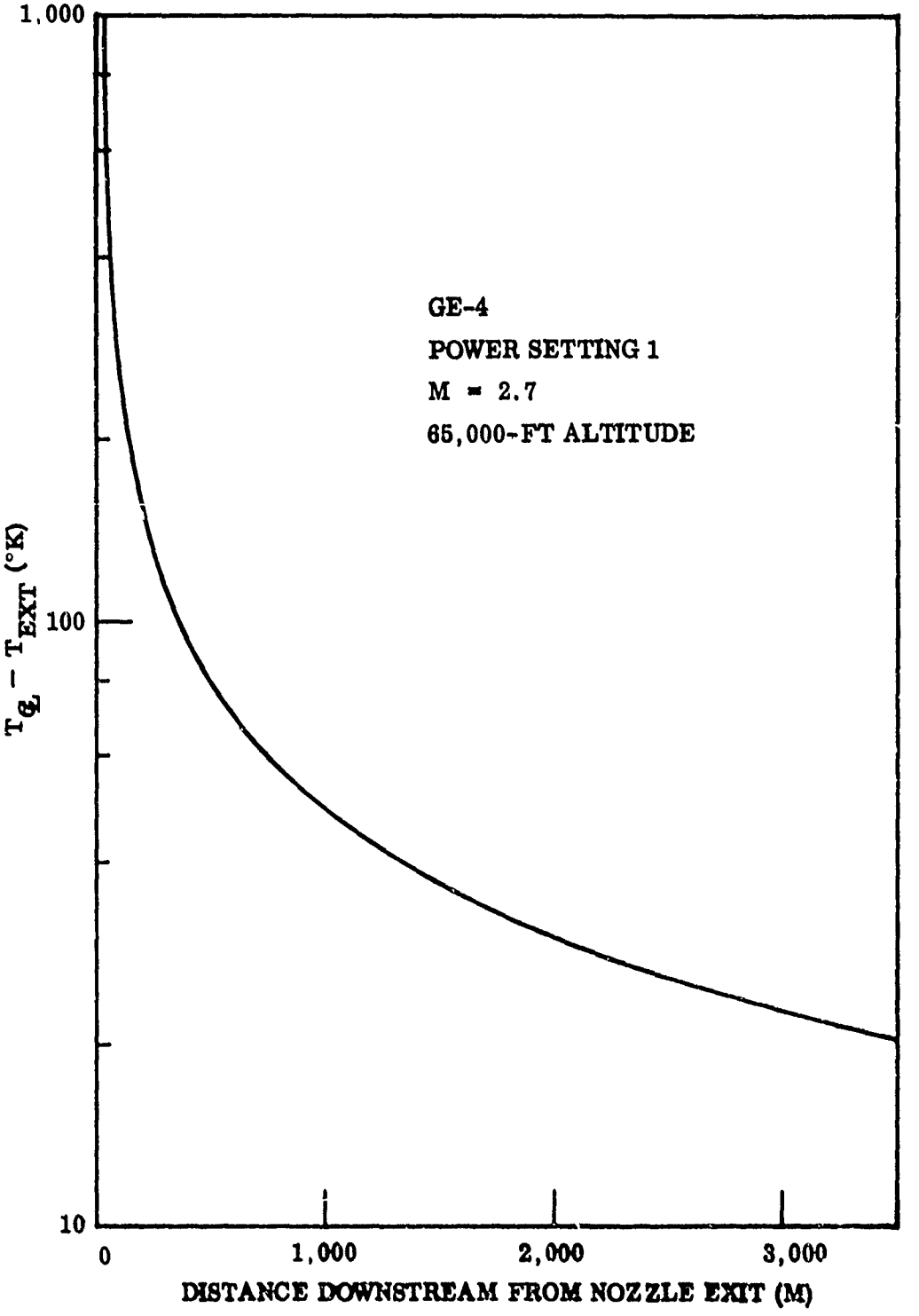

Figu. e 2-13 GE-4 Jet Centerline Temperature Profile

2.2.2 Vortex Regime

The vortex regime covers the section of exhaust trail extending from the end of the jet regime to the point where the trailing vortex pair breaks up. This corresponds to a time of the order of 100 sec. As indicated in section 2.1, the vortex pair in this regime dominates the dynamics of the wake. This vortex pair results from the roll-up of the vortex sheet shed from lifting surfaces, notably the aircraft wing. It can be shown that the edge of such a vortex sheet is unstable and rolls up because of mutual induction between the vortex filaments that make up the vortex sheet. This mutual induction is analogous to the electromagnetic phenomenon, and, in fact, obeys the same law (Biot-Savart). The roll-up of a trailing vortex sheet has been studied extensively (e.g., Ref. 2-7, and it is a well documented fact that after a time of approximately $\tau/10$ the edges have rolled up tightly about the two cores that contain most of the vorticity associated with the wing circulation. Thus, at times of order τ, that is, at the beginning of the vortex regime, the vortical wake of a finite wing is well represented by a classical vortex pair. This pair consists of two linear counterrotating vortices with cores that are small compared with the aircraft size and set apart a distance d of the order of wing span. [$d = (\pi/4)\ b$ for elliptically loaded wings.]

The dynamics of a vortex pair as described above is well understood (see Ref. 2-9). The pair cannot be stationary; due to mutual induction between the vortices, it travels at a steady speed. The sinking speed is given by

$$U = \frac{\Gamma}{2\pi d} \tag{2.4}$$

where Γ is the strength of either vortex. It can be shown that there is a mass of recirculating fluid, bounded by a closed streamline, that travels with the pair as shown in Figure 2-14, reproduced from the latter reference. In practice, the bounding streamline may sustain a weak shear layer due to velocity mismatch between the recirculating flow and the ambient fluid; otherwise, the boundary between vortex and ambient fluid is sharp. This explains the containment effect that the vortex has on the horizontal spread of the exhaust. For the case of a trailing vortex pair

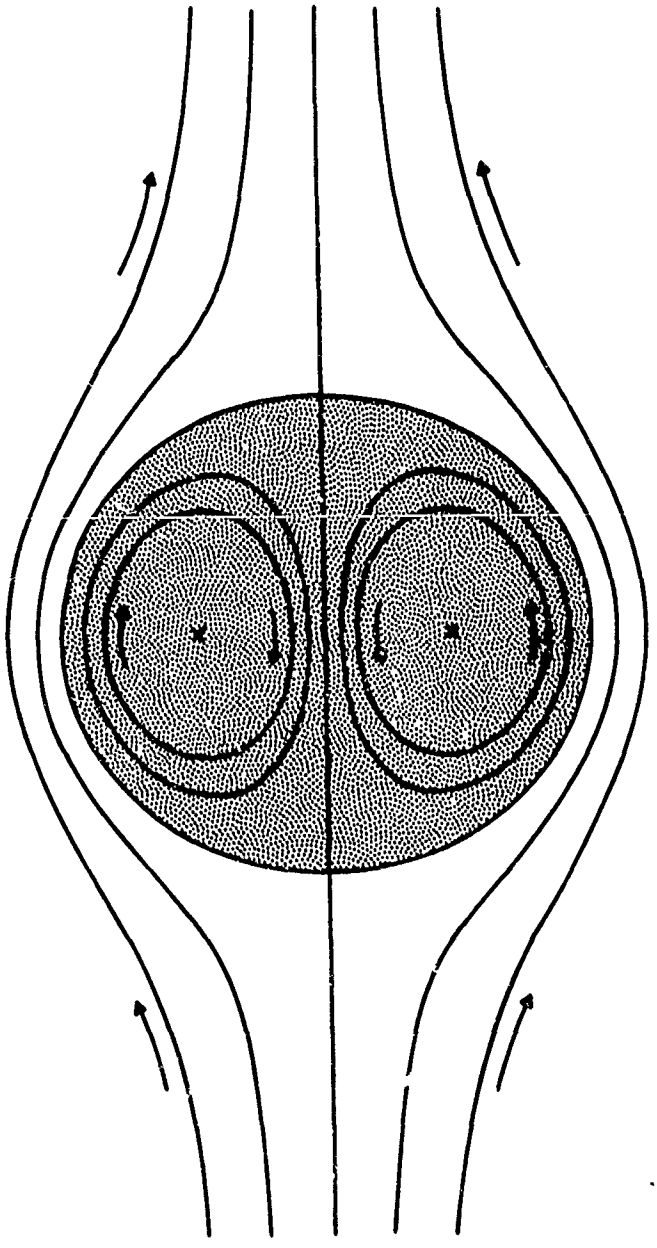

Figure 2-14 Streamlines of a Vortex Pair as Seen by an Observer Moving With the Pair. Shaded area marks recirculating flow trapped in the vortex

generated by a wing, the pair moves downward with a linear momentum per unit length

$$P = \rho \Gamma d \tag{2.5}$$

that balances the wing lift (which is related to Γ).

If the vortex pair were to behave ideally as described above, the aircraft wake would remain enclosed within its boundary. In practice, fluid becomes detrained from the vortex pair and deposited in a vertical band. It is believed that this detrainment is due to buoyancy forces, which detract from the downward momentum of the vortex pair, causing a decrease of circulation, detrainment of mass, and increase in sinking speed. The vortex is buoyant for two reasons; it contains exhaust gases, and it undergoes subsidence heating as it sinks in a generally stable environment. An approximate computation shows that the source of buoyancy is about equally divided between exhaust heat and subsidence, each contributing an increase in temperature of the order of 1°C. The upper central photograph in Figure 2-1 shows the cores of the sinking vortex pair and the detrained exhaust above them. This effect, which is induced entirely by the aircraft, has a lasting impact on the wake because the vertical growth exposes it to wind shear, which is one of the major mechanisms for further dispersal in the wake dispersion regime.

The vortex pair sinks at the speed U given by Eq. (2.4), which is relatively insensitive to buoyancy effects because the decrease in circulation and size tend to compensate each other. In a perfectly still environment, this process would continue for a long time because the dissipative effects are small. It is well known that frictional losses cannot account for the disappearance of the vortex pair in a matter of minutes as is usually the case. The most likely mechanism for destruction of the vortex pair seems to be the hydrodynamic instability studied in Ref. 2-2. According to this source, the time for instabilities to grow one e-fold is

$$t_B = 3.7\tau$$

where τ is defined by Eq. (2.3). A correlation of data from free flights and laboratory experiments (Ref. 2-3) shows that the time for the vortex cores to loop and start breaking up is best fitted by

$$t_B \approx 10\,\tau \qquad (2.6)$$

For modeling purposes, it will be assumed that the vortex pair sinks at a steady speed given by Eq. (2.4) or, equivalently, the wake in the vortex regime grows vertically at the rate

$$\frac{dh}{dt} = \frac{8}{\pi^3}\,\frac{W}{\rho V b^2}$$

From the previous discussion, it is clear that τ is a scaling time for the vortex regime. Thus, if lengths are referred to as the aircraft span b and times to τ, the last equation becomes

$$\frac{d\,(h/b)}{d(t/\tau)} = \frac{8}{\pi^3}$$

and a universal description of the vortex regime can be constructed as follows:

Initial time	$\frac{t_A}{\tau} = 1.5$
Final time	$\frac{t_B}{\tau} = 10$
Vertical rate of growth	$\frac{8}{\pi^3}$

It was previously noted in section 2.2.1 that the jet regime also scales with the time τ. Therefore, a simple model for jet and vortex regimes can be assembled, as will be shown in section 2.2.3.

2.2.3 Scaling Model For Jet and Vortex Regimes

The jet and vortex regimes scale with the same characteristic time τ and can be represented in a unified way as shown in Figure 2-15.

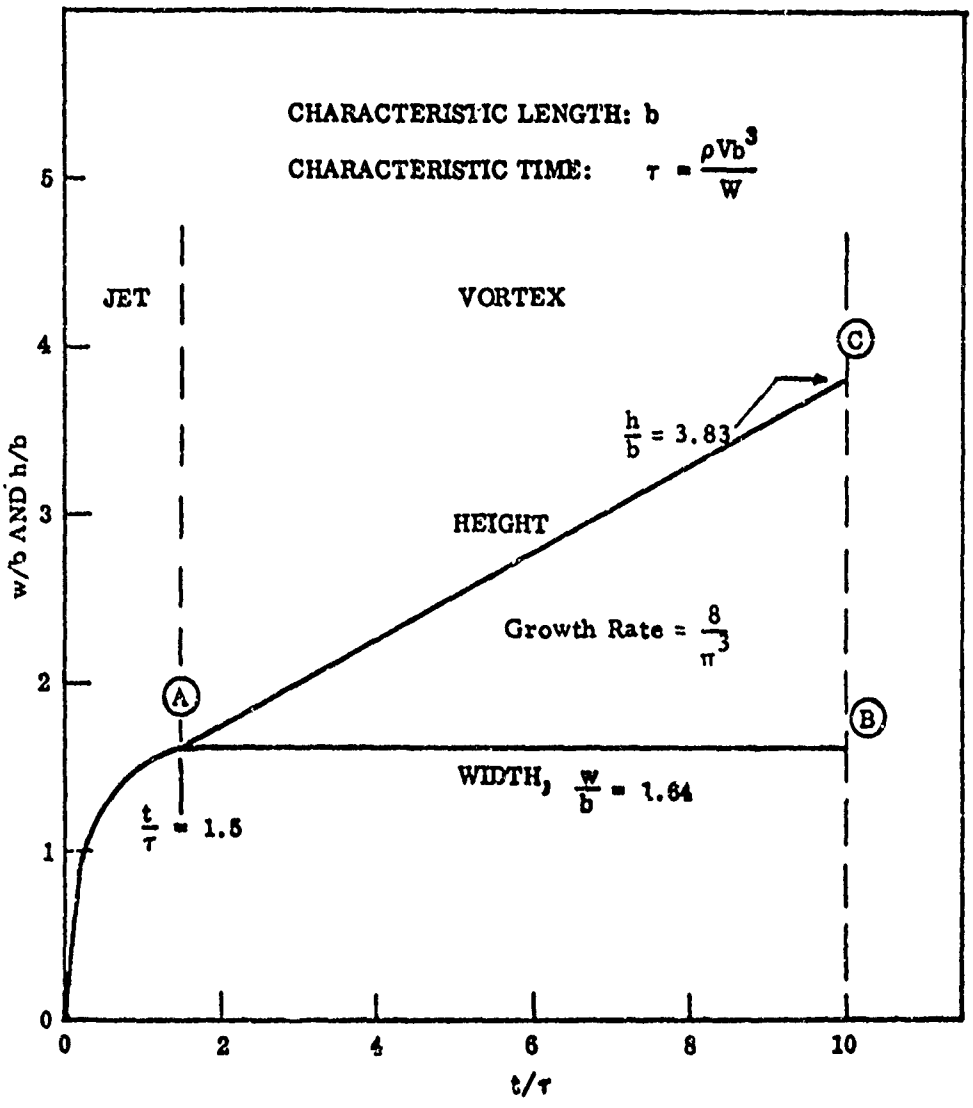

Figure 2-15 Scaling Model for Jet and Vortex Regimes

The jet regime starts at time zero and ends at $t_A/\tau = 1.5$ according to Eq. (2.2), which defines the abscissa of point A in the previous figure. The ordinate of point A is the width (dimensionless) of the vortex pair which, according to Ref. 2-9, is given by

$$w = 2.09\,d = 2.09(\pi/4)b = 1.64\,b$$

or

$$\frac{w}{b} = 1.64$$

for elliptically loaded wings. In the vortex regime, the width remains constant at this value (line A B) whereas the height grows at a rate $8/\pi^3$. (See section 2.2.2) The end of the vortex regime is at $t_B/\tau = 10$. This sets the final height of the wake (at vortex breakup) at $w/b = 3.83$. It is of interest to note that the height and width of the wake at vortex breakup depend on the aircraft span alone. Figures 2-16 and 2-17 show some data plotted in dimensionless form according to this scaling model. These data were obtained by LMSC and from Refs. 2-1 and 2-10.

It seems that in spite of its simplicity the model is reasonably good. One problem in testing the model is the scarcity of well-documented data. Flight and aircraft parameters must be known to reduce physical data such as that of Ref. 2-1 to dimensionless form.

2.2.4 Wake Dispersion Regime

Comparison of Data With Theoretical Estimate – The wake dispersion regime extends from vortex breakup to times at which the atmospheric dispersion is independent of the aircraft that deposited the exhaust trail. Thus, this regime spans the gap between the aircraft-dominated early regimes and the purely atmospheric processes. The wake dispersion regime is the most complex of the three presently defined regimes because it involves several modes of dispersal and because both aircraft-induced and atmospheric-induced processes coexist and are of comparable importance.

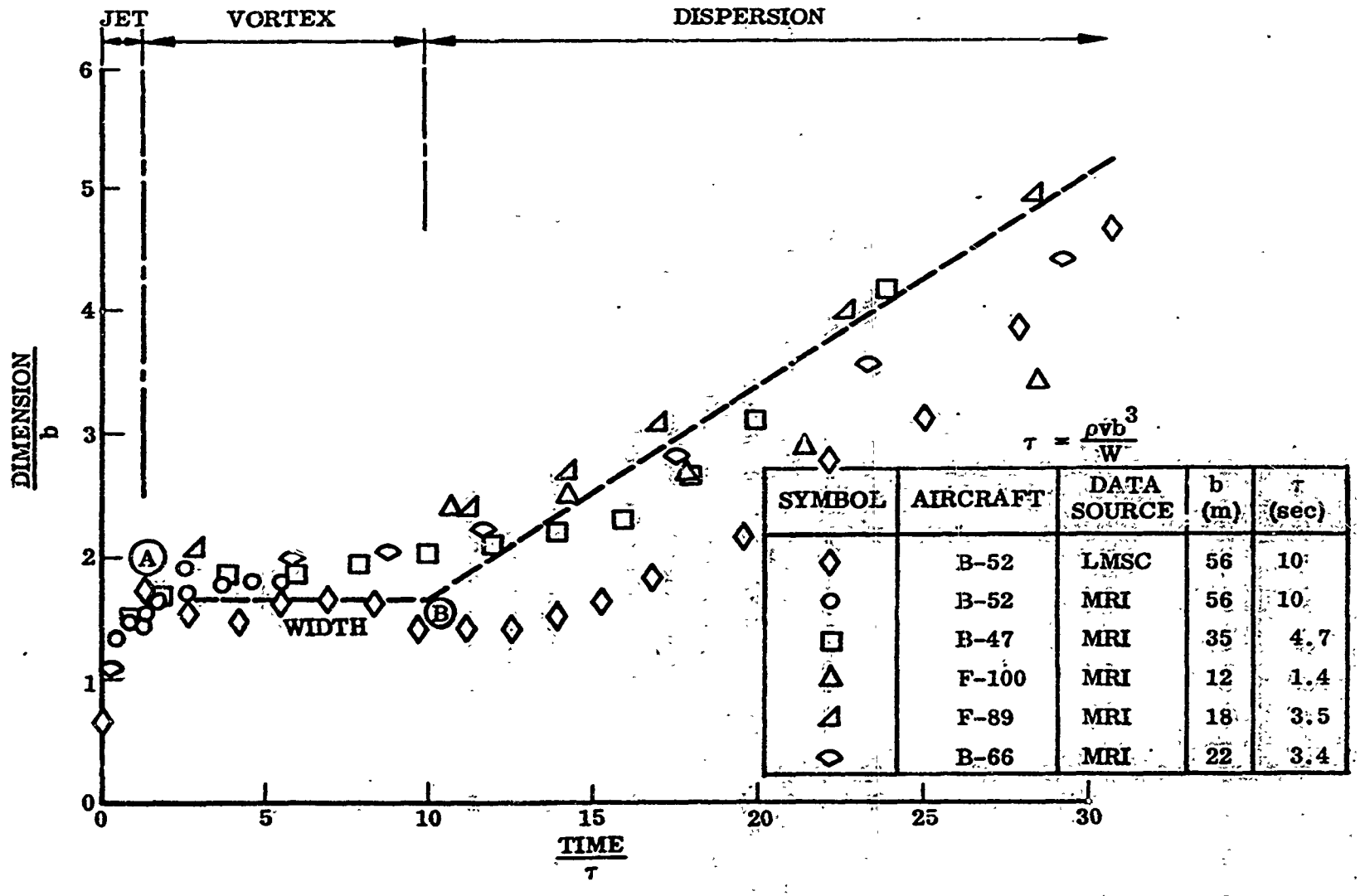

Figure 2-16 Comparison of Contrail Width Data With Scaling Model

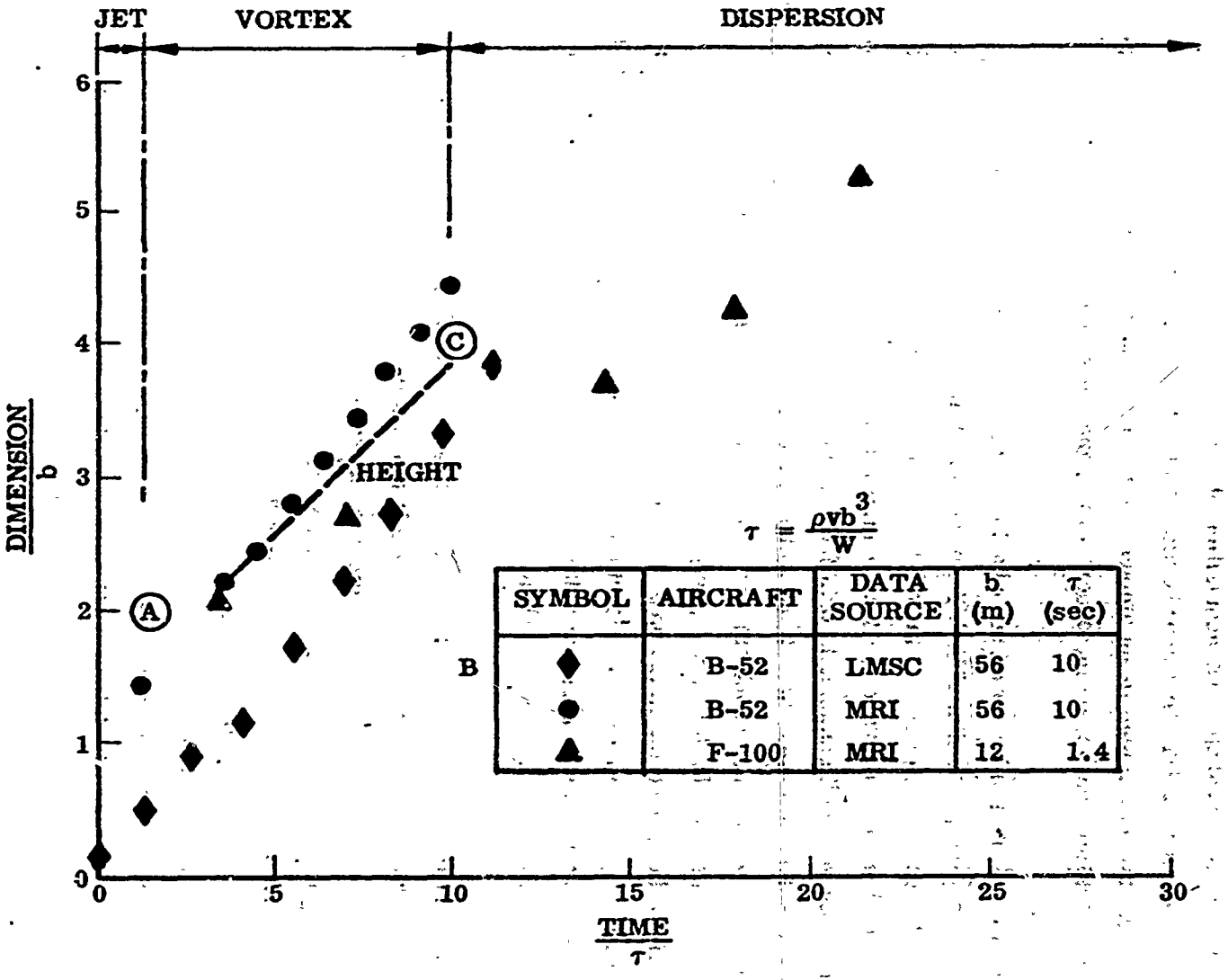

Figure 2-17 Comparison of Contrail Height Data With Scaling Model

It was an unexpected finding of the present study that aircraft-induced effects last for relatively long times. It has been generally assumed that aircraft effects die out rapidly after vortex breakup. Our acquisition of long time data and a closer look at the major processes contributing to wake dispersal indicate that aircraft-induced effects may be present in significant amounts up to times one order of magnitude larger than vortex breakup, that is, on the order of thousands of seconds.

The prediction of the fluid mechanical behavior of aircraft wakes in the dispersion regime involves the prediction of both the wake height and width. Unfortunately, clear-cut data on long-term wake growth in both the vertical and horizontal directions, which requires simultaneous coverage from two camera stations, are not currently available. However, combined width and height data from a single camera station have been obtained and resolved into wake height and width by means of certain assumptions, key data points and consistency requirements. The data previously presented in Figure 2-3 is a case in point. In this case, good data of the combined height and width were obtained from the ground for times up to 11 min at a moderate elevation angle (~35 deg) and between 15 and 25 min at a low elevation angle (~1 to 8 deg). In addition, several excellent photographs were taken from the aircraft — one of the contrail height at 7 min and another of the width at 33 min. These data were analyzed in the following manner.

For the first 11 min, the wake height was varied parametrically, and the wake width was computed from the observed combined height and width data. It was found that in order for the width to increase monotonically, the wake height had to first increase then decrease as shown in Figure 2-3. Another requirement was that the wake volume, computed as the product of height times the width, could not decrease. This latter requirement is not completely satisfied at all times for the preliminary data shown in Figure 2-3, but this slight deficiency can be corrected by additional massaging of the data. The wake width thus obtained was then faired into the data point obtained from the aircraft at 33 min. The faired-width data were then used to obtain the wake height from the low elevation ground data ($15 \leq t \leq 25$ min). The resulting height data were found to follow a consistent trend with the assumed height variation for the first 11 min.

One interesting result of this analysis is that the increase in wake height in the dispersion regime scales with the same characteristic length b and time t ($\tau = \rho V b^3/w$) as in the vortex regime. This correlation of the wake height growth is illustrated in Figure 2-16. The fact that the wake growth correlates with the same characteristic length and time suggest that the wake height growth in the dispersion regime is due to the residual downward momentum of the sinking vortex pair. At the present time it is thought that the increase in wake height due to the residual downward momentum is being opposed by gravitational forces (gravitational collapse mechanism), which exist when a well-mixed, uniform-density fluid is placed in a stable atmosphere. The densitometer trace shown in Figure 2-7 tends to support the contention that the wake is well mixed after vortex-pair breakdown. The gravitational force is proportional to wake height while the downward momentum per unit mass is inversely proportional to wake height, since the wake is being diluted as it grows. At some point ($t/\tau \approx 60$), the gravitational forces overcome the downward momentum and the wake begins to collapse. The wake collapse continues until the wake height is about 0.4 of its maximum height.

Based on the wake height variation observed for the Convair 990, long-term B-52 contrail data were also analyzed. These data along with a theoretical estimate of the contributions of wind shear, buoyant rise, gravitational collapse, and wake and atmospheric turbulence diffusion to the wake width are shown in Figure 2-19. Details of how these estimates were obtained are discussed in subsequent paragraphs. Unfortunately, time did not permit similar theoretical estimates to be made for the Convair 990 data.

Regarding the data and theoretical estimate shown in Figure 2-19, it can be seen that wind shear is the predominant dispersal mechanism. Mass entrainment due to buoyant rise, which results in an increase in wake width, is seen to be relatively small. Wake-width growth due to gravitational collapse is also relatively small and only occurs during the time the wake height is decreasing. The contribution due to turbulence deposited into the wake by vortex-pair breakdown is also small and is confined to early times, since the wake turbulence decays to the atmospheric level in a few minutes. Wake diffusion due to atmospheric turbulence is a sizable contributor to the overall wake dispersion, especially at late times. Although there is considerable scatter in the data, the agreement between data and the theoretical estimates is encouraging.

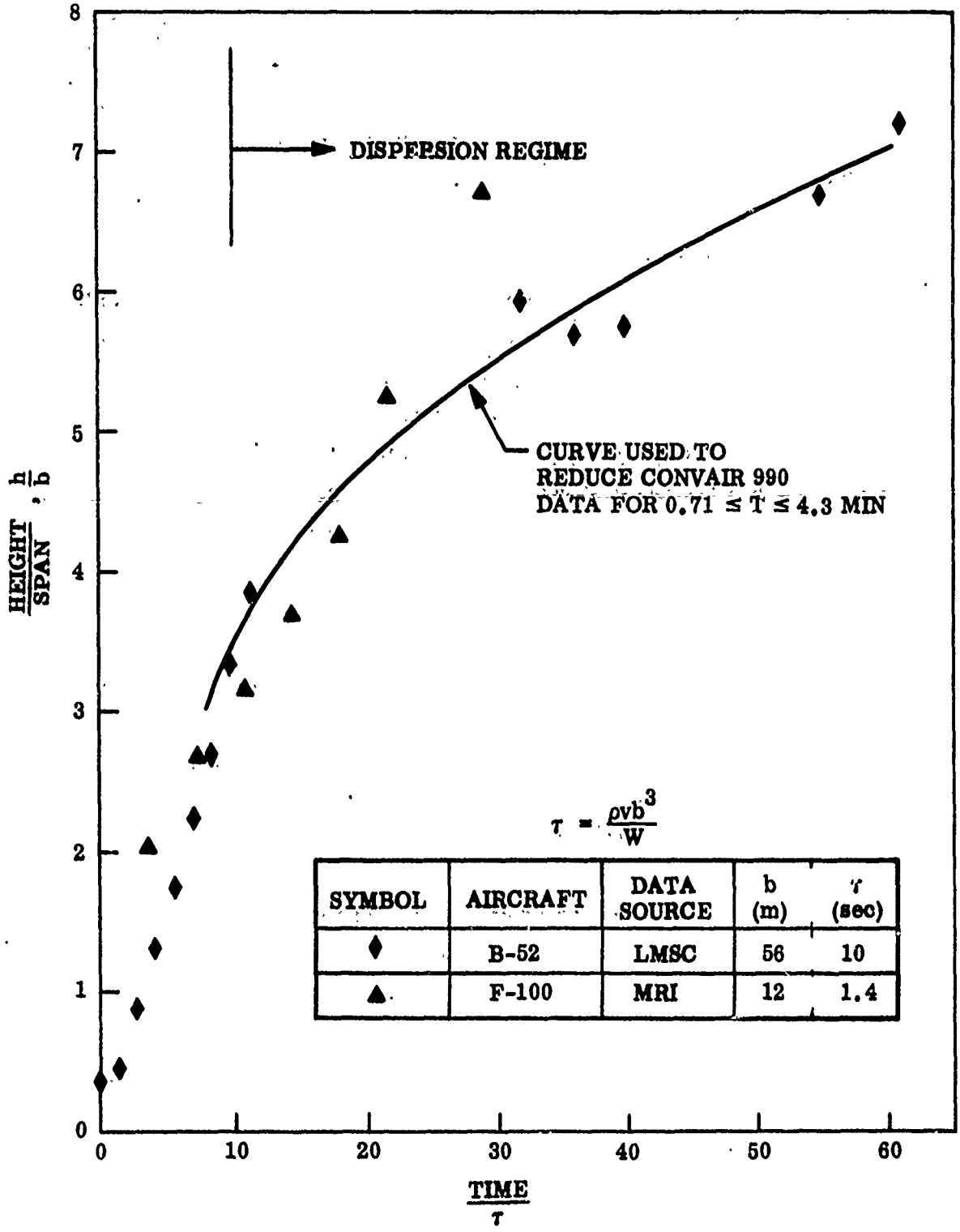

Figure 2-18 Dispersion Regime Wake Height Scaling

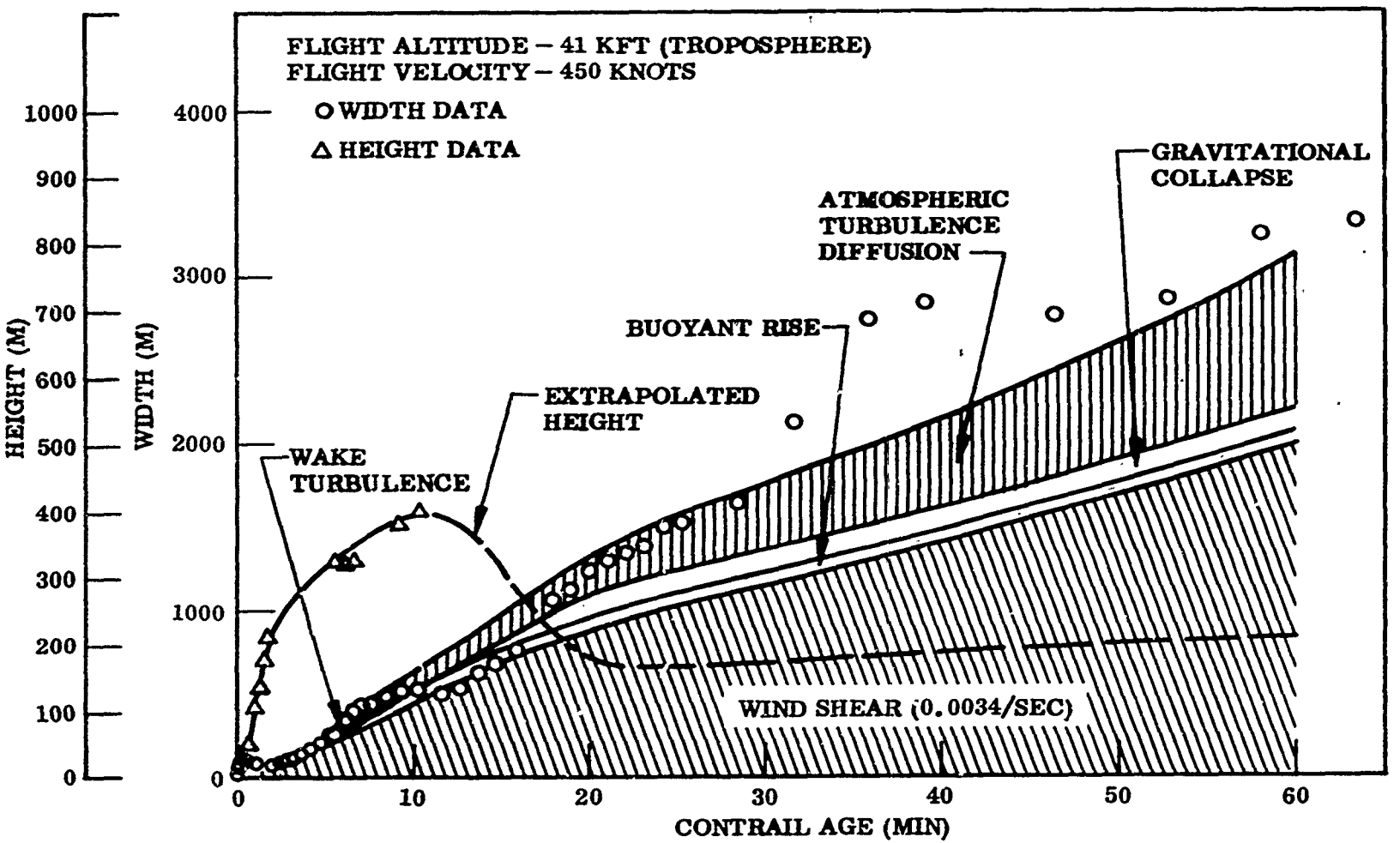

Figure 2-19 Comparison of B-52 Contrail Data With Theoretical Estimates

Wind Shear – Wind shear contributes to dispersal of the exhaust trail by advection of the top and bottom of the trail at different speeds. For simplicity, the wind velocity may be assumed linear through the trail height. This assumption seems justified in view of the coarseness and uncertainty associated with wind data. Under this assumption, the rate of growth of the trail width is given by

$$\frac{dw}{dt} = h \sin \theta \frac{dv}{dz} \tag{2.7}$$

where

- h = trail weight
- θ = angle between the wind and the trail axis
- v = wind speed
- z = vertical coordinate

The correction for wind shear is straightforward and will be easily implemented in the mathematical model. It is assumed that appropriate inputs of wind shear will be made available, a task that is considerably more difficult. As an illustration of some of the problems involved, Figure 2-20, reproduced from Ref. 2-11, shows the differences in wind shear that may be obtained by different manipulations of the same data.

An indication of the relative importance of wind shear is given in Figure 2-19 where the contribution of wind shear to horizontal dispersal was calculated on the basis of the local atmospheric sounding at the time the contrail was produced.

It can be expected that stratospheric flights will be subjected in the average to less wind shear than the one shown in the figure, which occurred in the high-shear region near the tropopause.

Wake Turbulence Diffusion – In the current model, it is assumed that wake growth by turbulent diffusion in the dispersion regime is due initially to turbulence deposited in the wake by vortex breakdown. The scale of turbulence created by vortex breakdown is assumed to be of the order of the wake width at the time of breakdown. The turbulent energy in the wake at wavelengths comparable to the wake width is initially much

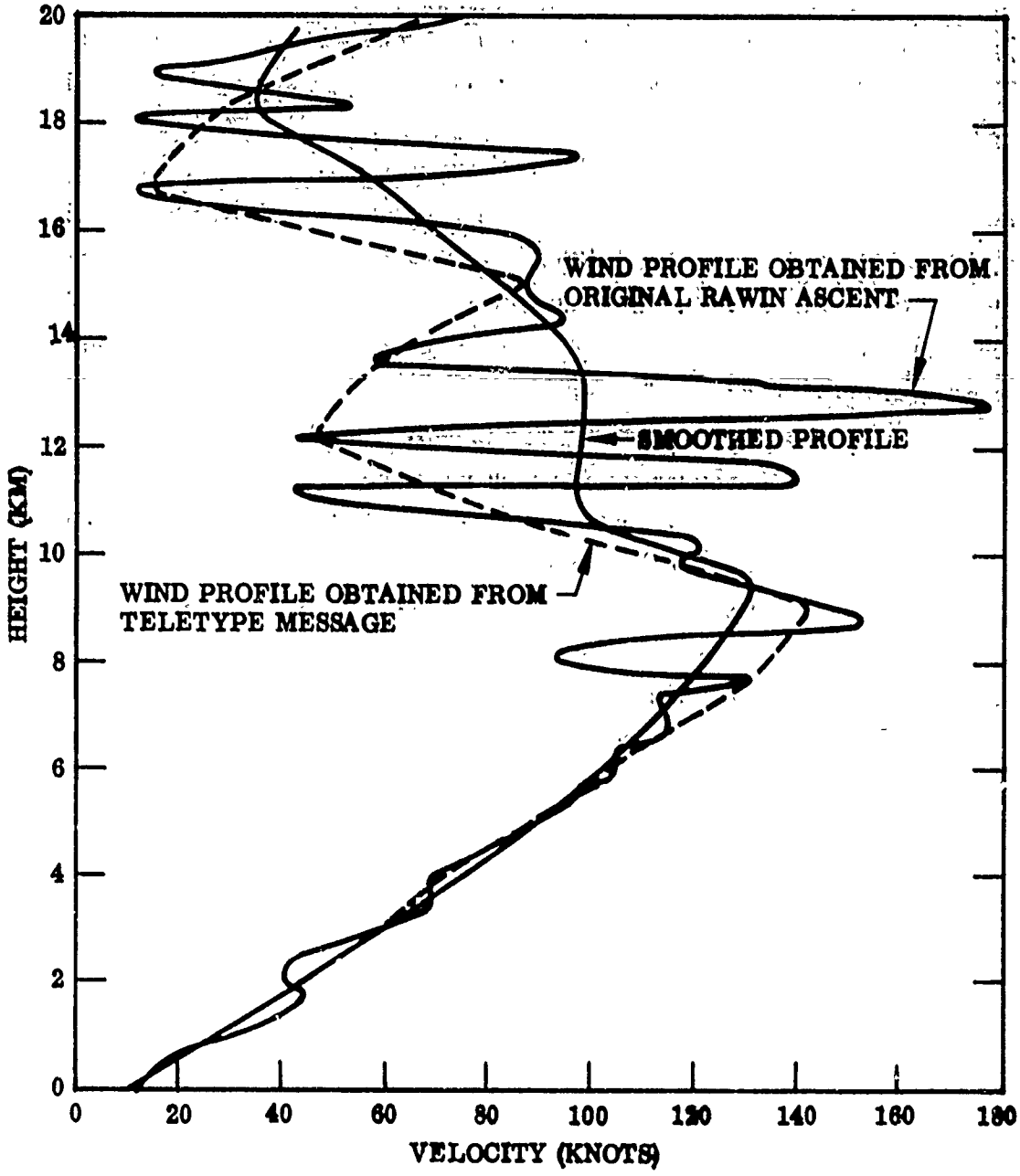

Figure 2-20 Rawin Measurements, Washington, D.C., 14 March 1954, 2100 GCT

greater than is present in the free atmosphere. As the wake grows in width and height, mixing with the atmosphere and viscous dissipation will decrease the wake turbulence level continuously until it attains the turbulence level in the free atmosphere. Additional turbulence will be deposited into the wake by the turbulent boundary layer and by viscous shear and mixing at the edge of the engine exhaust jets. The scale of this turbulence is probably of the order of 1 m or less and therefore should not play an important role in diffusing the overall wake.

The kinetic energy in the wake due to vortex pair breakdown was estimated by equating it to the induced drag and by assuming that the kinetic energy was distributed uniformly over the entire wake cross section. This estimate for the B-52 flight of interest yielded an average turbulence velocity of 2.4 m/sec. If it is further assumed that all of this energy is at the wavelength equal to the wake width, the resulting spectral density is somewhat higher than that present in what is qualitatively termed severe clear air turbulence. This estimate can be considered an upper bound, since the turbulence would be expected to distribute itself over some wavelength interval. According to the findings of many investigators, severe turbulence corresponds to a dissipation rate of about $\epsilon = 700\ cm^2/sec^3$. The order of magnitude of the initial dissipation rate can also be estimated from the relationship $\epsilon \sim \frac{u^3}{2\ell}$, where u is the turbulence velocity and ℓ is the scale length, which is assumed to be equal to the wake width. Based on the above relationship the initial dissipation rate is again estimated to be about $700\ cm^2/sec^3$.

If the dissipation rate is known, an estimate can be made of the wake growth by wake turbulence diffusion. Walton (Ref. 2-12) for example, has obtained a solution to the diffusion equation of the form

$$\sigma^2 = \sigma_o^2 + 2\epsilon^{1/3}\sigma_o^{4/3}t + \frac{4}{3}\left(\epsilon\sigma_o\right)^{2/3}t^2 + \frac{8}{27}t^3 \qquad (2.8)$$

where

σ = cloud size = standard deviation of concentration distribution
σ_o = initial cloud size
ϵ = dissipation rate
t = time

In this solution, the diffusion coefficient is taken to be

$$K = \epsilon^{1/3} \sigma^{4/3} (t) \tag{2.9}$$

In the aircraft wake, both dissipation rate and the wake size are functions of time. In the free atmosphere case, dissipation rate is taken to be a constant. An estimate of the wake growth by wake turbulence can be made by utilizing the above solution in a quasi-steady approximation. The approximation assumes that the rate of growth $(d\sigma/dt)$ for the case $\epsilon = \epsilon(t)$ and $\sigma = \sigma(t)$ can be approximated by solutions for ϵ = constant and $\sigma = \sigma(t)$.

The wake growth rate is then given by $\sigma = \int_0^t \frac{d\sigma}{dt} dt + \sigma_o$

where $d\sigma/dt$ is obtained from Eq. (2.8)

It now remains to estimate how the wake dissipation rate ϵ will decay from the initially high value of the order of 700 cm^2/sec^3 to the atmospheric value which is of the order of 1 cm^2/sec^3. There are three mechanisms for decreasing the dissipation rate in the wake: (1) dilution of the high-energy air in the wake by mixing with the low-energy atmospheric air, (2) an increase in wake scale due to wake growth, and (3) inviscid dissipation of large-scale turbulent energy.

The dilution effect can be estimated by

$$\epsilon = \epsilon_o \cdot \frac{A_o}{A} + \epsilon_{atm}$$

where A is the wake cross-sectional area and the subscript o refers to conditions at time of vortex breakdown. The scale change effect enters because the largest scale size of the turbulent energy deposited by vortex breakdown is of the order of the wake width at time of vortex breakdown. Since the wake grows because of various mechanisms and the turbulent scale of the deposited energy does not, the dissipation rate will decrease inversely as the wake width.

$$\epsilon = \left(\epsilon_o \frac{A_o}{A}\right) \cdot \frac{\ell_o}{\ell} + \epsilon_{atm}$$

The inviscid dissipation of large-scale turbulent energy to smaller scales will also decrease the dissipation rate. If we assume that the large scale eddies lose 1/e of their kinetic energy in the characteristic time ℓ/u, a rough estimate of the turbulent velocity decay can be obtained by means of a stepwise evaluation of the characteristic time. The dissipation rate, including all of the above decay mechanisms, is then estimated from

$$\epsilon = \left(\epsilon_o \frac{A_o}{A}\right) \frac{\ell_o}{\ell} \cdot \left(\frac{u}{u_o}\right)^3 + \epsilon_{atm}$$

The evaluation of the above estimate of the dissipation rate Figure 2-21 indicates that the wake turbulence will decay to the atmospheric value in about 2 to 3 min for $\epsilon_o = 700\ cm^2/sec^3$ and in about 1 to 2 min for $\epsilon_o = 100\ cm^2/sec^3$.

The wake and atmospheric turbulence contribution to wake growth was evaluated using the dissipation rate decay as estimated above in the quasi-steady approximation described previously. The results of these calculations are shown in Figure 2-19. The difference between the results for assumed initial values of ϵ_o of 700 and 100 cm^2/sec^3 is insignificant because of the rapid decay of dissipation rate to the atmospheric value. Diffusion of the wake a few minutes after vortex breakdown is due entirely to atmospheric turbulence.

In the present case, the wake diffusion is scale-dependent according to Eq. (2.9). Partial justification for this form of the diffusion coefficient relies on the comparison of predicted growth rates with observed growth rates of nuclear debris clouds (Ref. 2-12) and similar data. These data may include the combined effect of vertical transport and wind shear. In other words, the scale dependent diffusion prediction may include the effects of wind shear. If this is the case, the contribution of wake and atmospheric turbulence to the wake growth may be less than that currently estimated.

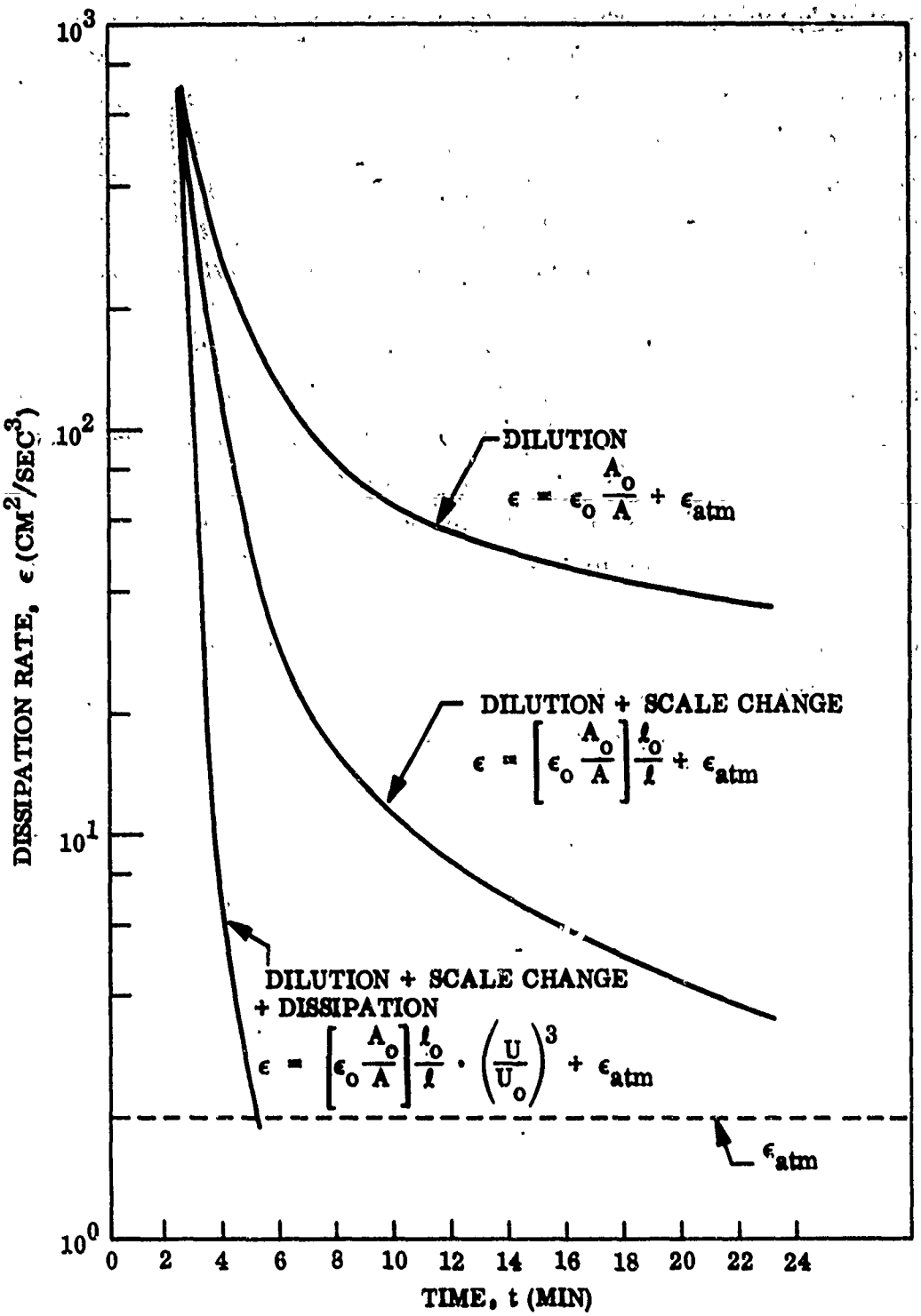

Figure 2-21 Estimate of Wake Dissipation Rate Decay

Gravitational Wake Collapse – When a well-mixed region is created locally in a stably stratified environment, the fluid in the well-mixed region tends to acquire neutral stability while the surrounding fluid remains stable. As a consequence local buoyancy forces are created, with the top of the mixed region becoming negatively buoyant and the bottom positively buoyant with respect to the environment. This creates a vertical collapse of the well-mixed region, which flattens and spreads horizontally as every parcel of mixed fluid seeks its own density level in the stratified environment.

A number of laboratory experiments have been carried out to study these effects in water tanks containing stratified solutions (Refs. 2-13, 2-14, and 2-15,). It has been observed that mixed regions created with various agitators or by the turbulent wakes of self-propelled bodies collapse as described above. The degree of collapse and the final shape depend on the initial degree of stratification and the thoroughness of the mixing process. The experiments generally involve much larger stratification than that of the standard stratosphere and, except for those of Ref. 2-15, are limited to relatively short times. Therefore, application of these results to aircraft wakes involves substantial extrapolation. Nevertheless, a certain amount of wake collapse should be expected in stratospheric wakes, and the extrapolation is justified within the error bounds of the present investigation.

The water-tank experiments mentioned above show that, in the wake-collapse process, the length scale is given by the size of the body generating the mixed region, and the time scale is given by the Brunt-Vaisala period

$$T = 2\pi \left(-g \frac{1}{\rho} \frac{\partial \rho}{\partial z}\right)^{-\frac{1}{2}} \qquad (2.10)$$

The theoretical estimate of the increase in wake width due to gravitational collapse shown in Figure 2-19 is based on conservation of mass. As the wake height decreases, the wake width must increase to compensate for the decrease in wake volume due to collapse. During collapse, other mechanisms are present which simultaneously increase the wake width. Since the wake height decrease for the B-52 was estimated from preliminary Convair 990 data, the estimate of the wake growth by gravitational collapse is somewhat uncertain.

Buoyant Rise – Buoyant rise of the exhaust trail has been proposed as a growth mechanism at late times (Ref. 2-16). The growth results from entrainment of ambient air, through turbulent mixing. The source of buoyancy in the wake is the thermal energy in the engine exhaust, and subsidence heating due to the vortex motion. A quick calculation shows that the temperature excess in the wake is not large but, on the other hand, small temperature differences can produce significant buoyant rise. In Ref. 2-16, the buoyant rise and associated rate of growth are calculated using chimney plume theories. In the present investigation, the problem was approached from a different point of view, namely, by considering the exhaust trail as a line thermal deposited instantaneously. Initially the thermal is assumed to have a finite, circular cross section and a finite amount of buoyancy per unit length, represented by the temperature difference above ambient. At time zero the thermal is allowed to rise freely in an environment of arbitrary stratification. The theoretical approach of Ref. 2-17 for instantaneous point sources was followed with the proper reformulation for the case of a line source. The basic assumptions are that the rate of turbulent entrainment is proportional to the speed of rise through an entrainment coefficient α, and that an incompressible formulation can be used for the atmosphere provided potential rather than physical density is used throughout.

The differential equations expressing conservation of volume, mass, and momentum

$$\frac{dr^2}{dt} = 2 r \alpha u \tag{2.11}$$

$$\frac{d}{dt}(\rho r^2) = 2 r \rho_a \alpha u \tag{2.12}$$

$$\frac{d}{dt}(r^2 \rho u) = g r^2 (\rho_a - \rho) \tag{2.13}$$

where r is the radius, ρ the potential wake density, and ρ_a the potential ambient density, an arbitrary function of altitude. This system can be solved in closed form in terms of quadratures containing the arbitrary ambient density. For present

purposes it was simpler to calculate numerical solutions to the differential equations with a high-speed computer. The entrainment coefficient suggested by Ref. 2-17 ($\alpha \approx 0.3$) was used, and the buoyant rise was calculated from time zero to the height of first velocity reversal. The initial temperature difference was given as an input parameter. Estimates of this difference were made (conservatively) by assigning the entire jet engine energy to the temperature rise in a cylindrical wake having uniform temperature and the same cross section as the observed wake. In an effort to account for all sources of heat, the average temperature rise due to subsidence was also calculated and added to the previous one. The results are shown in Figure 2-22 in the form of growth histories. It can be seen that for the B-52 wake the temperature increase due to the exhaust alone is 0.2°C, and including average subsidence it is 0.5°C. The maximum is about 1°C. For the case of an SST flying at 20 km in a standard stratosphere, the temperature difference is larger (due to the high-power output, particularly with afterburner) but the wake is smaller and the ambient more stable, resulting in total growth comparable to that of the B-52.

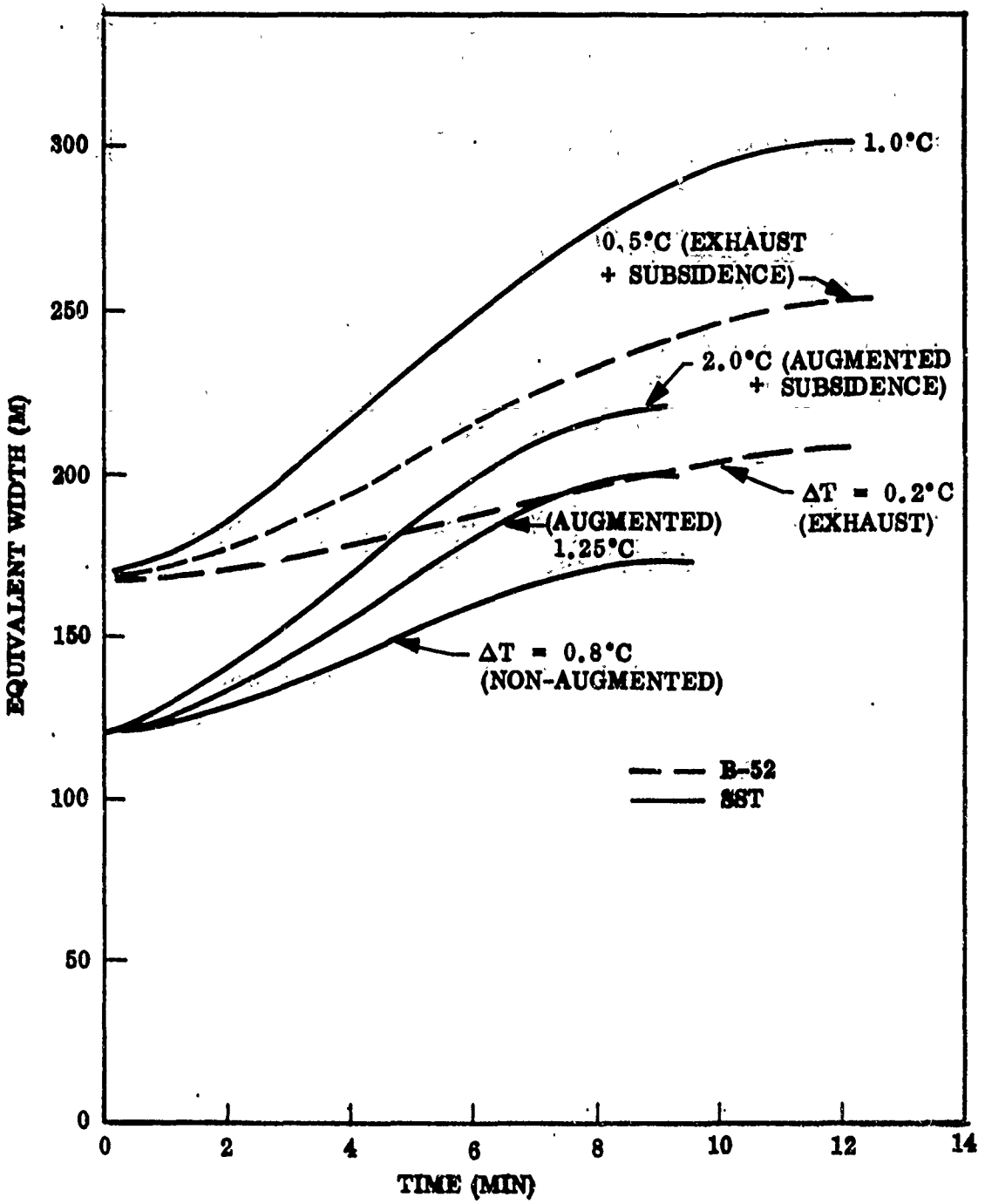

Figure 2-22 Growth Due to Buoyant Rise of Air Parcels Equivalent to B-52 and SST Exhaust Trails

2.3 REFERENCES FOR SECTION 2

2-1 T. B. Smith and K. M. Beesmer, Contrail Studies for Jet Aircraft, AFCRC TR-59-251, 1969

2-2 S. C. Crow, "Stability Theory for a Pair of Trailing Vortices," AIAA J., Vol. 8, p. 2172

2-3 Aircraft Wake Turbulence and Its Detection, ed., J. Olsen and A. Goldburg, Plenum Press, 1971

2-4 R. J. Procan, Development of a Method of Characteristics Solution for Supersonic Flow of an Ideal, Frozen, or Equilibrium Reacting Gas Mixture, LMSC/HREC A782535-A, Lockheed Missiles & Space Co., Huntsville

2-5 H. H. Korst et al., Compressible Two-Dimensional Jet Mixing at Constant Pressure, ME-TN-392-1, University of Illinois

2-6 Abramovich, The Theory of Turbulent Jets, MIT Press, 1963

2-7 J. R. Spreiter and A. H. Sacks, "The Rolling Up of the Trailing Vortex Sheet and Its Effect on the Downwash Behind Wings," J. Aero. Sci., Vol. 21

2-8 W. Forstall and A. Shapiro, Appl. Mech., Vol. 17, p. 399, 1950

2-9 H. Lamb, Hydrodynamics, Dover, 1945

2-10 T. B. Smith and R. J. Diamond, Study of Contrails From Jet Powered Aircraft, Final Report, Contract No. AF 19(604)-1495

2-11 E. R. Reiter, Jet Stream Meteorology, University of Chicago Press

2-12 J. J. Walton, Scale Dependent Diffusion, UCRL-74134, Lawrence Livermore Laboratory, 25 Aug 1972

2-13 A. H. Schooley and R. W. Stewart, "Experiments With a Self-Propelled Body Submerged in a Fluid With a Vertical Density Gradient," J. Fluid Mech., Vol. 15, p. 83

2-14 Wu, J., "Mixed Region Collapse With Internal Wave Generation in a Density-Stratified Medium, "J. Fluid Mech., Vol. 35, p. 531

2-15 Y. H. Pao, Private Communication

2-16 T. J. Overcamp and J. A. Fay, "Dispersion of SST Trails in the Stratosphere," AIAA Paper, 72-650, 1972

2-17 B. R. Morton, G. I. Taylor, and J. S. Turner, "Turbulent Gravitational Convection From Maintained and Instantaneous Sources," Proceed. Roy. Soc., Series A, Vol. 234, p. 1, 1956

Section 3
CHEMICAL KINETICS MODEL

3.1 SUMMARY

The present investigation is directed at the nature and extent of chemical reactions in the exhaust jets and wakes of high-altitude aircraft. The object is to determine what reactions might have an important effect on the composition of hot gases as they issue from the engine into the surrounding stratosphere. Experimentally measured exhaust compositions at the exit plane of an engine will not reflect accurately the final chemical composition of the exhaust in the stratosphere if reactions in the wake are important.

The objective of Task I, Problem Definition, is to identify essential features or considerations needed for subsequent development of a wake flow and chemistry model in order to define species concentrations and wake configurations at a time in the wake history when aircraft-induced motions have diminished and are dominated by the natural stratospheric motions. The technical approach for the wake-chemistry portion of Task I has been to screen the many possible chemical reactions to determine their probable importance in the engine exhaust jet, the near wake, and the far wake – i.e., to as late as 20 min after passage of the aircraft. To examine the reactions in the exhaust jet, however, it has been necessary for the calculations to cover areas even farther upstream – i.e., within the engine nozzle. This has been necessary to examine the rate histories for many of the species before they reach the nozzle exit so that their concentrations at the exit plane can be established. Many atoms and radicals are found to be present, and it cannot be reasonably anticipated that experimental test data on representative turbojet engines will be capable of quantitatively identifying all of the important species. Thus, the engine nozzle kinetics work is a necessary part of the chemical reaction screening process. In this approach, simplifying relationships have been sought, such as steady state and partial equilibrium relationships among

minor species, to discover when such relationships can be used for making reliable predictions. The reliability of the simplifying methods is ascertained by comparison of the results with fully coupled computer solutions of the reacting flow problem.

The emphasis in final development of the chemistry model will be influenced by the interface with and requirements of the chemical modeling program for the post-wake dispersion regime. It is anticipated that the NO_x concentrations and total NO_x will be first on the list of priorities. It is anticipated that any significant conversion of NO_x in the wake to HNO_3 will be of major interest. Formation of sulfate aerosol in the wake and diffusion and transport regime will also be of interest. It seems likely that the diffusion and transport regime and subsequent climatic analyses will be less sensitive to uncertainties in wake CO and hydrocarbon levels than to NO_x concentration. In light of this, a simplified wake-chemistry model may serve nicely. If, on the other hand, detailed information on minor wake species, exhaust generated radicals, etc., is required, a much more general and comprehensive wake kinetics model will be needed.

The scope of the chemical screening process is broad; i.e., thermochemical reactions, photochemistry, and particulate generating reactions are all considered. Because oxides of nitrogen are thought to play a particularly important role in the stratosphere, their reactions are given special attention, and analysis of the photochemical catalytic NO_x and ozone history following passage of an aircraft through the stratosphere is carried out to times well beyond the 20-min "end to wake" time.

For studies of thermal reactions in the engine exhaust regime, the analytical approach involves setting up a chemical kinetics model using those elementary reactions that play a role in changing the concentrations of engine emissions in the exhaust nozzle and the near jet downstream from the engine exit plane. Numerical methods are used to integrate the resulting governing chemical rate equations up to the point where the exhaust flow mixes with the ambient atmosphere. Initial conditions for the computations are compatible with available data on engine exhaust composition.

In particular, reactions affecting the oxidation of CO to CO_2, NO to NO_2, and SO_2 to SO_3, as well as conversion of NO_2 to HNO_3, are of interest. A model consisting of elementary forward and backward reactions pertinent to these exhaust chemical systems has been used in this study. Reaction rate constants are taken from recent evaluations available in the literature. The fluid-dynamic structure of the exhaust jet region was obtained from analytical predictions and experimental data available from the literature.

The major conclusions reached in the investigation are as follows:

- In an afterburning engine, with relatively low HC emissions, nonequilibrium effects are an important aspect of the chemistry in the engine exhaust expansion nozzle and exhaust jet regime. There is substantial oxidation of CO to CO_2 in the nozzle and jet, and the concomitant production of H atoms maintains the concentrations of H, O, and OH well above their equilibrium values. The partial equilibrium of some bimolecular reactions are the basis for useful relationships among the concentrations of H, O, OH, and H_2. However, these radicals cannot be related to major species because recombination reactions are far out of equilibrium.

- Hydrocarbons have a profound scavenging effect on exhaust inorganic radicals. Introduction of HC in quantities of the same order as CO reduce the H, OH, and O concentrations by many orders of magnitude.

- Oxidation of NO to NO_2 is not significant in the exhaust jet. If unburned hydrocarbons are not present, the NO_2/NO ratio is maintained well below its equilibrium value by fast reactions such as

$$NO_2 + H \rightarrow NO + OH$$

$$NO_2 + O \rightarrow NO + O_2$$

  With HC present and inorganic radicals consequently few, the effect is to freeze the NO_2 in the nozzle near its throat value.

- In the jet mixing region both reactions

$$NO + O + M \rightarrow NO_2 + M$$

$$NO_2 + OH \rightarrow HNO_3$$

are slow relative to OH recombination via

$$OH + OH + M \rightarrow H_2O_2 + M$$

Consequently, there is no regime of sufficient duration in which OH and NO_2 are simultaneously plentiful, and stable nitric acid is not formed in significant quantities.

- Oxidation of SO_2 to SO_3 in the hot exhaust jet is forestalled by H and O atom attack on SO_3 in a manner similar to the NO-NO_2 system.
- In the jet mixing region and the near wake, the possibility of aerosol formation by the following reaction pair can be ruled out:

$$SO_2 + O + M \rightarrow SO_3 + M$$

$$SO_3 + H_2O \rightarrow H_2SO_4$$

Other reactions that might lead to particulate formation appear to be too slow to contribute significantly in the wake regime.

- In ground tests the exhaust gases are maintained at substantially higher temperatures for longer residence than at high altitude. As observed, the chemical kinetics model predicts the occurrence of significantly more CO oxidation in the exhaust jet for an engine under static test conditions at sea level, than it predicts for stratospheric flight.
- The subject of chemical kinetics in turbulent flows is considered. To a large extent, chemistry is found to be "diffusion limited" in the exhaust jet core and "reaction rate limited" in the wake. The simple, "well-mixed" kinetics model, which ignores diffusion and turbulence in the exhaust jet, appears to agree reasonably well with ground-test data on CO profiles. This may mean that the net influence of turbulence on the chemistry is small.
- Addition of unburned exhaust hydrocarbons to the stratosphere does not appear to be significant. Catalytic chain effects of hydrocarbons on ozone/NO_x cycles degrade the hydrocarbons and are unimportant. Removal of NO_x by

hydrocarbons in the stratosphere is an important area for study, but the contribution from engine exhaust hydrocarbons is dwarfed by the ambient methane.

- The release of chemical enthalpy due to reaction of exhaust species is too small to have an important effect on the fluid mechanics. Thus, the chemistry may be uncoupled energetically from the flow field calculations.
- The species of primary interest in evaluating possible climatic effects of high-altitude aircraft – NO_x - is not removed or depleted by gas-phase chemical reactions in the aircraft wake regime.

3.2 CARBON MONOXIDE OXIDATION – EQUILIBRIUM OH TREATMENT

3.2.1 Major Oxidation Reaction

A two-reaction zone model is generally accepted as the most useful for kinetic interpretation (Ref. 3-1). The gas turbine combustor exhibits a two-reaction zone behavior wherein CO is formed in the regions near the fuel nozzle and further oxidation to CO_2 takes place downstream of this point. The degree of conversion to CO_2 is strongly dependent upon equivalence ratio.

The accepted rate controlling step in CO oxidation in hydrocarbon systems is the reaction (Refs. 3-1 and 3-2):

$$CO + OH \overset{k_1}{\rightleftharpoons} CO_2 + H \qquad (3.1)$$

The reactions $CO + O \rightarrow CO_2$ and $CO + O_2 \rightarrow CO_2 + O$ are much too slow (Ref. 3-1).

3.2.2 Kinetic Details

In general, it is necessary to consider the reaction mechanism including all reactions affecting OH and H to arrive at the proper OH concentration. This reaction scheme (Ref. 3-3) is as follows:

$$CO + OH \rightleftharpoons CO_2 + H$$

$$H + O_2 \rightleftharpoons OH + O$$

$$OH + OH \rightleftharpoons H_2O + O$$

$$O + H_2 \rightleftharpoons H + OH$$

$$H_2 + OH \rightleftharpoons H_2O + H$$

$$H_2 + M \rightleftharpoons H + H + M$$

$$O_2 + M \rightleftharpoons O + O + M$$

$$H + OH \rightleftharpoons H_2O + M$$

3.2.3 Overall Kinetics

In those situations in which one slow reaction determines the overall reaction rate, the overall or global rate approach is often quite useful, and can circumvent the rigors of integrating a complete reaction scheme (Ref. 3-1). The oxidation of CO controlled by Eq. (3.1) provides just such a situation, and many authors have given overall expressions for CO oxidation. These various expressions are reviewed by Singh and Sawyer (Ref. 3-2) and will not be discussed here.

The major problem with empirically determined overall rate equations is that they may only be valid for the particular conditions under which they were measured. One approach to overall CO oxidation is to consider partial equilibration of some of the reactions above.

In post-combustion zone mixtures of hot gases with excess O_2 and H_2O, the assumption of OH equilibrium is quite good (Ref. 3-1). Gas-turbine exhaust streams typically meet these conditions, and the time involved in passing from the combustor to the exit will allow OH equilibration. Using the equilibrium relations

$$O + H_2O = OH + OH \ , \ K_{P_1} = \frac{(P_{OH})^2}{(P_O)(P_{H_2O})} \tag{3.2}$$

$$O + O = O_2 \ , \ K_{P_2} = \frac{P_{O_2}}{(P_O)^2} \tag{3.3}$$

the OH concentration may be written as

$$[OH] = \frac{K_{P_1}^{1/2} [H_2O]^{1/2} [O_2]^{1/4}}{K_{P_2}^{1/4} (RT)^{1/4}} \tag{3.4}$$

[The $(RT)^{1/4}$ factor results from the use of equilibrium constants in terms of pressure.]

The equilibrium constants K_{P_1} and K_{P_2} are, of course, well known from thermochemical tables and can be fitted to an equation of the form

$$K_P = AT^{\alpha} e^{-E/RT}$$

The latest recommended value for k_1 in Eq. (3.1) is (Ref. 3-4)

$$k_1 = 4.2 \times 10^{11} e^{-1080/RT} \text{ cm}^3\text{-mole}^{-1}\text{-sec}^{-1}$$

Using the foregoing k_1 expression, the fitted forms for K_p in Eq. (3.4), combining with Eq. (3.5) for the disappearance of CO according to Eq. (3.1), and eliminating a weak $T^{-0.218}$ dependence through its evaluation at T = 1500°K, in the range of interest, one obtains Eq. (3.6).

$$\frac{d[CO]}{dt} = -k_1 [CO] [OH] \tag{3.5}$$

$$\frac{d[CO]}{dt} = -10^{12.6} e^{-39800/RT} [CO] [H_2O]^{1/2} [O_2]^{1/4} \tag{3.6}$$

The H_2O and O_2 concentrations are given by their equilibrium values. The example of CO oxidation for given profiles follows.

To compute the relative change in the CO mole fraction when jet engine exhaust gases expand over specified temperature and pressure profiles, one may recast Eq. (3.6) and integrate stepwise according to Eq. (3.7):

$$-\ln \frac{X_{CO}}{(X_{CO})_o} = \frac{10^{12.6}}{\bar{M}^{0.75}} \int_o^{\Delta t} e^{-39800/RT} \rho^{0.75} X_{H_2O}^{0.25} X_{O_2}^{0.25} dt \qquad (3.7)$$

where

X = mole fraction

ρ = gas density

$\bar{M}$ = average molecular weight (assumed constant)

Δt = time step taken during integration

$( )_o$ = initial value

Additional simplification usually results because the mole fractions of H_2O and O_2 are frequently almost constant in the nozzle, and these terms have small exponents in Eq. (3.7).

For the GE-4 engine at maximum power, Eq. (3.7) has been integrated numerically for temperature, pressure, time, and distance relationships obtained from fluid mechanics analysis. These relationships appear in Figure 3-1. Equilibrium fractions of H_2O and O_2 at the secondary nozzle throat were computed for the overall equivalence ratios given by the following engine manufacturer's data for the corresponding power setting;

Condition	Altitude (ft)	Mach Number	Power Setting
Maximum Power	65,000	2.7	1

The results appear in Figure 3-3. Clearly, the centerline CO mole fraction stops decreasing almost immediately after the nozzle expansion begins. Examination of the strong temperature dependence of the CO reaction rate in Eq. (3.7) shows why this result is obtained, in view of the temperature histories shown in Fig. 3-1. As will be seen, however, this very severe freezing of CO is not, in fact, obtained. Thus.

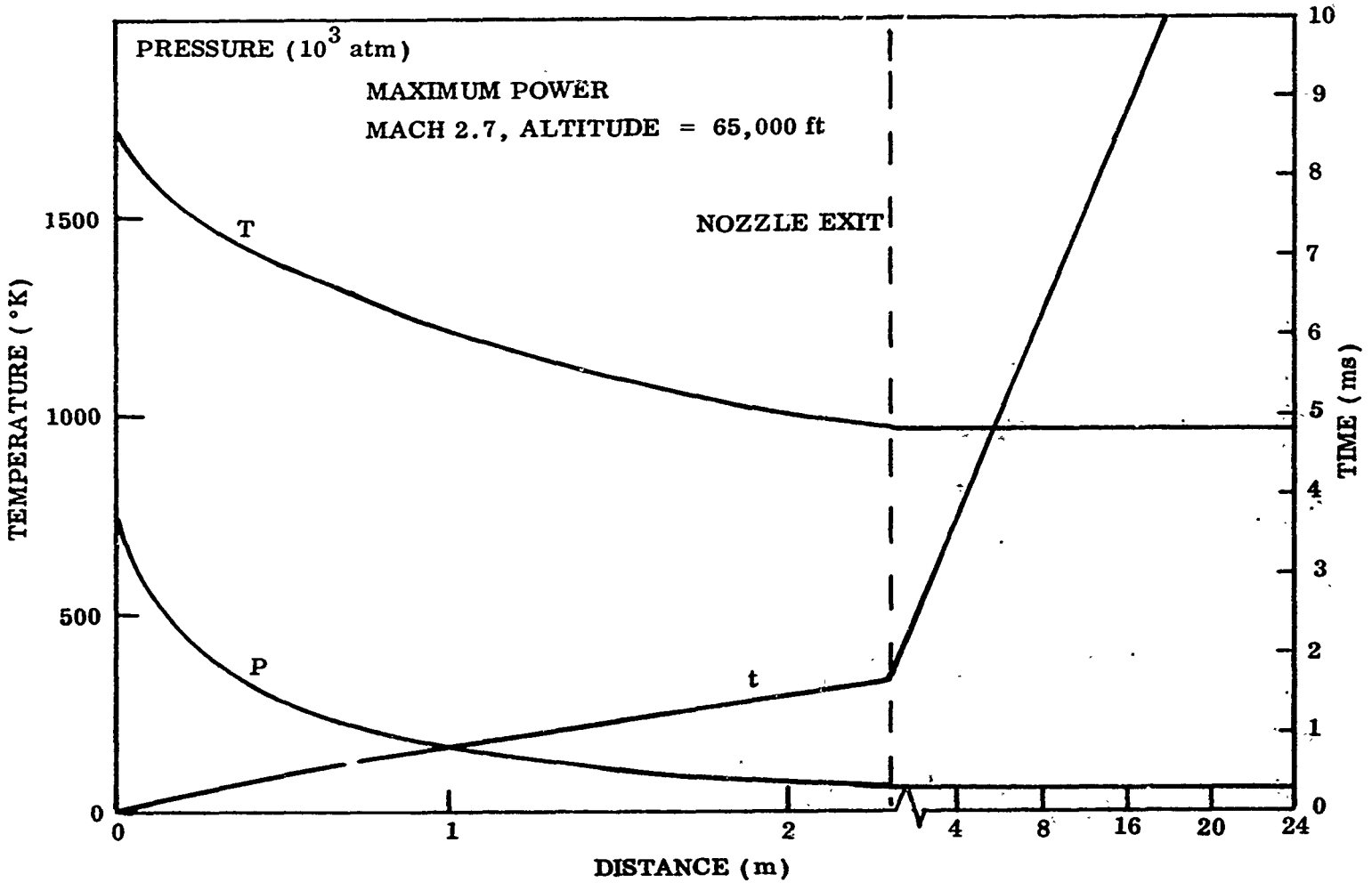

Figure 3-1 GE-4 Secondary Nozzle Flow Properties

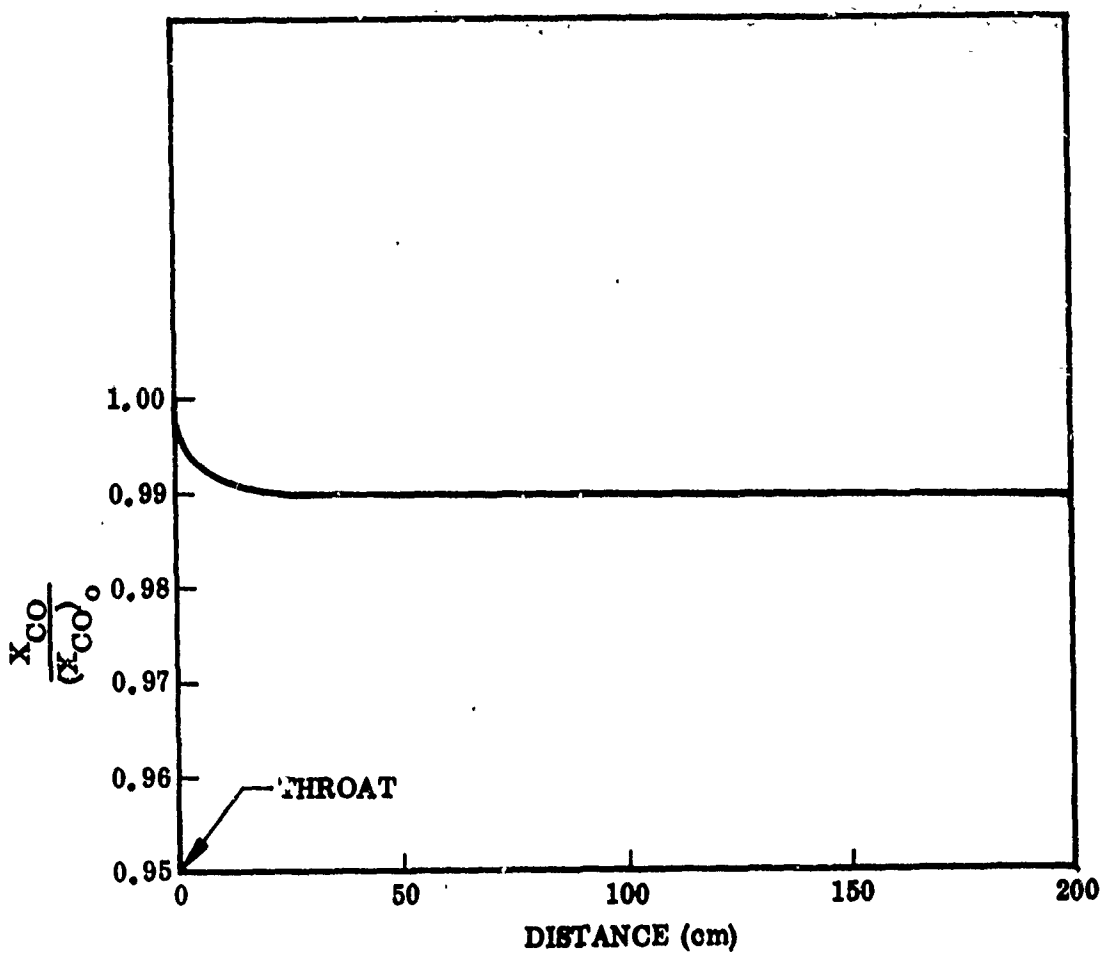

Figure 3-2 CO Concentration Ratio Profile for GE-4 at Maximum Power

this equilibrium OH assumption is not justified for the engine exhaust analysis, in light of results from detailed chemical kinetics numerical analysis. Actually, the OH is maintained far in excess of its equilibrium concentration by a chain sequence initiated by H atoms generated in CO oxidation by the reaction shown in Eq. (3.1).

3.3 NITRIC OXIDE

3.3.1 General

Nitric oxide emissions from gas turbine combustors are, in general, much less than those predicted by thermochemical equilibrium considerations. Experimental measurements (Ref. 3-5) and theoretical kinetic models (Ref. 3-6) have established that the NO is formed in the high-temperature post-flame gases in the primary zone of the combustor. The residence time in this zone is not long enough for the NO to reach its equilibrium concentration, and rapid quenching in the secondary zone freezes the NO concentration at its subequilibrium level (Ref. 3-6). Both Heywood et al. (Ref. 3-7) and Caretto et al. (Ref. 3-8) have pointed out that the NO should not decompose when its concentration is less than the local equilibrium value.

In a gas turbine engine with an afterburner, there is the possibility of additional NO formation in the afterburning region. However, it is expected that the short residence times and lower temperatures in this region, as compared with the primary zone, will prevent significant NO formation in the afterburner.

3.3.2 Kinetics

The accepted mechanism for NO formation in a high-temperature combustion system is (Refs. 3-7 and 3-8):

$$N + NO \rightleftarrows N_2 + O \tag{3.8}$$

$$N + O_2 \rightleftarrows NO + O \tag{3.9}$$

$$N + OH \rightleftarrows NO + H \tag{3.10}$$

$$H + N_2O \rightleftarrows N_2 + OH \tag{3.11}$$

$$O + N_2O \rightleftarrows N_2 + O_2 \tag{3.12}$$

$$O + N_2O \rightleftarrows 2\,NO \tag{3.13}$$

The first two reactions represent the well known Zeldovich (Ref. 3-9) mechanism and are generally sufficient to account for NO production in high-temperature combustion systems. The last three reactions can be important at lower temperatures in lean mixtures. The $[N_2]$, $[O]$, $[O_2]$, $[OH]$, and $[H]$ are given by their equilibrium values, and if $[N]$ and $[N_2O]$ are given by their steady-state values, then the mole fraction of NO can be shown to be given by (Ref. 3-6)

$$\frac{dX_{NO}}{dt} = \frac{2\bar{M}}{\rho}(1 - \alpha^2)\left(\frac{R_1}{1 + \alpha\underline{K}_1} + \frac{R_6}{1 + \underline{K}_2}\right)$$

Here, $\alpha = [NO]/[NO]_{equil.}$, R_i = "one-way" equilibrium rate of ith reaction ($R_1 = K_1[N]_e[NO]_e$), $\underline{K}_1 = R_1/(R_2 + R_3)$, and $\underline{K}_2 = R_6/(R_4 + R_5)$. When $dX_{NO}/dt\big|_o$ is evaluated for initial conditions in the GE-13 jet expansion case previously given,

$$\left.\frac{dX_{NO}}{dt}\right|_o = 0.113 \times 10^{-5}/\text{sec} \qquad (\alpha << 1)$$

Thus, for the time scale of the jet expansion, there will be no change in NO mole fraction due to the reaction scheme (3.8) to (3.13).

3.3.3 Other Reactions

The question arises as to the possibility of decomposition of NO in the outer cooler portion of the jet where $[NO]$ exceeds its equilibrium value.

Laurendeau and Sawyer (Ref. 3-10) have considered NO decomposition due to the reaction scheme:

$$NO + N \rightarrow O + N_2 \qquad (3.14)$$

$$NO + O \rightarrow N + O_2 \qquad (3.15)$$

$$NO_2 + M \rightleftarrows NO + O + M \qquad (3.16)$$

$$NO + O_2 \rightleftarrows O + NO_2 \qquad (3.17)$$

$$NO + NO \rightarrow N_2O + O \qquad (3.18)$$

$$N_2O + M \rightarrow N_2 + O + M \qquad (3.19)$$

Starting with an initial mixture of 10% NO and 90% inert, they computed the NO decomposition at 1700°K and 0.7 atm. Their results show that the time scale for the beginning of significant NO decomposition is on the order of 10 sec under these conditions. NO_2 levels resulting from this reaction scheme are 3 to 4 orders of magnitude less than the NO levels. Thus, in the GE-13 exhaust jet considered previously, for example, where $X_{NO} << 0.1$ and $T < 1700°K$, the decomposition of NO due to reaction (3.14) to (3.19) will be insignificant.

Possible reactions involved in converting NO to NO_2 in the outer jet are:

$$NO + O + M \rightarrow NO_2 + M \qquad (3.20)$$

$$NO + O \rightarrow NO_2 + h\nu \qquad (3.21)$$

$$NO + NO + O_2 \rightarrow NO_2 + NO_2 \qquad (3.22)$$

$$NO_2 + NO_2 \rightarrow NO + NO + O_2 \qquad (3.23)$$

$$NO + NO \rightarrow NO_2 + N \qquad (3.24)$$

A discussion of these reactions and their respective rate constants is given in Refs. 3-11 and 3-12. Reaction Eq. (3.23) is insignificant at temperatures less than 5000°K and can be eliminated immediately. The rate constants for reactions (3.20) to (3.23) are:

$$k_{3.20} = 1.05 \times 10^{15} \exp\left(\frac{1870}{RT}\right) \text{cm}^6\text{-mile}^{-2}\text{-sec}^{-1}$$

$$k_{3.21} = 3.9 \times 10^{7} \left(\frac{T}{296}\right)^{-1.94} \text{cm}^3\text{-mole}^{-1}\text{-sec}^{-1}$$

$$k_{3.22} = 2.4 \times 10^{9}\, e^{+1046/RT} \text{cm}^6\text{-mole}^{-2}\text{-sec}^{-1}$$

$$k_{3.23} = 4 \times 10^{12}\, e^{-26900/RT} \text{cm}^3\text{-mole}^{-1}\text{-sec}^{-1}$$

Considering the low temperatures and very small equilibrium O atom concentrations in the outer jet region, reaction (3.22) will dominate NO_2 formation in this region. The NO decomposition rate under this scheme is thus given by

$$-\frac{d[NO]}{dt} = (4.8 \times 10^{9}\, e^{1046/RT})\, [NO]^2 [O_2]$$

or in terms of mole fractions

$$-\frac{dX_{NO}}{dt} = (4.8 \times 10^{9}\, e^{1046/RT})\, \frac{(\rho)^2}{M}\, X_{NO}^2 X_{O_2}$$

Taking the last data point in the GE-13 jet expansion as typical outer jet conditions gives:

$$\rho = 0.37 \times 10^{-4} \text{ g/cm}^3$$

$$T = 950°K$$

$$-\frac{dX_{NO}}{dt} = 1.4 \times 10^{-2}\, X_{NO}^2 X_{O_2}$$

Considering that typical magnitudes for the mole fractions are

$$X_{NO} < 0.001$$

$$X_{O_2} < 0.2$$

dX_{NO}/dt will be of order 10^{-9}/SEC. Thus, there will be no significant change in NO mole fraction in the jet due to formation of NO_2.

The overall conclusion is that based on the equilibrium assumption, the mole fraction of NO remains constant in the exhaust jet. A complete analysis presented in the following sections demonstrates that equilibrium is not attained and thus invalidates this analysis.

3.4 CARBON MONOXIDE OXIDATION AND NO_x KINETICS – COMPLETE KINETIC TREATMENT

3.4.1 Rationale

The equilibrium analysis utilized in section 3.2 is questionable in the light of observed high OH concentrations in jet engine exhausts (Ref. 3-13). Therefore, to further investigate changes in CO and NO_x concentrations in the wake region of high-altitude aircraft, simplified treatments had to be abandoned. It was necessary to set up a chemical kinetics model including all elementary reactions which might conceivably contribute to the alteration of emission levels.

3.4.2 Reaction System

- CO oxidation to CO_2 has only one important elementary reaction (Refs. 3-1, 3-2, 3-3:

$$CO + OH \rightleftharpoons CO_2 + H$$

- This necessitates inclusion of all reaction controlling OH and H levels:

$$\left.\begin{aligned} H + O_2 &\rightleftharpoons OH + O \\ OH + OH &\rightleftharpoons H_2O + O \\ O + H_2 &\rightleftharpoons H + OH \\ H_2 + OH &\rightleftharpoons H_2O + H \end{aligned}\right\} \text{fast bimolecular radical shuffle reactions}$$

$$\left.\begin{aligned} H + H + M &\rightleftharpoons H_2 + M \\ O + O + M &\rightleftharpoons O_2 + M \\ H + OH + M &\rightleftharpoons H_2O + M \end{aligned}\right\} \text{3 body association reactions}$$

- Reactions involving HO_2 also affect the pool of radical species:

$$H + O_2 + M \rightleftharpoons HO_2 + M$$

$$H + HO_2 \rightleftharpoons OH + OH$$

$$OH + HO_2 \rightleftharpoons H_2O + O_2$$

$$O + HO_2 \rightleftharpoons OH + O_2$$

$$H + HO_2 \rightleftharpoons H_2 + O_2$$

$$H + HO_2 \rightleftharpoons H_2O + O$$

- H_2O_2 Reactions:

$$OH + OH + M \rightleftharpoons H_2O_2 + M$$

$$HO_2 + HO_2 \rightleftharpoons H_2O_2 + O_2$$

$$H_2O_2 + OH \rightleftharpoons H_2O + HO_2$$

$$H + H_2O_2 \rightleftharpoons H_2 + HO_2$$

- Nitric acid reactions:

$$NO_2 + OH \rightleftharpoons HNO_3$$

- Sulfur reactions:

$$SO_2 + O + M \rightleftharpoons SO_2 + M$$

$$H + SO_3 \rightleftharpoons SO_2 + OH$$

$$O + SO_3 \rightleftharpoons SO_2 + O_2$$

- Principal reactions exchanging NO and NO_2:

$$NO + O + M \rightleftharpoons NO_2 + M$$
$$H + NO_2 \rightleftharpoons NO + OH$$
$$O + NO_2 \rightleftharpoons NO + O_2$$
$$NO + HO_2 \rightleftharpoons NO_2 + OH$$

- Other reactions involving NO, NO_2, N_2, and N_2O:

$$O + N_2 \rightleftharpoons NO + N$$
$$N + O_2 \rightleftharpoons NO + O$$

} Zellovitch NO formation, important at high temperature only

$$NO + NO \rightleftharpoons N_2O + O$$
$$H + N_2O \rightleftharpoons N_2 + OH$$
$$O + N_2O \rightleftharpoons N_2 + O_2$$
$$N_2 + NO_2 \rightleftharpoons NO + N_2O$$
$$N_2O + M \rightleftharpoons N_2 + O$$
$$N_2 + NO_2 \rightleftharpoons NO + N_2O$$

- Ozone reactions:

$$O + O_2 + M \rightleftharpoons O_3 + M$$
$$O + O_3 \rightleftharpoons O_2 + O_2$$
$$H + O_3 \rightleftharpoons OH + O_2$$
$$NO + O_3 \rightleftharpoons NO_2 + O_2$$

- Methane Oxidation:

$$CH_4 + H \rightleftharpoons CH_3 + H_2$$
$$CH_4 + OH \rightleftharpoons CH_3 + H_2O$$
$$CH_4 + O \rightleftharpoons CH_3 + OH$$
$$CH_4 + O_2 \rightleftharpoons CH_3 + HO_2$$
$$CH_3 + O \rightleftharpoons CH_2O + H$$
$$CH_3 + O_2 \rightleftharpoons CH_2O + OH$$
$$CH_2O + H \rightleftharpoons HCO + H_2$$
$$CH_2O + OH \rightleftharpoons HCO + H_2O$$
$$CH_2O + O \rightleftharpoons HCO + OH$$
$$HCO + O \rightleftharpoons CO + OH$$
$$HCO + OH \rightleftharpoons CO + H_2O$$
$$HCO + H \rightleftharpoons CO + H_2$$

The above 76 reactions (forward and reverse), excluding the methane oxidation reactions, can be taken to describe the fuel-lean chemistry in the engine exhaust nozzle and plume up to the point where mixing between the exhaust plume and the surrounding atmosphere becomes important. A necessary condition for their sufficiency is that the hydrocarbon emissions be very low so that carbon monoxide oxidation is dominant. For local conditions where this is not the case, the above well-known methane oxidation scheme is convenient to represent HC oxidation. Since the number of possible species and reactions is exceedingly large, the assembly of a complete mechanism with rate constants to represent higher HC (e.g., C_8H_{18}) oxidation is probably not possible at this time.

The reactions and their respective rates are summarized in Table 3-1. Reverse reaction-rate constants are calculated from equilibrium constants. References given in the table refer to the special reference list given in section 3.7.

Table 3-1

CHEMICAL REACTIONS IN THE $CO_x/NO_x/SO_x/CH_4$/AIR SYSTEM

Reaction Number	Reaction	Reaction Rate Variables[a]			Ref (b)
		A	n	F	
1	$H + N_2O = N_2 + OH$	3.01×10^{13}	0	10,800	19
2	$N + OH = NO + H$	4.21×10^{13}	0	0	19
3	$O + N_2O = N_2 + O_2$	3.61×10^{13}	0	24,000	13
4	$N_2 + NO_2 = NO + N_2O$	1.41×10^{14}	0	83,000	13
5	$H + NO_2 = NO + OH$	7.25×10^{14}	0	1,930	6
6	$HO_2 + NO = OH + NO_2$	6.00×10^{11}	0	0	18
7	$O + N_2 = NO + N$	1.44×10^{14}	0	75,580	13
8	$NO + O = N + O_2$	4.10×10^{9}	0	38,340	13
9	$NO + O + M = NO_2 + M$	1.05×10^{15}	0	-1,870	3
10	$NO_2 + O = NO + O_2$	1.0×10^{13}	0	600	3
11	$NO + NO = N_2O + O$	7.05×10^{11}	0	65,000	13
12	$M + N_2O = N_2 + O + M$	6.30×10^{14}	0	56,800	13
13	$CO + OH = CO_2 + H$	4.20×10^{11}	0	1,080	1
14	$H + O_2 = OH + O$	2.20×10^{14}	0	16,800	7
15	$OH + OH = H_2O + O$	6.30×10^{12}	0	1,100	7
16	$O + H_2 = H + OH$	1.80×10^{10}	1	8,900	7
17	$H_2 + OH = H_2O + H$	2.20×10^{13}	0	5,150	7
18	$M + H_2 = H + H + M$	2.20×10^{14}	0	96,000	7
19	$M + H + OH = H_2O + M$	1.40×10^{23}	-2	0	7
20	$M + O_2 = O + O + M$	2.50×10^{18}	-1	118,500	6
21	$M + H + O_2 = HO_2 + M$	1.50×10^{15}	0	-1,000	7
22	$H + HO_2 = OH + OH$	2.50×10^{14}	0	1,900	7
23	$OH + HO_2 = H_2O + O_2$	1.00×10^{13}	0	1,000	7
24	$O + HO_2 = OH + O_2$	5.00×10^{13}	0	1,000	7
25	$H + HO_2 = H_2 + O_2$	2.50×10^{13}	0	700	7

(a) Reaction rate constant $k = A T^n \exp(E/RT)$. Units are moles, cm, sec, °K, cal.

(b) References in this table appear as a special reference list in Section 3.7.

Table 3-1 (Cont)

Reaction Number	Reaction	Reaction Rate Variables			Ref
		A	n	E	
26	$H + HO_2 = H_2O + O$	1.00×10^{13}	0	1,000	7
27	$NO_2 + OH = HNO_3$	2.90×10^{12}	0	0	8
28	$H_2O_2 + OH = H_2O + HO_2$	1.00×10^{13}	0	1,800	7
29	$OH + OH + M = H_2O_2 + M$	7.1×10^{14}	0	-5,100	7
30	$HO_2 + HO2 = H_2O2 + O_2$	6.5×10^{13}	0	0	7
31	$SO_2 + O + M = SO_3 + M$	4.5×10^{14}	0	0	12
32	$SO_3 + H = SO_2 + OH$	6.5×10^{14}	0	10,800	12
33	$SO_3 + O = SO_2 + O_2$	6.5×10^{14}	0	10,800	12
34	$CH_4 + H = CH_3 + H_2$	5.1×10^{13}	0	12,900	9
35	$CH_4 + OH = CH_3 + H_2O$	7.9×10^{13}	0	5,800	9
36	$CH_4 + O = CH_3 + OH$	2.0×10^{13}	0	9,200	15
37	$CH_4 + O_2 = CH_3 + HO_2$	1.0×10^{13}	0	63,000	15
38	$CH_3 + O = CH_2O + H$	1.9×10^{13}	0	0	10
39	$CH_3 + O_2 = CH_2O + OH$	7.5×10^{10}	0	0	10
40	$CH_2O + H = HCO + H_2$	1.0×10^{13}	0	2,000	10
41	$CH_2O + OH = HCO + H_2O$	7.0×10^{10}	0.7	1,000	15
42	$CH_2O + O = HCO + OH$	4.0×10^{11}	0.6	4,000	10
43	$HCO + O = CO + OH$	1.8×10^{11}	0.5	0	10
44	$HCO + OH = CO + H_2O$	1.1×10^{11}	0.5	0	10
45	$HCO + H = CO + H_2$	1.5×10^{12}	0.5	0	10
46	$O + O_2 + M = O_3 + M$	7.2×10^{12}	0	-1,050	17
47	$O + O_3 = O_2 + O_2$	1.2×10^{13}	0	4,800	17
48	$H + O_3 = OH + O_2$	1.6×10^{13}	0	0	6
49	$NO + O_3 = NC_2 + O_2$	6.7×10^{11}	0	2,450	6
50	$H + H_2O_2 = H_2 + HO_2$	1.7×10^{12}	0	3,800	7

It turns out that many of these reactions are not important in the nozzle and wake regimes. A condensed list of essential reactions is given in a later section.

3.4.3 Analysis

The analysis of the effect of the chemical reactions in the engine exhaust nozzle and exhaust plume was carried out using the NASA Lewis general kinetics program (Ref3-14)and other Lockheed programs. The NASA program is capable of treating reacting flows with the fluid mechanical equations coupled to the chemical rate equations.

The GE-4 engine operating at maximum power at 65,000-ft altitude and flight Mach number 2.7 was taken as the most conservative case for evaluating exhaust reactions. This operating condition gives the highest engine temperatures and hence the greatest possibility of significant chemical reaction in the wake.

- The engine exhaust nozzle conditions as determined from engine manufacturer's data are as follows:
  - Nozzle throat radius 57.9 cm
  - Throat static temperature 1730°
  - Throat static pressure 0.839 atm
- Equivalent fuel C_8H_{18}, $\phi = 0.715$
- The nozzle shape is approximately conical with the radius given by

$$r - r^* = 0.26\,x$$

  where r is the nozzle radius, x the length, and * indicates the throat
- The nozzle is designed to expand the flow to ambient pressure – 0.0562 atm at 65,000 ft.

With the pressure-matched condition at the nozzle exit plane, the exhaust flow continues at constant temperature and pressure until the shear layer generated at the exhaust jet/ambient-atmosphere interface closes in and mixes with the exhaust jet.

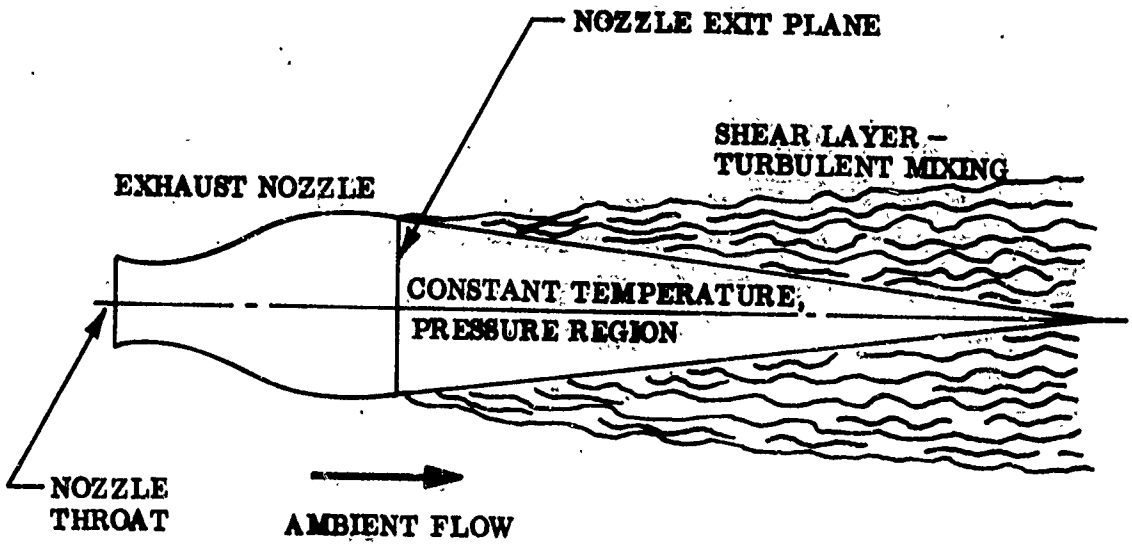

Figure 3-3 Near Jet Exhaust

After leaving the nozzle, the exhaust forms a turbulent jet with characteristics illustrated by Fig. 3-3. The boundaries of this jet grow as free turbulent shear layers between the jet core and the supersonic freestream. These shear layers grow as the jet proceeds downstream until they meet at the center, after which the exhaust becomes a fully developed turbulent jet. In the region between this meeting point and the exit plane of the exhaust nozzle there exists a conical shaped region in the center of the jet which is unaffected by the external stream, and assuming that the nozzle expansion is matched to ambient pressure, the flow properties are constant in this region. Thus, the exhaust gas temperature on the jet centerline will be constant, equal to its value at the nozzle exit, downstream to the point where the shear layers meet.

The jet exhaust forms a compressible turbulent jet flow in a co-flowing external stream. For the purposes of conservative analysis, it is necessary to determine the longest possible initial constant temperature core. For this case, compressibility effects which tend to shorten this initial region are not included. The conditions at the engine nozzle exit plane were calculated from published data for the GE-4 engine at power setting 1, that is full power with afterburner. The flow was isentropically expanded

with $\gamma = 1.28$ in the nozzle to the exit plane where the static pressure was matched with ambient for 65,000-ft altitude.

Using the theory of Abramovich (Ref. 3-15) for these conditions and an aircraft Mach number of 2.7, the length of the initial core region of constant temperature was found to be 22.15 m. Experiments pertaining to this situation were carried out by Forstall and Shapiro (Ref. 3-16) and an expression was derived for the length of this core by curve fitting data. Use of this expression yields a value of 22.0 m for the length of the constant temperature core.

Therefore, for the conditions mentioned above—full power operation of the GE-4 with afterburner at Mach 2.7 at 65,000 ft—the centerline jet temperature will be 954°K and this value will be constant for, at most, 22 m downstream of the exhaust plane.

The complete chemical kinetic model analysis then involves two steps. First, the model is run subject to the constraint of the conical nozzle flow, and second, the calculations are continued at exit plane temperature and pressure, out to the end of the unmixed region. Possible reactions in the mixing zone and beyond are considered in later sections.

The initial composition for the nozzle expansion was taken to be that determined by chemical equilibrium at the nozzle throat, with the exception of CO, NO, and NO_2 (equilibrium calculations were performed using a Lockheed Thermo-chemical equilibrium program). The species CO and NO are well known to be out of equilibrium in jet exhaust because of chemical kinetic freezing effects in the combustor region. CO and NO concentrations have been estimated by a review of available aircraft exhaust emission data. NO_2 concentration has been arbitrarily given a large value – 10 percent of the NO concentration – for the purpose of illustrating the difficulty of preserving NO_2. Actual NO_2 levels in jet exhausts are highly uncertain at present.

Initial throat concentrations of all species considered in the first runs are given in Table 3-2. Hydrocarbons and H_2O_2 were not taken into consideration for this particular case.

Table 3-2

INITIAL THROAT CONCENTRATIONS

Species	Concentration (moles/cm^3)	Mole Fraction
H	4.47 E-12	7.57 E-07
N_2O	4.79 E-13	8.11 E-08
N_2	4.41 E-06	7.47 E-01
OH	1.97 E-09	3.33 E-04
N	5.56 E-17	9.41 E-12
NO	1.77 E-09	3.00 E-04
O	9.25 E-11	1.56 E-05
O_2	3.30 E-07	5.59 E-02
NO_2	1.77 E-10	3.00 E-05
HO_2	8.09 E-13	1.36 E-07
CO	1.77 E-08	3.00 E-03
CO_2	5.37 E-07	9.10 E-02
H_2O	6.04 E-07	1.02 E-01
H_2	7.58 E-11	1.28 E-05
HNO_3	3.80 E-17	6.43 E-12
SO_2	5.91 E-09	1.00 E-04

3.4.4 Discussion of Kinetic Results Without Excess Hydrocarbons

Under these starting conditions, the model calculations yielded the concentration profiles shown in Figure 3-4. Excluded from Figure 3-4 are the trace species SO_3, N, and HNO_3, whose concentration levels remain at all times less than 1 ppb, and the major species CO_2, O_2, N_2, and H_2O. Concentrations calculated from thermodynamic equilibrium considerations are indicated on the far right of the figure for comparison

The results in Figure 3-4 show that a nonequilibrium, but only slowly changing, chemical balance exists in the exhaust plume. Evidently, at the low density corresponding to 65,000-ft altitude, recombination is very slow. All of the active inorganic radical and atomic species are found to exist in super-equilibrium concentrations.

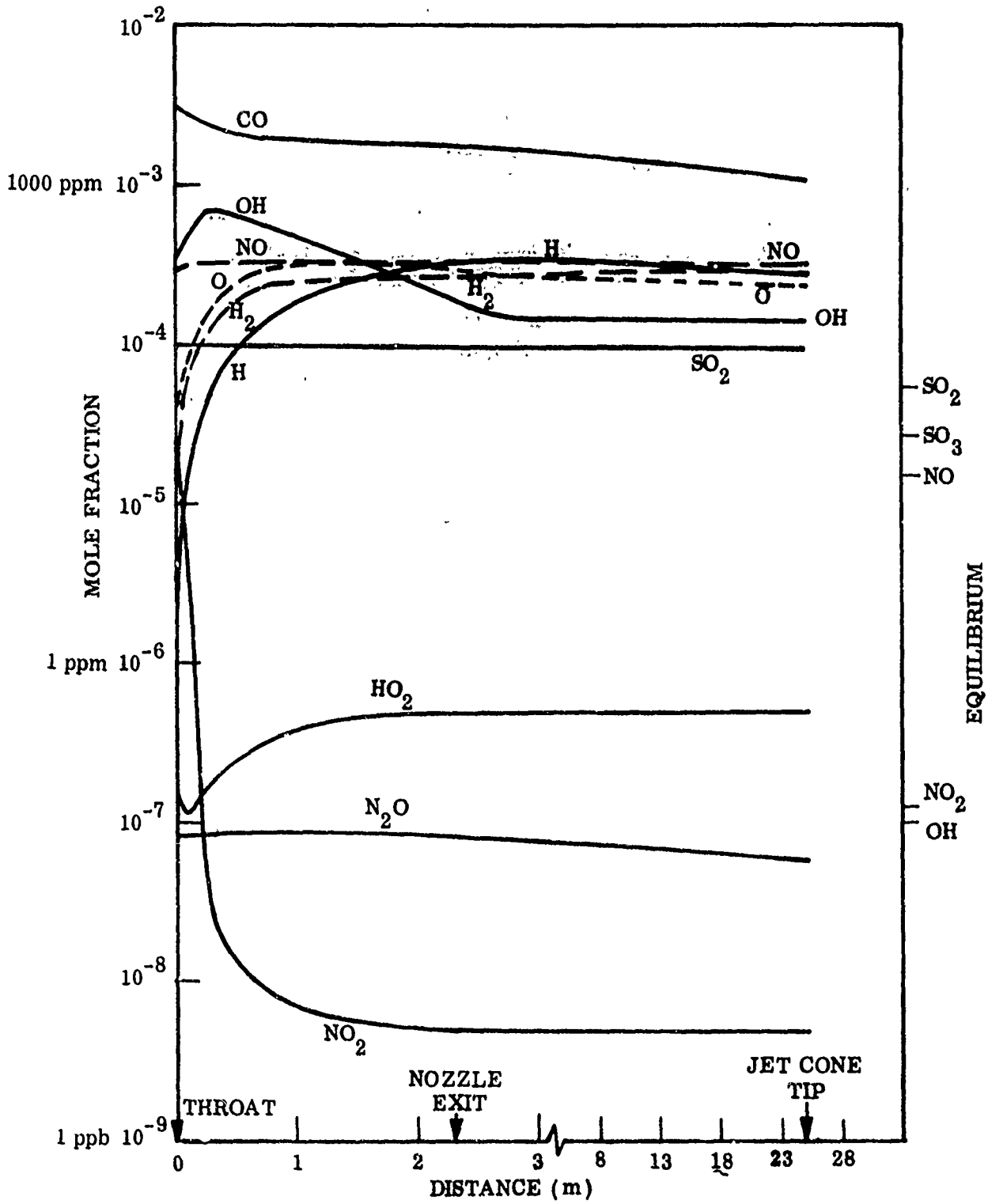

Figure 3-4 Centerline Concentration Profiles, GE-4 Secondary Nozzle and Exhaust (Zero CH_4)

The origin and maintenance of these radicals is a consequence of carbon monoxide oxidation. At throat temperature, $CO + OH \rightarrow CO_2 + H$ is essentially a branching step because the H atoms produced react via $H + O_2 \rightarrow O + OH$, followed by $O + H_2O \rightarrow OH + OH$ and $H + H_2O \rightarrow H_2 + OH$. This chain branching effect is confirmed by the numerical results in Table 3-3. There are given reaction rates and net radical species production for the six reactions mainly governing H, O, and OH levels. It can be seen that while the CO oxidation reaction rapidly consumes OH, the net effect of all six reactions is a rapid generation of additional OH as well as O and H radicals.

Table 3-3

RADICAL FORMATION AT STATION 10-cm DOWNSTREAM OF NOZZLE THROAT

	Reaction	Net Reaction Rate, $r_n \rightarrow$ (moles/cm^3-sec)
5	$H + NO_2 \rightleftharpoons NO + OH$	0.46 E-6
13	$CO + OH \rightleftharpoons CO_2 + H$	7.74 E-6
14	$H + O_2 \rightleftharpoons OH + O$	5.03 E-6
15	$OH + OH \rightleftharpoons H_2O + O$	-2.64 E-6
16	$O + H_2 \rightleftharpoons H + OH$	-0.06 E-6
17	$H_2 + OH \rightleftharpoons H_2O + H$	-1.49 E-6

Net Effect on Radicals

$$\text{net } \frac{d[H]}{dt} = -r_5 + r_{13} - r_{14} + r_{16} + r_{17} = 0.7 \text{ E-6}^*$$

$$\text{net } \frac{d[O]}{dt} = r_{14} + r_{15} - r_{16} = 2.5 \text{ E-6}^*$$

$$\text{net } \frac{d[OH]}{dt} = r_5 - r_{13} + r_{14} - 2r_{15} + r_{16} - r_{17} = 4.5 \text{ E-6}^*$$

*(moles/cm^3-sec)

The initial fast reaction only serves to demonstrate that the assumption that the radicals were in equilibrium with major species in the throat is unrealistic. It is, of course, generally not possible for one species (e.g., H) to be in equilibrium and another

(e.g., CO) to be out of equilibrium, when there is a fast reaction (e.g., CO + OH CO_2 + H) available to exchange them.

In the cooler exhaust jet, CO oxidation is still a chain mechanism since now CO + OH CO_2 + H is followed mainly by H + O_2 + M → HO_2 + M and then H + HO_2 → OH + OH. This notion that the high radical concentrations are a result of carbon monoxide oxidation as the driving reaction is confirmed by computations in which the CO oxidation rate is arbitrarily reduced to negligible values. The output then shows about an order of magnitude lower concentration of O, H, and OH radicals in the nozzle.

It is encouraging to note that a recent optical measurement (Ref. 3-13) of OH concentration in a relevant afterburning situation under altitude condition gives an OH concentration in good agreement with the super-equilibrium value computed here.

Understanding of the details of the various chemical balances in the exhaust jet is aided by Table 3-4. There are listed rate constants, foward reaction rates, and net rates for the various reactions at a position 2 m downstream from the nozzle exit plane. Table 3-4 can then, in turn, be used to identify the reactions that are of importance to individual species rates. For example, the OH balance shown in Table 3-5 is instructive. This gives all the important reactions involving OH as well as their rates and the net effect. As can be seen in the table, the aforementioned CO oxidation chain has the consequence that the net disappearance of OH is more than an order of magnitude less than its rate of participation in CO + OH → CO_2 + H. Hence, it would be a good approximation to assume the OH concentration constant in computing the rate of CO oxidation. The very sluggish nature of the net recombination means that the radicals will persist out into the region where the plume mixes with ambient air.

3.4.5 Exhaust Chemistry With Significant Hydrocarbons

Test data are somewhat scarce for SST engines, but existing data show that quantities of unburned hydrocarbons (measured as total C) may be large along certain streamlines with afterburning (Refs. 3-17 and 3-18). To take some account of the effect of hydrocarbons on the chemistry, reactions 34 through 45 (Table 3-1), a methane oxidation scheme,

Table 3-4

CHEMICAL KINETIC SITUATION TWO METERS DOWNSTREAM OF NOZZLE EXIT PLANE

	REACTION $\sum_i \nu_i A_i \rightleftharpoons \sum_j \nu_j A_j$		FORWARD RATE CONSTANT k^f	FORWARD REACTION RATE $r^f = k^f \prod_i [A_i]^{\nu_i}$	NET REACTION RATE $r^f - k^r \prod_j [A_j]^{\nu_j}$	COMMENTS*
1	$H + N_2O$	$\rightleftharpoons N_2 + OH$	1.01 E+11	1.57 E-12	1.57 E-12	F
2	$N + OH$	$\rightleftharpoons NO + H$	4.21 E+13	3.21 E-17	-3.63 E-17	B
3	$O + N_2O$	$\rightleftharpoons N_2 + O_2$	1.14 E+8	1.39 E-15	1.39 E-15	F
4	$N_2 + NO_2$	$\rightleftharpoons NO + N_2O$	1.35 E-5	1.94 E-26	-7.46 E-21	R
5	$H + NO_2$	$\rightleftharpoons NO + OH$	2.62 E+14	1.86 E-10	1.86 E-10	F
6	$HO_2 + NO$	$\rightleftharpoons OH + NO_2$	1.25 E+11	1.51 E-11	1.51 E-11	F
7	$O + N_2$	$\rightleftharpoons NO + N$	6.93 E-4	7.69 E-20	-3.66 E-17	R
8	$NO + O$	$\rightleftharpoons N + O_2$	6.73 E+0	3.30 E-19	1.78 E-19	B
9	$NO_2 + M$	$\rightleftharpoons NO + O + M$	1.41 E+1	2.72 E-20	-1.75 E-10	R
10	$NO + O_2$	$\rightleftharpoons O + NO_2$	4.20 E+1	3.93 E-16	-4.01 E-12	R
11	$NO + NO$	$\rightleftharpoons N_2O + O$	9.01 E-4	5.06 E-23	-1.94 E-16	R
12	$N_2O + M$	$\rightleftharpoons N_2 + O + M$	6.09 E+1	2.56 E-18	-4.62 E-14	R
13	$CO + OH$	$\rightleftharpoons CO_2 + H$	3.17 E+11	2.32 E-8	1.85 E-8	B
14	$H + O_2$	$\rightleftharpoons OH + O$	3.11 E+10	3.26 E-7	-2.30 E-9	FASTEST REACTION BUT VERY NEAR PE
15	$OH + OH$	$\rightleftharpoons H_2O + O$	3.53 E+12	5.91 E-8	-8.41 E-12	PE
16	$O + H_2$	$\rightleftharpoons H + OH$	1.57 E+11	8.06 E-9	9.74 E-10	NEAR PE
17	$H_2 + CH$	$\rightleftharpoons H_2O + H$	1.45 E+12	4.65 E-8	5.63 E-9	NEAR PE
18	$H_2 + M$	$\rightleftharpoons H + H + M$	2.22 E-8	3.96 E-24	-2.26 E-10	R
19	$H + OH + M$	$\rightleftharpoons H_2O + M$	1.54 E+17	3.80 E-3	3.78 E-9	F
20	$O_2 + M$	$\rightleftharpoons O + O + M$	1.85 E-12	5.26 E-26	-3.46 E-12	R
21	$M + H + O_2$	$\rightleftharpoons HO_2 + M$	2.54 E+15	1.91 E-8	1.91 E-8	F
22	$H + HO_2$	$\rightleftharpoons OH + OH$	9.175 E+13	1.24 E-8	1.24 E-8	F
23	$OH + HO_2$	$\rightleftharpoons H_2O + O_2$	5.90 E+12	3.90 E-10	3.90 E-10	F
24	$O + HO_2$	$\rightleftharpoons OH + O_2$	2.95 E+13	3.12 E-9	3.12 E-9	F
25	$H + HO_2$	$\rightleftharpoons H_2 + O_2$	1.73 E+13	2.34 E-9	2.34 E-9	F
26	$H + HO_2$	$\rightleftharpoons H_2O + O$	5.90 E+12	7.98 E-10	7.98 E-10	F
27	$NO_2 + OH$	$\rightleftharpoons HNO_3$	2.90 E+12	1.00 E-12	-1.62 E-17	PE

*F – FORWARD REACTION DOMINATES.
R – REVERSE REACTION DOMINATES.
PE – FORWARD RATE = REVERSE RATE, REACTION IN PARTIAL EQUILIBRIUM.
B – BOTH FORWARD AND BACK RATES SIGNIFICANT AND NONEQUAL.

Table 3-5

PREDOMINANT CONTRIBUTIONS TO OH BALANCE TWO METERS DOWNSTREAM OF EXHAUST NOZZLE EXIT PLANE

NO.	REACTION	COMMENT
		OH FORMATIONS
22[f]	$H + HO_2 \rightarrow OH + OH$	PRIMARY
24[f]	$O + HO_2 \rightarrow OH + O_2$	SECONDARY
16	$O + H_2 \rightarrow OH + H$	SMALL CONTRIBUTIONS
5[f]	$H + NO_2 \rightarrow OH + NO$	SMALL CONTRIBUTIONS
		OH DESTRUCTIONS
13	$CO + OH \rightleftarrows CO_2 + H$	PRIMARY
17	$H_2 + OH \rightleftarrows H_2O + H$	SECONDARY
19[f]	$H + OH + M \rightarrow H_2O + M$	SECONDARY
14	$O + OH \rightleftarrows H + O_2$	SECONDARY
23[f]	$HO_2 + OH \rightarrow H_2O + O_2$	SMALL CONTRIBUTION

NET CHANGE OH

$$r_{22}^f = 2.48\ E\text{-}8 \quad (MOLE/CM^3\text{-}SEC)$$
$$r_{24}^f = 0.31\ E\text{-}8 \quad (MOLE/CM^3\text{-}SEC)$$
$$r_{16} = 0.10\ E\text{-}8 \quad (MOLE/CM^3\text{-}SEC)$$
$$r_5^f = 0.02\ E\text{-}8 \quad (MOLE/CM^3\text{-}SEC)$$
$$-r_{13} = -1.85\ E\text{-}8 \quad (MOLE/CM^3\text{-}SEC)$$
$$-r_{17} = -0.56\ E\text{-}8 \quad (MOLE/CM^3\text{-}SEC)$$
$$-r_{19}^f = -0.38\ E\text{-}8 \quad (MOLE/CM^3\text{-}SEC)$$
$$-r_{14} = -0.23\ E\text{-}8 \quad (MOLE/CM^3\text{-}SEC)$$
$$-r_{23}^f = -0.04\ E\text{-}8 \quad (MOLE/CM^3\text{-}SEC)$$

$$\frac{d[OH]}{dt} = \Sigma r = -0.15\ E\text{-}8 \quad (MOLE/CM^3\text{-}SEC)$$

TO BE COMPARED WITH $\frac{d[CO]}{dt} = -r_{13} = -1.85\ E\text{-}8$ (MOLE/CM^3-SEC)

have been included at this point. As we shall see, sacrifice of $\mathcal{P}$ (defined as $\mathcal{P}$ = H, OH, and O together) in favor of CH_3, CH_2O, HCO, and CO is the net effect on the exhaust chemistry. The magnitude of $\mathcal{P}$ radical reduction is highly dependent on the HC quantities.

Two sets of concentration profiles are shown in Figures 3-5 and 3-6. Both are for the same operating condition as Figure 3-4. Starting throat concentrations of all species are taken as before, except that the portion of CH_4 is assumed initially at 500 ppm in Figure 3-5 and 3,000 ppm in Figure 3-6. In the first case most of the CH_4 is oxidized in the nozzle and jet, with only 50 ppm total HC (including CHO and CH_2O) remaining at the exit plane and subsequently disappearing in the near wake. Total $\mathcal{P}$ is forced down to about one-fifth of its zero HC level at the exit plane, but builds up somewhat in the wake as the last of the HC vanishes.

When the CH_4 is set at 3,000 ppm throat concentration, very little is completely oxidized; i.e., the wake HC level is frozen at 3,000 ppm with about half of it present as CH_4 and the rest as CH_2O and CHO. This has the consequence of nearly eliminating $\mathcal{P}$ from the wake, as shown in Figure 3-6.

Although it may seem peculiar at first that the addition of CH_4 reduces the levels of H, OH, and O, it should be emphasized that this is a highly nonequilibrium situation, where super-equilibrium amounts of methane are introduced and in turn produce super-equilibrium amounts of hydrocarbon radicals (CH_3, CH_2O, and HCO) at the expense of H, OH, and O. In fact, Figure 3-5 shows that H, OH, and O begin to return as the added hydrocarbons disappear. For higher levels of added CH_4, as in Figure 3-6, the hydrocarbon oxidation is incomplete and the H, OH, and O remain bound in the frozen hydrocarbon radicals. The levels for the three cases are shown plotted together in Figure 3-7 for comparison.

These calculations serve to point out the profound difference of carbon monoxide and hydrocarbon oxidation at nozzle expansion temperatures. The former, CO + OH → CO + H, builds up $\mathcal{P}$ through activity of the H atom, whereas the hydrocarbon oxidation cannot sustain production of $\mathcal{P}$, and freezing occurs as soon as the available radicals are scavenged. The general conclusion drawn here is that, if the HC levels are high the radical H, OH, or O cannot be present in significantly large concentrations.

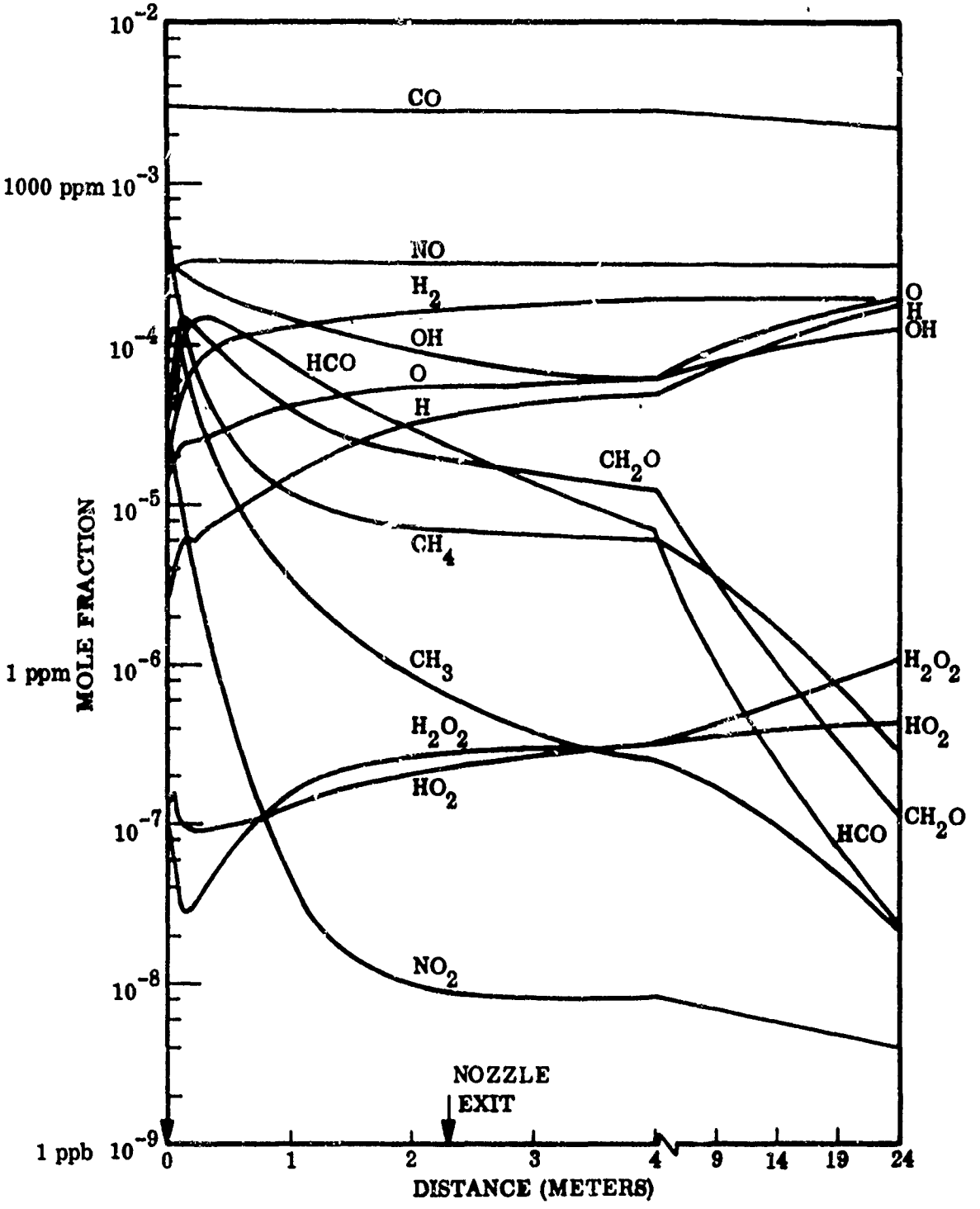

Figure 3-5 Centerline Concentration Profiles, GE-4 Secondary Nozzle and Exhaust (500 ppm CH_4 at Throat)

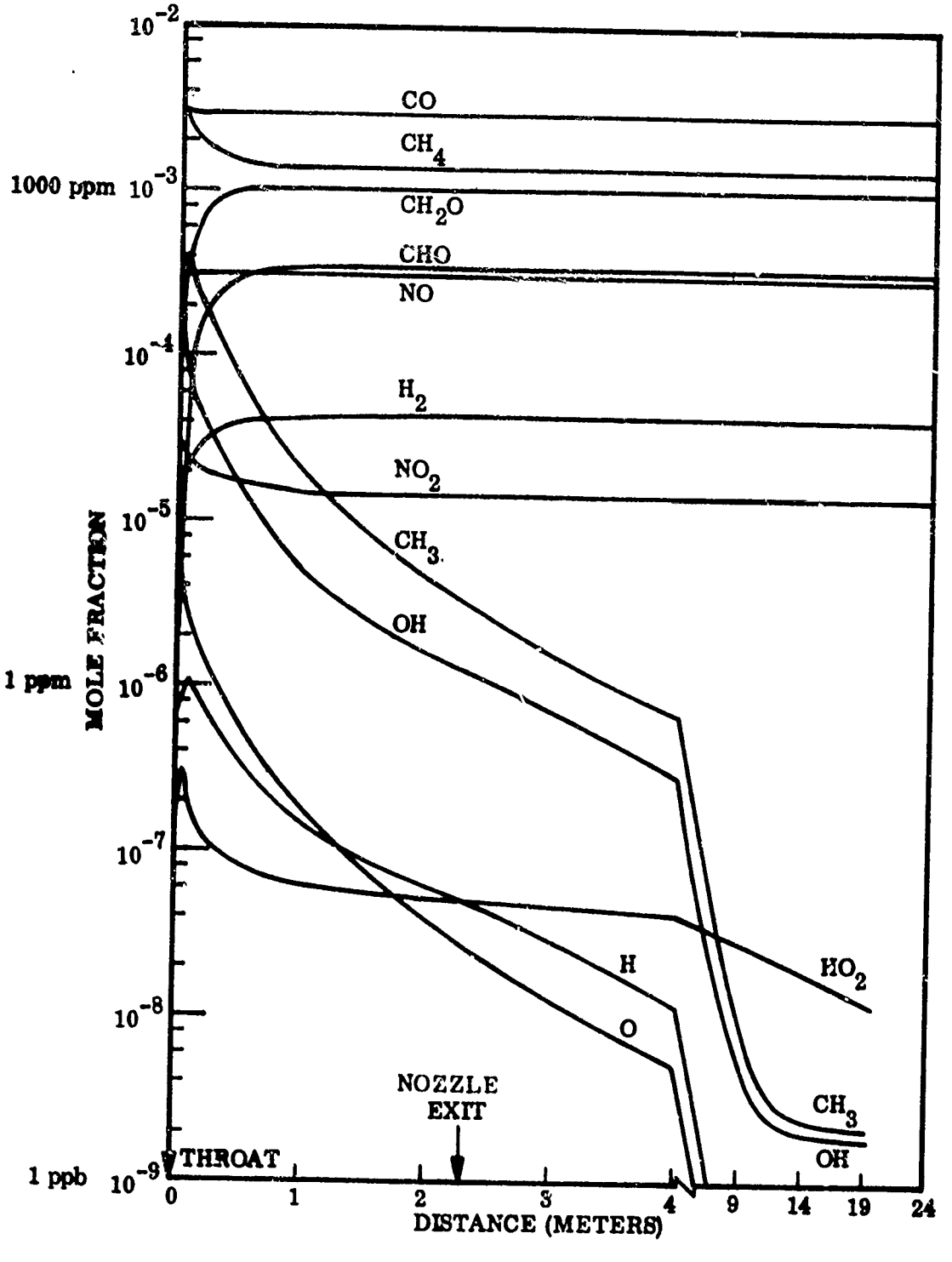

Figure 3-6 Centerline Concentration Profiles, GE-4 Secondary Nozzle and Exhaust (3,000 ppm CH_4 at Throat)

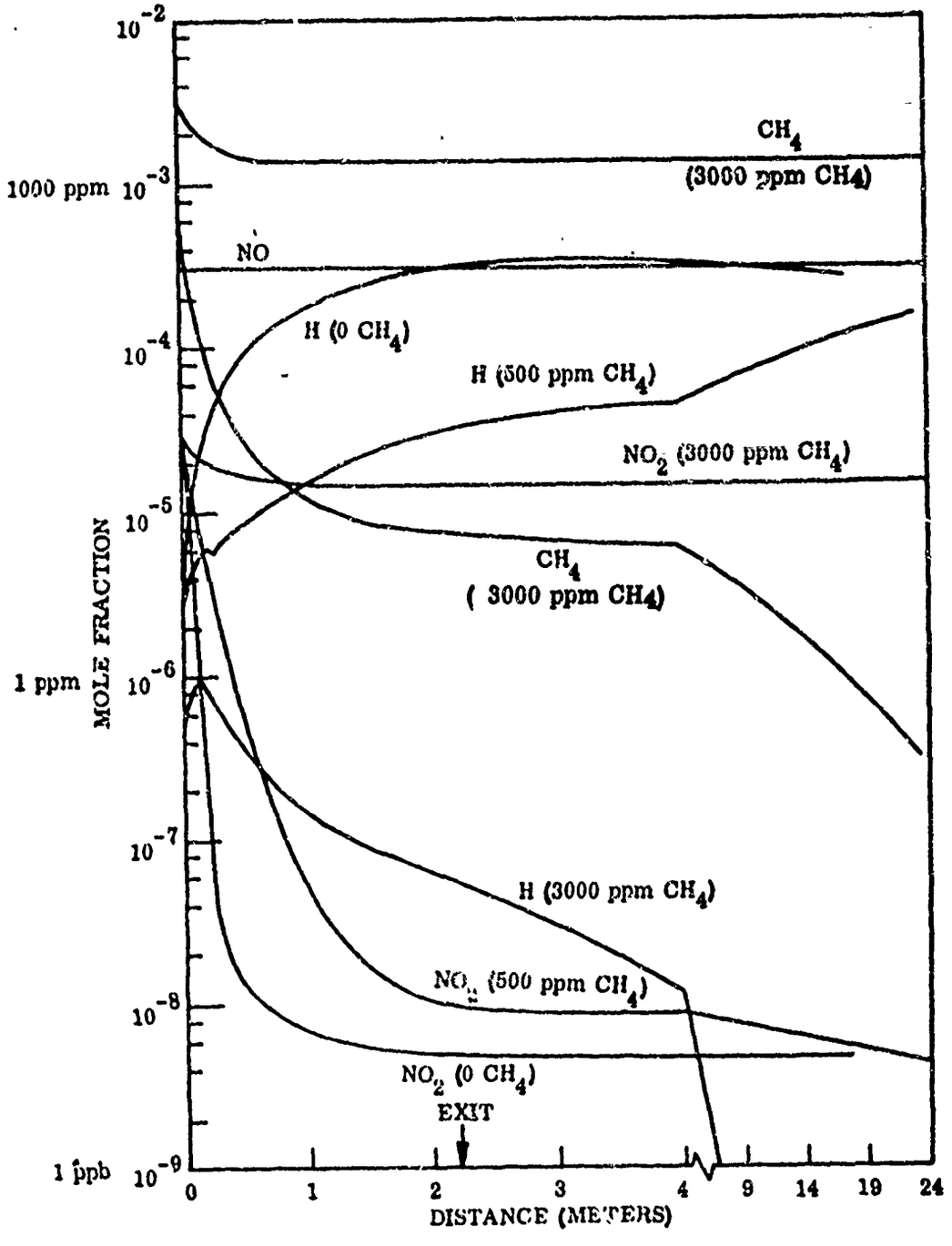

Figure 3-7 Effect of Hydrocarbon on NO_2 in GE-4 Secondary Nozzle and Jet Exhaust

3.4.6 Radical Partial Equilibrium

Another simplifying condition evident from Table 3-4 is that the bimolecular shuffle reactions 14 through 17 are in partial equilibrium. That is, their forward reaction rates are approximateiy equal to their reverse rates. This condition is exhibited in the table by the fact that the forward rate is much larger than the net rate. Since the ratio of forward to back rate constant is the equilibrium constant, an algebraic equation can be written relating the concentration of species in each of these reactions, as follows:

$$K_{14} = \frac{[OH]\,[O]}{[H]\,[O_2]} \quad ; \quad K_{15} = \frac{[H_2O]\,[O]}{[OH^2]}$$

$$K_{16} = \frac{[H]\,[OH]}{[O]\,[H_2]} \quad ; \quad K_{17} = \frac{[H_2O]\,[H]}{[H_2]\,[OH]} = K_{15}K_{16}$$

where K represents the equilibrium constants and the brackets signify concentrations. Since only three of these equations are independent, a complete solution is not obtainable, but the concentration of the variable species H, OH, H_2, and O can be expressed as a function of just one. If OH is selected as the independent quantity, we have

$$[H] = \frac{K_{15}}{K_{14}\,[O_2]\,[H_2O]}\,[OH]^3$$

$$[O] = \frac{K_{15}}{[H_2O]}\,[OH]^2$$

$$[H_2] = \frac{1}{K_{14}\,K_{16}\,[O_2]}\,[OH]^2$$

$$\frac{[H]}{[O]} = \frac{[OH]}{K_{14}\,[O_2]}$$

These relations are expected to be of value in setting initial nozzle exit conditions from test-cell measurements of OH. All the inorganic radical concentrations must be known if meaningful downstream calculations are to be made. It is clear from the results in the last two sections that probably none of these radicals are in absolute chemical equilibrium anywhere in the nozzle. Some experimental measurements are therefore essential.

3.4.7 Discussion of Axial CO Oxidation

The initial CO concentration far exceeds its local equilibrium value and therefore tends to oxidize to CO_2 in the nozzle and exhaust jet. Oxidation of CO is governed by its reaction with OH radicals, $CO + OH \rightarrow CO_2 + H$. The H atoms produced by this reaction then enter the fast bimolecular shuffle reactions 14 through 17 (Table 3-1) and OH is regenerated. These fast reactions, coupled with the slow recombination, act to maintain O, H, and OH at super-equilibrium concentrations.

The phenomenological aspects of CO oxidation have already been discussed earlier. Numerical results show that a considerable decrease in CO can occur in the nozzle and jet under low HC conditions. Calculations for the zero HC run, presented in Figure 3-4 show that the proportion of CO in the exhaust is decreased from 3,000 ppm in the nozzle throat to 1,780 ppm at the exit and then is further reduced to 1,150 ppm at the tip of the jet core region.

The corresponding levels for the runs with 500 ppm CH_4 initially, where CO was again 3,000 ppm at the throat, are 2,810 ppm at the exit, and 2,180 ppm finally. When the portion of CH_4 was set at 3,000 ppm, the CO level remained essentially frozen throughout.

The kinetic model is run at constant pressure for the jet calculations so a chemically induced temperature change is computed between the nozzle exit and the jet cone tip. In the zero HC case, which had the largest amount of CO oxidized, the magnitude of this change was still only 5° K (in 950° K). This tends to confirm our intuitively held notion that the exhaust species chemistry can have no meaningful effect on the fluid mechanic properties.

3.4.8 Integrated CO Oxidation in Exhaust Jet Core

The above results without hydrocarbons show oxidation of 35% of the available CO occurs between the nozzle exit plane and the tip of the constant properties region. However, this result is for the centerline of the wake; streamlines nearer the jet boundary encounter the reaction quenching inward propagating shear layer earlier, so the total integrated CO oxidation is not so great.

If the wake zone of constant conditions is assumed to be exactly conical, the total reduction can be estimated in a simple manner. Let L be the length of the undisturbed exhaust cone; x be the streamline distance; CO (x) be the axial CO profile calculated assuming constant properties; r be the local radius for nozzle centerline; and subscript E refer to the exit plane. Clearly the CO contained in the annulus of area $dA = 2\pi\, r\, dr$ is frozen at the position

$$x = \left(\frac{r_E - r}{r_E}\right) L$$

Therefore, the portion of the total CO remaining

$$T = \frac{\text{Total CO}}{\text{Total CO in exit plane}} \text{ contributed by this element}$$

is

$$dT = \frac{[CO(x)]\ 2\pi\, r\, dr}{[CO]_E\, A_E} = \frac{[CO(x)]}{[CO]_E} \frac{2\, r}{r_E^2}\, dr$$

and with $r = r_E\,(1 - x/L)$ and $dr = \frac{-r_E}{L}\, dx$

$$\therefore dT = \frac{[CO(x)]}{[CO]_E} (2) \frac{(L - x)}{L^2}\, dx$$

so that the total remaining is given by

$$T = \int_{-L}^{0} - \frac{[CO(x)]}{[CO]_E} \frac{2\,(L - x)}{L^2}\,dx = \int_{0}^{L} 2\,\frac{[CO(x)]}{[CO]_E}\,\frac{(L - x)}{L^2}\,dx$$

A numerical integration of this equation using the [CO(x)] profile data presented in Figure 3-4 yields the value T = 0.87 corresponding to a 13% total CO oxidation beyond the nozzle exit.

The extent of CO oxidation in the far wake beyond the jet core depends almost entirely on the rate at which the exhaust becomes diluted, the rate falling off as the square of the dilution. The significance of the CO oxidation is not the final wake concentration of CO or the total CO added to the stratosphere. The estimated total impact of the CO added by an SST fleet is to increase ambient stratospheric levels by approximately 0.2 ppb/30 ppb = 0.7% (Ref. 3-19).

Carbon monoxide is not a "pollutant" in this sense. The significance of CO oxidation is the resultant production of hydrogen atoms. These contribute substantially to reactions which tend to prevent oxidation of pollutants like NO and SO_2 in the exhaust jet. This point will be discussed more fully in later paragraphs.

3.4.9 Discussion of NO_x Results

Oxides of nitrogon are the species of major interest with regard to environmental impact. The portion of NO_x as NO_2 in the hot exhaust is of importance because of the possibility of nitric acid formation to provide an NO_x "sink" in the wake,

$$NO_2 + OH \rightarrow HNO_3$$

Experimental evidence (Refs. 3-20, 3-21) indicates that the afterburning region in augmented turbojet engines produces very little NO so that NO levels in the exhaust are associated with the NO production ir the main combustors. Typical combustor

NO exit levels range from 100 to 500 ppm (Refs. 3-22, 3-23). The initial NO concentration is taken here as 300 ppm.

Emission levels of NO_2 are more uncertain than the NO levels. Both Fletcher (Ref. 3-23) and Caretto (Ref. 3-24) indicate that at full power the oxides of nitrogen will be essentially all nitric oxide, NO. However, recent test data (Ref. 3-25) seem to indicate that significant NO_2 levels exist at all engine power levels.

In the measurement of NO_2 levels, one method is to use a chemilumescent detector with a converter to convert NO_2 to NO so that the detector measures total NO_x. NO_2 is then determined by the difference between NO_x and NO. Mellor (Ref. 3-26) has recently reported problems in using the NO_2-NO converters and has attributed lack of reproducibility of results to catalytic reactions in the converter. This illustrates the point that the presence of catalytic walls, such as sampling probes in the flow, can promote reactions between NO_x and oxygen species which might not take place in the gas phase. Recent test data (Ref. 3-25) utilized an electrochemical device to measure NO_2 and NO_x.

Thus, at the present time NO_2 emission levels are quite uncertain. For this investigations we have taken 30 ppm for the NO_2 concentration at the nozzle throat.

Thermodynamic equilibrium considerations give an NO_2/NO ratio of 0.01 at exit plane conditions. The results of the kinetic calculations without HC, as shown in Figure 3-4, reveal that conversion of NO to NO_2 actually does not occur. In fact, any NO_2 assumed present at the throat is quickly destroyed. At the exit plane the concentration has fallen to 4 ppb, corresponding to an NO_2/NO ratio of only 10^{-5}.

NO_2 is kept far below its equilibrium level by fast reaction such as

$$9^r \quad NO + O + M \rightarrow NO_2 + M$$

$$6^f \quad NO + HO_2 \rightarrow NO_2 + OH$$

$$5^f \quad H + NO_2 \rightarrow NO + OH$$

$$10^r \quad O + NO_2 \rightarrow NO + O_2$$

and the fact that the H and the O levels are maintained far above their equilibrium concentrations. The second and fourth reactions above become unimportant as the temperature drops and are already much slower than the other two reactions at the exit plane.

The contributions of the NO_2 balance at the 2-m position can be tabulated as follows. Net Change NO_2, No Excess HC:

$$r_9^r = 1.86 \times 10^{-10} \text{ (moles/cm}^3\text{-sec)}$$

$$r_6^f = 0.15 \times 10^{-10} \text{ (moles/cm}^3\text{-sec)}$$

$$-r_5^f = -1.97 \times 10^{-10} \text{ (moles/cm}^3\text{-sec)}$$

$$-r_{10}^r = -0.04 \times 10^{-10} \text{ (moles/cm}^3\text{-sec)}$$

$$\frac{d[NO_2]}{dt} = \Sigma r < 0.01 \times 10^{-10} \text{ (moles/cm}^3\text{-sec)}$$

Thus, in the absence of HC the NO_2 level is largely controlled by a steady state between its formation by reaction with O atoms and destruction by H atoms. Given such a balance between reactions 9 and 5, an expression for the steady-state NO_2/NO ratio is obtained as follows:

$$O = \frac{d[NO_2]}{dt} = k_9 [NO] [O] [M] - k_5 [H] [NO_2]$$

Therefore

$$\left(\frac{[NO_2]}{[NO]}\right)_{SS} = \frac{k_9\,[M]\,[O]}{k_5\,[H]}$$

The O/H ratio is thus the controlling quantity.

Substituting the zero HC exit plane concentrations of M, O, and H, and k_5 and k_9 evaluated at the exit plane temperature, in the expression yields

$$\frac{(NO_2)}{(NO)_{\text{exit, steady state}}} = 0.62 \times 10^{-5}$$

This result compares favorably with the results of the full computer solution, i.e.,

$$\frac{(NO_2)}{(NO)_{\text{exit, finite rate}}} = 1.1 \times 10^{-5}$$

For minor species resulting from rapid formation and even faster destruction processes, a simple local steady state approximation can often furnish a useful order-of-magnitude estimate of the ratio between the oxidized and reduced forms of the species in question.

When sufficient hydrocarbons are present, the steady-state NO_x position is not reached. The expression above is still a good approximation in the case of 500 ppm CH_4, but with 3,000 ppm CH_4 the H is driven so low that NO_2 is no longer destroyed and $([NO_2] / [NO]) = 0.05$. Of course, any formation would also be slowed since O is driven equally as low as H.

3.4.10 H, O, and OH Recombination in Cooling Wake

An assessment of predominant radical recombination paths, as air is entrained and the wake cools, can be based on calculations such as presented in Table 3-6. There are listed rate constants and initial reaction rates for recombination and contributing bimolecular reactions, assuming the exit plane species are cooled instantaneously to 220°K. A ten-fold air dilution has also been assumed for these sample calculations. The original exit plane concentrations are those corresponding to Figure 3-4.

It is evident from the tabulated results that each radical has one prevailing recombination reaction that is at least an order of magnitude faster than its competitors. For H atoms this reaction is (4)* $H + O_2 + M \rightarrow HO_2 + M$, for OH radicals it is reaction (6) $OH + OH + M \rightarrow H_2O_2 + M$, and for O atoms reaction (9) $O + O_2 + M \rightarrow O_3 + M$ dominates.

The half time for O atom recombination via (9) at 220°K is given by:

$$t_{1/2} = \frac{\ln 2}{k_9[O_2][M]}$$

$$= 4 \times 10^{-4} \text{ sec at 20 km}$$

H and OH recombination are similarly fast.

Reaction (7) $SO_2 + O + M \rightarrow SO_3 + M$ and (8) $NO + O + M \rightarrow NO_2 + M$ are slow compared to loss of O atoms in (9). Keeping in mind that (9) becomes relatively even faster with more air dilution, it is apparent that the extent of SO_2 and NO oxidation in the cooling wake by (7) and (8) will be small.

*Return number in this discussion refer to those used in Table 3-6.

Table 3-6

REACTION RATES FOR SUDDEN COOLING OF EXHAUST TO 220 K

	Reaction	k (mole, cm, sec)	r → (male/cm^3-sec)	
(1)	$H + OH + M \rightarrow H_2O + M$	2.9 E18	3.2 E-8	
(2)	$H + H + M \rightarrow H_2 + M$	3.0 E15	4.2 E-11	
(3)	$O + O + M \rightarrow O_2 + M$	1.7 E15	2.3 E-11	
(4)	$H + O_2 + M \rightarrow HO_2 + M$	1.5 E16	2.2 E-6	Prevailing H sink
(5)	$H + O + M \rightarrow OH + M$	5.0 E15	7.3 E-11	
(6)	$OH + OH + M \rightarrow H_2O_2 + M$	1.1 E20	8.0 E-7	Prevailing OH sink
(7)	$SO_2 + O + M \rightarrow SO_3 + M$	4.0 E15	2.6 E-11	
(8)	$NO + O + M \rightarrow NO_2 + M$	7.6 E16	1.6 E-9	
(9)	$O + O_2 + M \rightarrow O_3 + M$	9.0 E14	1.2 E-7	Prevailing O sink
(10)	$OH + O \rightarrow O_2 + M$	1.5 E13	5.0 E-8	
(11)	$OH + OH \rightarrow H_2O + O$	5.1 E11	1.2 E-9	

3.4.11 NO_x in the Near Wake

Another possible oxidation process for NO is the Bodenstein mechanism

$$NO + NO + O_2 \rightarrow NO_2 + NO_2$$

This has the rate equation

$$-\frac{d(NO)}{dt} = 2 k_b (NO)^2 (O_2)$$

and hence a half time for NO disappearance of

$$\tau_{1/2} = \frac{1}{2 k_b (NO)_o (O_2)}$$

This relationship between $\tau_{1/2}$ and $(NO)_o$ is shown plotted in Figure 3-8 for some altitudes of interest. The rate constant is $k_b = 2.4 \times 10^9 \exp(+1046/RT)$ $cm^6\text{-mole}^{-2}\text{-sec}^{-1}$ (Ref. 3-27). Figure 3-8 shows that the Bodenstein oxidation is insignificant in the wake.

Upon mixing of the exhaust with ambient air, ozone is introduced and the subsequent effect of the reaction

$$NO + O_3 \xrightarrow{k_a} NO_2 + O_2 \qquad (3.25)$$

must be considered from the standpoint of NO oxidation.

The NO depletion rate of Eq. (3.25) is given by

$$\frac{d(NO)}{dt} = -k_a (NO)(O_3)$$

Integrating the rate,

$$\int_{(NO)_o}^{NO} \frac{d(NO)}{(NO)} = \int_0^{\tau} -k_a (O_3)\, dt$$

or

$$\ln \frac{(NO)_o}{(NO)} = k_a \int_0^{\tau} (O_3)\, dt$$

Now if the exhaust mixing is extensive enough so that $(O_3) >> (NO)$, the ozone concentration will be constant, and the half-time is

$$\tau_{1/2} = \frac{\ln 2}{k_a (O_3)}$$

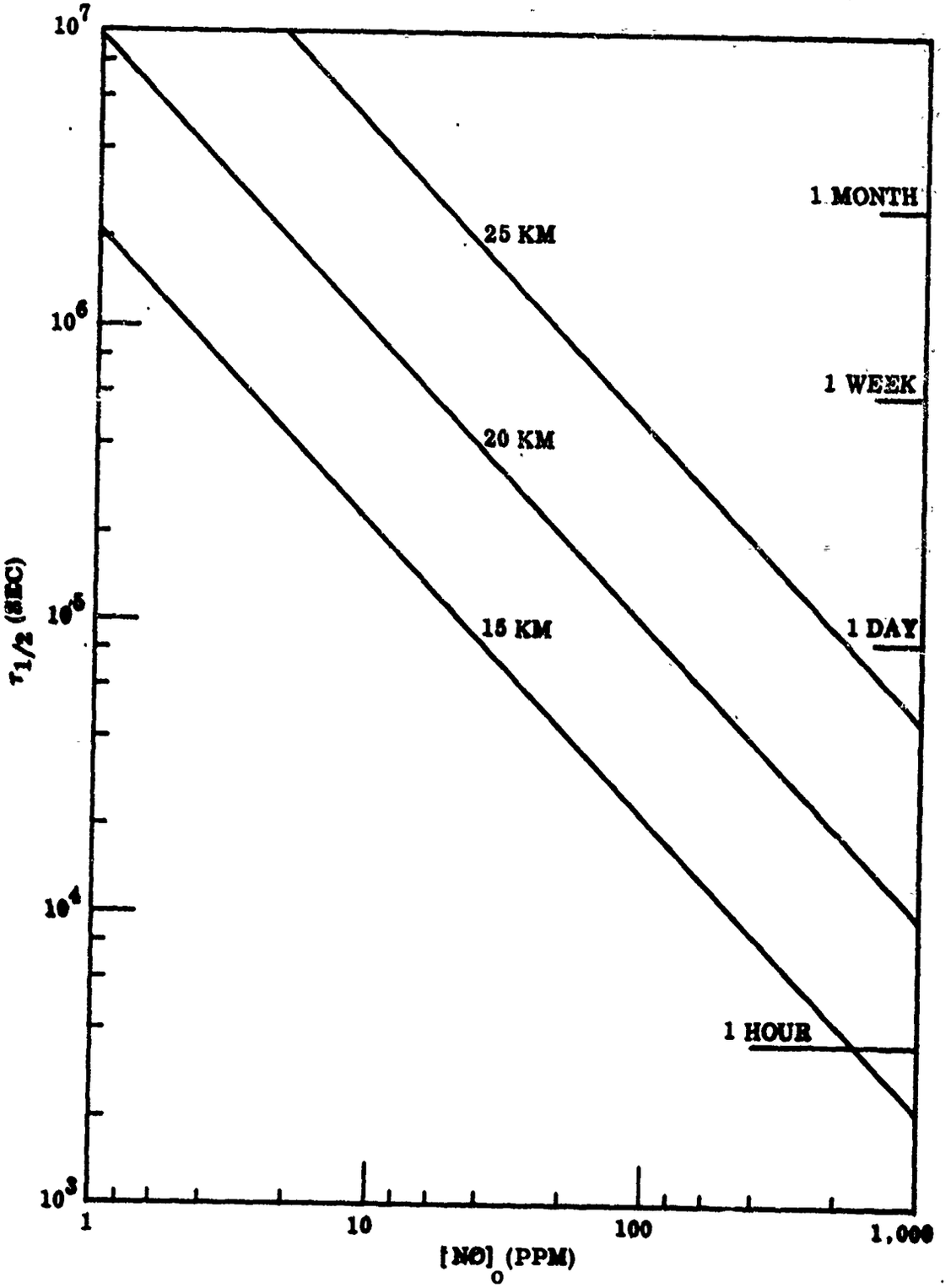

Figure 3-8 Half Time for NO Oxidation by $NO + NO + O_2 \rightarrow NO_2 + NO_2$

For 20-km altitude conditions, Johnston (Ref. 3-27) gives $k_a = 10^{-14.40}$ cm^3-molecule^{-1}-sec^{-1} and $(O_3) \approx 10^{12}$ molecule-cm^{-3}

Therefore

$$\tau_{1/2} = 175 \text{ sec} \approx 3 \text{ min}$$

It is also instructive to compute the half-time in the event that $(O_3)_o = (NO)_o$ with no diffusional replenishment of O_3 as the reaction proceeds.

In this case, the half-time expression is

$$\tau_{1/2} = \frac{1}{k_a (O_3)_o}$$

which, when evaluated for the same initial conditions as before, yields

$$\tau_{1/2} = 252 \text{ sec} \approx 4 \text{ min}$$

Thus, it is clear that the oxidation of NO by ozone is rapid enough to be significant in the wake regime. In the near wake the rate will be limited by the ozone supply. The O_3/NO_x approach to steady state in the irradiated environment is treated more fully in Section 4.

3.4.12 Oxidation of NO_2 to HNO_3 in Wake

In the mixing region, when a sufficiently low temperature is reached for nitric acid to be stable, NO_2 can be oxidized by the reaction

$$NO_2 + OH \overset{k_a}{\rightarrow} HNO_3 \qquad (3.26a)$$

Although it would appear from foregoing calculations that the hot exhaust will contain very little NO_x as NO_2, this is unconfirmed by test data and, therefore, reaction (3.26a) must be considered. However, even assuming all NO_x is emitted as NO_2, the following argument will demonstrate that NO_x removal by reaction (3.26a) is still not of an important magnitude.

As discussed in Section 3.4.10 the reaction

$$OH + OH + M \xrightarrow{k_b} H_2O_2 + M \qquad (3.26b)$$

is fast. If it is sufficiently so, OH will be totally removed before reaction (a) can proceed to a significant degree. This is confirmed by the following analysis of the reaction system (3.26a) plus (3.26b).

The rate of OH disappearance from reactions (3.26a) and (3.26b) is given by:

$$\frac{d[OH]}{dt} = -2\,k_b\,[OH]^2\,[M] - k_a\,[NO_2]\,[OH]$$

approximating $[NO_2]$ by an average value $[\overline{NO_2}]$, (justified in the light of results) an integration produces the relation

$$[OH] = \frac{k_a\,[OH]_0\,[\overline{NO_2}]\,e^{-k_a\,[\overline{NO_2}]\,t}}{k_a\,[\overline{NO_2}] + 2k_b\,[OH]_0\,[M]\left[1 - \exp\left(-k_a\,[\overline{NO_2}]\,t\right)\right]}$$

where subscript zero denotes initial conditions.

This expression, when substituted for OH in the NO_2 rate equation

$$\frac{d[NO_2]}{dt} = -k_a\,[NO_2]\,[OH]$$

yields

$$\frac{1}{[\overline{NO_2}]}\frac{d[NO_2]}{dt} = \frac{-k_a^2[\overline{OH}]_0[\overline{NO_2}]\exp\left(-k_a[\overline{NO_2}]t\right)}{k_a[\overline{NO_2}] + 2k_b[OH]_0[M]\left[1 - \exp\left(-k_a[\overline{NO_2}]t\right)\right]}$$

Another integration then gives:

$$\frac{[NO_2]}{[NO_2]_0} = \left[\frac{\alpha}{\alpha + \frac{[OH]_0}{[\overline{NO_2}]}\left[1 - \exp\left(-k_a[\overline{NO_2}]t\right)\right]}\right]^{\alpha}$$

where

$$\alpha = \frac{k_a}{2k_b[M]}$$

Taking the limit as $t \to \infty$ gives the final quantity of NO_2 in the wake as

$$[NO_2]_\infty = [NO_2]_0\left\{\frac{\alpha}{\alpha + \frac{[OH]_0}{[\overline{NO_2}]}}\right\}^{\alpha}$$

This expression may be evaluated by assuming $[\overline{NO_2}] = [NO_2]_0$ as a first approximation, calculating $[NO_2]_\infty$ on this basis, and then taking $[\overline{NO_2}] = \frac{[NO_2]_0 + [NO_2]}{2}$ and repeating the calculation.

Results of the calculations are presented in Figure 3-9 in terms of the fraction of NO_2 oxidized to HNO_3, $1 - [NO_2]_\infty/[NO_2]_0$, as a function of the initial ratio $[NO_2]_0/[OH]_0$ for altitudes of interest.

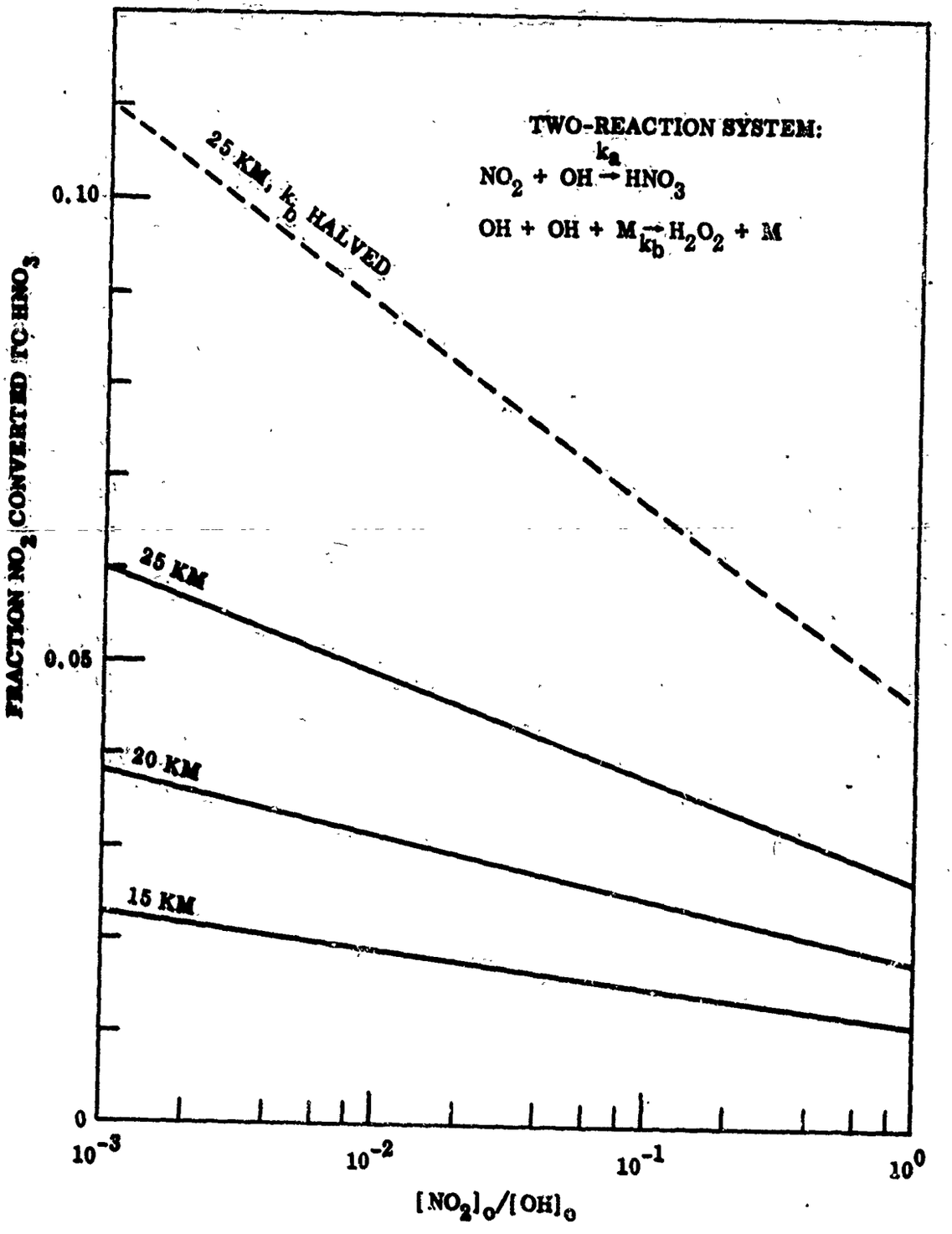

Figure 3-9 Fraction of NO_2 Oxidized to HNO_3 in Infinite Time

In generating Figure 3-9, the rate constant k_a was evaluated using the parameters given in Table 3-1. For k_a the recent expression cited by Crutzen (Ref. 3-28) was used:

$$k_a = 6.3 \times 10^{12} \exp\left(\frac{-170}{T}\right) \frac{2.4 \times 10^{13} [M]}{2.4 \times 10^{13} [M] + 10^{13} / \left(1 + \frac{5000}{T}\right)^4}$$

Here his expression has been converted to mole, cm^3, sec units.

By using these rate data, the three solid lines on Figure 3-9 can be computed. The maximum extent of NO_2 oxidation is only 6 percent and occurs at 25 km when the ratio $[NO_2]_o/[OH]_o$ is reduced to 10^{-3}. Thus it appears that a very conservative upper limit on the possible extent of NO_x depletion by the nitric acid reaction could be placed at 10 percent.

To test the consequences of the uncertainties (about a factor of 2) in the rate constants, the α parameter was doubled (equivalent to doubling k_a or halving k_b), producing the dotted 25-km line shown in Figure 3-9. The corresponding maximum figure is then increased to 11 percent when $[NO_2]_o/[OH]_o$ is 10^{-3}. In the unlikely event that α is multiplied by 4, the maximum goes up to 20 percent. However, since only a fraction of emitted NO_x is actually NO_2, the above conclusion should still be valid.

In present engines, $[NO_x]$ and $[OH]$ are of comparable orders of magnitude in the exhaust jet. Measures to reduce NO_x formation in combustion should not affect the level of OH, so the condition $[NO_2]_o/[OH]_o < 10^{-3}$ implies more than a 1,000-fold reduction of NO_x emissions over present engines. In that event there is no need to predict the fraction of NO_x oxidized to nitric acid because there is no NO_x problem.

3.4.13 Oxides of Sulfur

At the combustor exit, both thermodynamic and kinetic considerations predict the well-known result that virtually all sulfur is present at SO_2. In the nozzle and jet, the kinetics of the sulfur oxides will be dominated by three reactions (Ref. 3-29). These are the homogeneous formation of SO_3

$$SO_2 + O + M \xrightarrow{k_a} SO_3 + M \qquad (3.27a)$$

and its reduction by H or O atoms

$$SO_3 + H \text{ (or O)} \xrightarrow{k_b} SO_2 + OH \text{ (or } O_2) \qquad (3.27b)$$

This mechanism is analogous to the $NO\text{-}NO_2$ cycle in the nozzle and jet discussed previously.

A steady-state analysis can be applied as before, with SO_3 replacing NO_2 as the steady-state species. The analysis gives the expression:

$$\frac{(SO_3)}{(SO_2)_{SS}} = \frac{k_a\,(O)\,(M)}{k_b\,[(O)+(H)]}$$

Recent published values (Ref. 3-29) for k_a are in the range $k_a = 1.5 \times 10^{15}$ to 10^{16} $(cm^5\text{-}mole^{-2}\text{-}sec^{-1})$

For k_b the expression $k_b = 6.5 \times 10^{14} \exp(-10800/RT)$ $(cm^3\text{-}mole^{-1}\text{-}sec^{-1})$ has been used. (Ref. 3-29).

Using k_b above, $k_a = 4 \times 10^{15}$, and nozzle exit properties (T = 954° K), the steady-state relationship yields

$$\frac{(SO_3)}{(SO_2)_{SS}} = 6 \times 10^{-4} \qquad \text{(nozzle exit)}$$

Therefore, it can be concluded that at the nozzle exit there is only a negligible quantity of SO_3.

This is much less than the 1 to 2 percent SO_3/SO_2 ratio commonly observed in cooler combustion systems such as flue gases (Ref. 3-29). The explanation lies in the 10.8-kcal activation energy for the SO_3 destruction reaction, e.g., Eq. (3.27b). Under lower temperature conditions, the SO_3 removal would be greatly slowed. For example, if T = 500°K, but the same radical concentrations are retained, then

$$\frac{(SO_3)}{(SO_2)_{SS}} = 0.1 \qquad (T = 500°K)$$

For such conditions the assumption of steady state might be invalid.

It is instructive to consider just the formation of SO_3 by Eq. (3.27a) and neglect its destructions. If the (O) remains constant, this reaction has a half time

$$t_{1/2} = \frac{\ln 2}{k_a (O) (M)}$$

which corresponds to $t_{1/2} = 1$ sec. As shown in Section 3.4.10 the half time for O atom removal by $O + O_2 + M \rightarrow O_3 + M$ is a great deal less – $0(10^{-3})$ sec. This suggests that O will not be available in the diluted low-temperature wake long enough for a non-negligible fraction of SO_2 to be oxidized to SO_3.

In the presence of water vapor, SO_3 rapidly forms sulfuric acid aerosols. Possible sulfur aerosol reactions in the wake will be discussed more fully in Section 4.2, but it appears from the above discussion that SO_3, and hence acid aerosol, will be absent from the wake.

3.4.14 Comparison of Kinetic Model With Ground Test Data

Test data obtained from the wake of a J-85 engine at sea-level static maximum A/B conditions (Ref. 3-25) indicate substantial CO oxidation in the exhaust jet. This has been confirmed by calculations with the present kinetic model using plume temperature profiles given for the J-85 under similar conditions. A comparison between the test data and computed CO concentrations is given in Figure 3-10. The kinetic model calculations were carried out only for a short distance beyond the nozzle exit. Exact agreement should not be expected since the temperature profile used was not confirmed to be compatible with the test. In addition, the test data have not been corrected for dilution of the plume by surrounding air.

The rapid oxidation of CO behind the exit plane of a J-85 engine operating at sea level is quite a different result from the slow change in CO mole fraction with distance behind a GE-4 engine in supersonic flight in the stratosphere. The kinetic model is able to account for and explain the differences. In both cases the model predicts almost no conversion of NO to NO_2, however, as discussed previously.

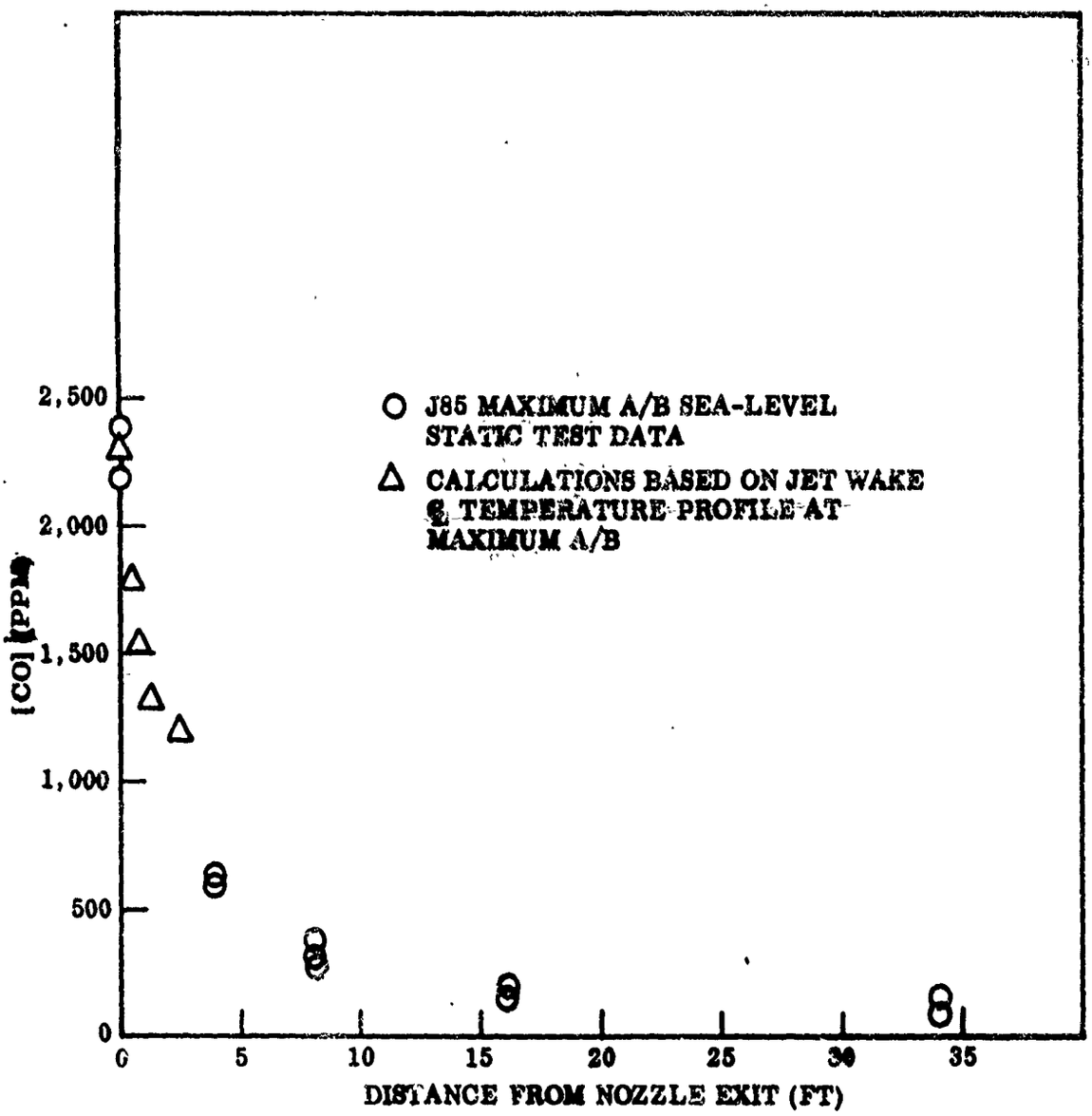

Figure 3-10 Comparison of Kinetic Model With Ground Test Data

3.4.15 Essential Exhaust Reactions

In the light of the complete analysis, many of the reactions in Table 3-1 can be eliminated from consideration. The deletions can be divided into three catagories First, some species are present only in negligibly small concentrations. Providing this condition is not the result of a dynamic balance which can shift (e.g., by the removal of a destructive radical), these species can be neglected. Second, reactions that are very slow in both forward and reverse directions can be eliminated. Third, frequently one direction of reaction can be neglected in comparison to the other. In the kinetic calculations presented in this report the reverse reactions have been included automatically, with the reverse rate constants calculated from the forward rate constants and thermodynamic data. In the wake model program under development, forward and reverse reactions will be treated as completely separate reactions.

On the basis of the first two catagories, all reactions involving the species N and N_2O can be omitted. For all practical purposes N atoms are not present in the engine exhaust. Figure 3-4 and Table 3-4 show that the N_2O is virtually frozen at 0.1 ppm because of slow reactions; this is a tiny fraction (10^{-3}) of the total NO_x, and hence N_2O may be neglected.

As exemplified by Table 3-4, nearly all three body reactions fall into the third category. Only the recombination directions of these reactions need to be considered; the direct thermal disassociation of all species except HNO_3 can be neglected.

A list of the reactions deemed essential for engine exhaust nozzle and jet kinetic calculations is given in Table 3-7. Forward and reverse reactions are tabulated separately and the rate constant parameters are listed in both molar and molecular units for convenience. The indicated references can be found in the reaction rate data reference list (section 3.7) as before. The stated uncertainties in the rate constants are also included under $\pm \log k$ column. No entry appears in this column if no confidence level was given by the evaluator. In such a case, the probable uncertainty can usually be taken to be large.

Table 3-7

ESSENTIAL EXHAUST REACTIONS

	REACTION						LOG10 A (MOLE,CM,SEC)	E(KCAL)	N	LOG10 A (PARTICLES,CM,SEC)	E/1000K K	N	+=LOG K	REF*
1	H	O2		= OH	O		14.340	16.80	.0	-9.440	8.45	.0	.10	7
2	OH	O		= H	O2		13.110	.00	.0	-10.670	.00	.0		7
3	OH	OH		= H2O	O		12.780	1.10	.0	-11.080	.55	.0	.20	7
4	H2O	O		= OH	OH		13.830	18.48	.0	-9.950	9.30	.0	.20	7
5	O	H2		= H	OH		13.250	8.98	1.0	-10.530	4.48	1.0	.10	7
6	H	OH		= O	H2		9.920	7.00	1.0	-13.460	3.52	1.0	.10	7
7	H2	OH		= H2O	H		13.340	5.15	.0	-10.440	2.59	.0	.10	7
8	H2	OH		= H2O	H		13.576	5.20	.0	-10.202	2.62	.0	.30	16
9	H2O	H		= H2	OH		13.970	20.50	.0	-9.810	10.32	.0	.20	7
10	H	O2	M	= HO2	M		15.176	-1.00	.0	-32.584	-.50	.0	.20	7
11	H	OH	M	= H2O	M		23.146	.00	-2.0	-24.418	.00	-2.0	.20	7
12	H	H	M	= H2	M		15.476	.00	.0	-32.088	.00	.0	.20	7
13	O	O	M	= O2	M		17.410	.00	-.9	-30.150	.00	-.9	.30	9
14	O	O	M	= O2	M		18.138	-.48	-1.0	-29.422	-.17	-1.0	.50	17
15	OH	OH	M	= H2O2	M		14.958	-5.10	.0	-32.602	-2.57	.0	.10	7
16	OH	OH	M	= H2O2	M		14.923	-5.30	.0	-32.637	-2.67	.0	.50	16
17	NO	O	M	= NO2	M		15.920	-1.67	.0	-32.640	-.84	.0	.00	5
18	O	O2	M	= O2	M		13.224	-2.10	.0	-34.536	-1.06	.0	.20	17
19	SO2	O	M	= SO3	M		15.681	.00	.0	-31.959	.00	.0	.50	12
20	H	HO2		= OH	OH		14.398	1.90	.0	-9.582	.96	.0	.30	7
21	H	HO2		= H2O	O		13.000	1.00	.0	-10.780	.50	.0		7
22	H	HO2		= H2	O2		13.390	.70	.0	-10.582	.35	.0	.40	7
23	OH	HO2		= H2O	O2		13.000	.00	.0	-10.780	.00	.0		6
24	O	HO2		= OH	O2		13.699	1.00	.0	-10.081	.50	.0		7
25	OH	H2O2		= H2O	HO2		13.000	3.00	.0	-10.780	1.81	.0	.70	16
26	H	O3		= O2	OH		13.204	.00	.0	-10.576	.00	.0	.10	6
27	O	O3		= O2	O2		13.076	.70	.0	-10.704	2.41	.0	.20	17
28	NO	O3		= NO2	O2		11.730	2.40	.0	-12.050	1.21	.0	.20	6
29	CO	OH		= CO2	H		11.748	1.68	.0	-12.032	.54	.0	.50	10
30	CO	OH		= CO2	H		11.491	.50	.0	-12.289	.30	.0	.30	16
31	CO	OH		= CO2	H		11.590	.41	.0	-12.190	.41	.0	.07	9
32	CO2	H		= CO	OH		14.070	25.10	.0	-9.710	12.07	.0	.10	9
33	SO3	H		= SO2	OH		14.012	10.48	.0	-8.966	5.44	.0		12
34	SO3	O		= SO2	O2		14.012	10.88	.0	-8.966	5.44	.0		12
35	SO3	O		= SO2	O2		12.000	.00	.0	-11.780	.00	.0		9
36	HO2	NO		= NO2	OH		11.778	.00	.0	-12.002	.00	.0		16
37	H	HO2		= NO	OH		14.060	1.93	.0	-8.920	.97	.0	.10	6
38	O	NO2		= NO	O2		13.298	1.16	.0	-10.498	.58	.0	.00	6
39	NO	O3		= NO2	O2		11.826	2.45	.0	-11.954	1.23	.0	.20	6
40	NO2	OH		= HNO3			12.387	.09	.0	-11.393	.38	.0	.30	20 (15 bar)

*References in this Table appear as a special reference list in Section 3.7.

Table 3-7 (Cont.)

	REACTION					LOG10 A (MOLE-CM-SEC)	E(KCAL)	N	LOG10 A (PARTICLES-CM-SEC)	E/1000R K	N	+-LOG K	REF	
41	NO2	OH	= HNO3			12.313	.00	.0	-11.467	.00	.0	.3	20	(20 km)
42	NO2	OH	= HNO3			12.160	.00	.0	-11.612	.00	.0	.3	20	(35 km)
43	HNO3	M	= NO2	OH	M	15.200	30.60	.0	-6.580	15.40	.0	1.00	21	
44	CH4	OH	= CH3	H2O		13.453	5.00	.0	-10.527	2.52	.0	.70	16	
45	CH4	M	= CH3	H2		13.710	12.90	.0	-10.070	6.49	.0	.40	9	
46	O	CH4	= CH3	OH		13.300	9.20	.0	-10.480	4.63	.0		15	
47	CH4	OH	= CH3	H2O		13.900	5.70	.0	-9.880	2.91	.0	.00	9	
48	O	CH3	= CH2O	H		13.278	.00	.0	-10.502	.00	.0		10	
49	CH3	O2	= CH2O	OH		10.674	.00	.0	-12.986	.00	.0		15	
50	CH2O	H	= HCO	H2		13.500	4.23	.0	-10.280	2.13	.0		9	
51	CH2O	M	= HCO	H2		13.000	2.00	.0	-10.780	1.01	.0		10	
52	CH2O	OH	= HCO	H2O		13.900	2.50	.0	-9.906	1.20	.0		9	
53	CH2O	OH	= HCO	H2O		13.780	.00	.0	-10.060	.00	.0	1600	10	
54	CH2O	O	= HCO	OH		11.602	4.00	.6	-12.178	2.01	.6		10	
55	HCO	O	= CO	OH		11.250	.00	.5	-12.526	.00	.5		10	
56	HCO	OH	= CO	H2O		11.040	.00	.5	-12.740	.00	.5		10	
57	HCO	H	= CO	H2		12.175	.00	.5	-11.605	.00	.5		10	

Table 3-7 may not constitute a completely sufficient list since unknown (e.g., hydrocarbon) reactions undoubtedly are possible in addition to the ones shown (e.g., the methane oxidation sequence). The addition of other HC reactions would not cause any foreseeable change of such a magnitude as to have an environmental impact. On the contrary, the higher hydrocarbons tend to have more reactive groups such as reactive (α) hydrogen, tending to speed up termination reactions. Thus, the previous conclusions attributed to rapid removal of inorganic radicals by unburned hydrocarbons are apt to be even more strongly reinforced by inclusion of oxidation mechanisms for the higher weight unburned hydrocarbon fractions. Of course, "unknown" reactions need not be limited to those involving organic species.

3.4.16 Sensitivity of Results to Input Data

The objective of a sensitivity analysis is to identify those factors to which computed results are most sensitive. In the present case, the computed results will be the final wake concentrations of species with a potentially significant climatic impact. Obviously, the stated objective cannot be achieved fully until the model is developed and exercised during the next phases of the program. However, some discussion is warranted there, because identification of the essential features of the model has been dependent throughout on the data that have been consulted.

The two categories of results for which sensitivity analyses are needed are:

- Dependence of model features on uncertainties in the data underlying the model formulation
- Sensitivity of results computed by the model to input data uncertainties

In either of the above cases, a systematic investigation may be divided into two parts: (1) sensitivity to uncertainties in rate constants, and (2) sensitivity to input species concentrations.

The simplified chemical model that is currently being developed has evolved from broader considerations. The most important factor that can influence the nature of the

model is the possible extent of conversion of NO_x to HNO_3. This is discussed in section 3.4.12, where it is seen that the maximum uncertainties in radical recombination rate constants are insufficient to allow for significant formation of HNO_3 in the near field. Even for a worst-on-worst situation corresponding to maximum uncertainty in each rate constant, in opposite directions, and for an unrealistically cooperative assumption that all NO_x is NO_2, the fraction converted to HNO_3 only begins to approach significent values in terms of climatic impact analyses. If this had not been the case, i.e., if HNO_3 formation appeared to be extensive, then a much more complicated and general model, cumbersome and expensive to run, might have been necessary.

The model will "turn on" at the nozzle exit plane. However, the model characteristics will depend on the various simplifying relationships discovered in the chemistry farther upstream — i.e., within the nozzle. For purposes of illustration, one important factor mentioned previously — the NO which is converted to NO_2 — will be discussed in terms of its sensitivity to uncertainties in a specific reaction. This example is chosen to illustrate the principles involved in performing the sensitivity analysis.

Table 3-7 lists the set of essential reactions needed for the kinetics model and shows the rate-constant uncertainties given by the evaluators. Sensitivity to rate-constant uncertainties may be handled parametrically as illustrated below for one NO oxidation reaction.

It is known that, under certain conditions, the hydroperoxyl radical can rapidly oxidize nitric oxide, as follows:

$$HO_2 + NO \xrightarrow{k_{36}} NO_2 + OH$$

The value for k_{36} listed in Table 3-7 is a "latest upper limit" estimate. The published value for $k_{36} = 1.25 \times 10^{11}$ cm^3/mole-sec had been used previously. From the computer output, the five-fold increase in k_{36} results in only a 0.25

increase in NO_2 concentration. Thus, NO_2 is not found to be particularly sensitive to k_{36} under the present conditions. As will be seen below, this simple "substitution of values, run the computer" approach is often wasteful and unnecessary.

The sensitivities of species concentrations to their input values at the throat can be assessed readily with Figures 3-4 to 3-7. Where there are reactions tending to drastically and rapidly alter initial concentrations — illustrated by the strong non-equilibrium production of radicals at 10 cm downstream from the throat as discussed in section 3.4.4, for example — the sensitivity to initial concentration is very small. The rapid destruction of NO_2 seen in Figure 3-4 shows this — where an artificially high initial concentration of NO_2 was used. Such cases can be identified easily by rapid approach to steady-state levels that are very different from the starting concentrations. On the other hand, species concentrations that do not change appreciably from their starting values may or may not be highly sensitive to those values. Obviously, any inert species will have concentrations at any point which are linearly dependent on their initial values. Although the NO profile in Figure 3-4 is flat, it certainly does not follow that NO is inert. It behaves so only because initial NO_2 concentrations are so small. If the intial NO_2/NO ratio were large, say one-half or more, then there would be a very rapid increase in NO from its initial to its steady-state value.

To aid in discussion of sensitivity of a species to local concentrations of a particular reactant of associated rate constants, or to uncertainties in such data, the HO_2 radical mentioned above is again a convenient choice. It might be supposed, for example, that sufficiently high levels of HO_2 would raise the NO_2 levels. The primary destruction reaction tending to keep NO_2 small in Figure 3-4 is attack of NO_2 by H atoms, which are present in high concentration. However, in many private discussions it was frequently asserted that high concentrations of hydrogen atoms implied high HO_2 concentrations because of the following rapid reaction:

$$H + O_2 + M \rightarrow HO_2 + M$$

The relationship of HO_2 to H can be assessed readily with the help of Table 3-4, which shows that reactions 21, 22, and 25 define the major formation and destruction processes for HO_2. In this event the rate expression is

$$\frac{d[HO_2]}{dt} = k_{21}[H][O_2][M] - (k_{22} + k_{25})[H][HO_2]$$

When HO_2 is in a steady state, however, the following equation may be derived

$$\left(\frac{[HO_2]}{[M]}\right)_{SS} = \frac{k_{21}}{k_{22} + k_{25}}[O_2]$$

Thus, the HO_2 concentration is independent of H. This condition obviates the need for a parametric sensitivity study based on uncertainties in the concentrations of hydrogen atoms. Also, it is clear that the above equation defines the sensitivity of HO_2 formation to uncertainties in the rate data for reactions 21, 22, and 25. Hence, a parametric study is again unnecessary.

Considerations of the above types have been made throughout the work to define the model. It is felt that, except for "unknown" reactions, the sensitivities of the chemical model features to rate data have been treated adequately. As was indicated, if OH recombination and NO_2 oxidation rates had been vastly different than they are, a multidimensional model capable of handling, for example, cross stream and radial diffusion reactions of OH and NO_2 might have been needed. Fortunately, this is not the case, and a simple stream tube approach should suffice.

Finally, sensitivity of the output results calculated by the model to uncertainties in its input data, such as measured exit-plane exhaust concentrations, can be better defined in subsequent phases of the program, after final model programming and executions for test cases of interest are in progress.

3.5 SIGNIFICANCE OF UNBURNED HYDROCARBONS

3.5.1 General and Summary

Aircraft turbojet engines without afterburners yield extremely low concentrations of unburned hydrocarbons (Ref. 3-30). However, with afterburning "reheat" the concentrations of unburned hydrocarbons increase drastically (Refs. 3-31 through 3-33). With maximum reheat, the unburned hydrocarbons may equal carbon monoxide concentration levels; i.e., hydrocarbon levels of over 1,000 ppm may be present in the exhaust. Even at maximum reheat, overall equivalence ratios are still considerably less than 1, and there is ample oxygen present to burn these hydrocarbons in the hot exhaust stream. In fact, their presence in the first place cannot arise from thermochemical limitations, but must depend on reaction and mixing rate limitations of combustion in the afterburner. As seen previously, the concentrations of reactive species – i.e., O, H, and OH – may be high in this exhaust mixture. It appears unlikely that the requisite rate constants and detailed mechanisms can be assembled readily for meaningful chemical-kinetics numerical analysis of this complex system. However, it is clear that concentrations of unburned hydrocarbons in the final wake will be equal to or less than values based on their measured concentrations at the exit plane after accounting for appropriate dilution in the wake. The question then arises whether it is necessary to specify these concentrations with any greater accuracy than an appropriate upper limit corresponding to freezing in the nozzle and subsequent dilution. In the following arguments it is shown that the impact of the added unburned hydrocarbons on the chemical processes occurring in the wake, dispersion, and transport regimes and, ultimately, their climatic impact, is negligible.

Four reaction categories are considered, which encompass the spectrum of thermochemical hydrocarbon reactions in the stratospheric flight environment. Results of these considerations may be summarized for each of the four categories as follows:

- Hydrocarbons do not enter into long chain-length catalytic cycles that can affect ozone. The reactions degrade the hydrocarbon chains, and the maximum total effect on ozone is negligible.

- Although hydrocarbon reactions that remove NO_x appear to be possible in the stratosphere, for mechanistic reasons and because the total quantities of added hydrocarbons are dwarfed by the ambient methane, the impact on both the local rate and final total NO_x removal by the hydrocarbons added from the exhaust is negligible.
- The destruction of oxygen atoms by organics in the exhaust is not competitive with faster processes. Thus, the impact of unburned hydrocarbons on exhaust SO_x and NO_x is small. If the concentrations of unsaturated hydrocarbons in the exhaust are well below the SO_2 emission levels, the hydrocarbon influence on particulate formation is negligible.
- Reactions with organic radicals that can accelerate conversion of NO to NO_2 in the stratosphere are of negligible importance for at least four reasons:
  - Competing rates are faster.
  - Processes are noncyclic.
  - Stable products are formed.
  - Hydrocarbons are degraded.

3.5.2 Hydrocarbon/Ozone Catalytic Chains

By analogy to NO_x and HO_x catalytic cycles that can conceptually destroy ozone, one is tempted to investigate RO_x cycles, i.e.,

$$RO\cdot + O_3 \rightarrow RO_2\cdot + O_2$$

$$RO_2\cdot + O \rightarrow RO\cdot + O_2$$

or

$$R\cdot + O_3 \rightarrow RO\cdot + O_2$$

$$RO\cdot + O \rightarrow R\cdot + O_2$$

The net effect in either case is

$$O + O_3 \rightarrow 2O_2$$

Aside from difficulties in achieving the first reactions on each of these cycles, the main point to be made is that R· is not N or H; i.e., R is not stable and cannot "go around the cycle" very many times. First of all, there is competition for RO by molecular oxygen, which is in great excess over O_3 or O:

$$RO\cdot + O_2 \rightarrow \text{aldehyde} + \text{peroxyl}$$

If RO is CH_3O at room temperature*

$$CH_3O\cdot + O_2 \rightarrow CH_2O + HO_2\cdot, \qquad k = 3 \times 10^{-18}\ cm^3/\text{molecule sec}$$

Although this rate constant is as much as six orders of magnitude lower than those for some of the competing reactions, the concentration of O_2 is at least six orders of magnitude higher than the competing reactant levels. For example, the oxygen atom and hydroxyl radical concentrations are about 11 orders of magnitude lower than molecular oxygen levels at 20-km altitude.

---

*All rate constants are taken from the compilation in Ref. 3-34 unless otherwise indicated.

The formaldehyde formed by the above reaction is relatively stable and is slowly converted to carbon dioxide by several reactions:

$$CH_2O + OH \rightarrow CHO\cdot + H_2O, \qquad k = 1.6 \times 10^{-11}$$

$$CH_2O + h\nu \rightarrow CHO\cdot + H$$

$$CHO\cdot + O_2 \rightarrow CO + HO_2\cdot, \qquad k > 2 \times 10^{-15}$$

$$CO + OH \rightarrow CO_2 + H$$

Secondly, the reactions are energetic and lead to decomposition of the radicals.

For example, from thermochemical estimates (Ref. 3-35) one finds that the second reaction in the proposed catalytic cycle is highly exothermic:

$$RO_2\cdot + O \rightarrow RO\cdot + O_2 \qquad \Delta H \sim -60 \text{ kcal/mole}$$

It is unlikely that all of the reaction energy would be partitioned solely among translational modes of the products. It is well known that very little residual energy in the alcoxy radical will result in its decomposition. Ethoxy radicals, for example, decompose rapidly with energy inputs as small as 10 kcal/mole (Ref. 3-36)

$$CH_3CH_2O \rightarrow CH_3\cdot + CH_2O$$

The products would react further, formaldehyde going to CO_2 as previously discussed, and $CH_3\cdot$ entering the degradative cycle thus:

$$CH_3\cdot + O_2 \rightarrow CH_3O_2\cdot, \qquad k > 2.5 \times 10^{-15}$$

$$\Delta H = -27.3$$

One may write a large number of mechanisms for stepwise degradation of RO. One such sequence follows, where NO_x is also present:

$$RCH_2O\cdot + O_2 \rightarrow RCHO + HO_2\cdot$$

$$RCHO + OH \rightarrow RC\dot{=}O + H_2O, \qquad k \sim 3\times10^{-13} \ (R \equiv CH_3)$$

$$RC\dot{=}O + O_2 \rightarrow R\overset{O}{\overset{\|}{C}}O_2\cdot, \qquad k \sim 2\times10^{-15}$$

$$R\overset{O}{\overset{\|}{C}}O_2\cdot + NO \rightarrow RCO_2\cdot + NO_2, \qquad k \sim 1\times10^{-12}$$

$$RCO_2\cdot \rightarrow R\cdot + CO_2, \qquad k \sim 1\times10^{12}$$

Also, reaction of the alkoxy radical with nitrogen dioxide gives stable products.

3.5.3 Hydrocarbon-Assisted Nitric Oxide Oxidation

Acceleration of the reaction

$$O_2 + NO \rightarrow NO_2$$

by intermediates such as

$$O_2 + R\cdot \rightarrow RO_2\cdot$$

$$NO + RO_2\cdot \rightarrow NO_2 + RO\cdot$$

will affect ozone through NO_2 photolysis if the net rate exceeds the rate of nitric oxide oxidation by ozone, i.e.,

$$NO + O_3 \rightarrow NO_2 + O_2$$

However, this is not likely to be the case as indicated in the following methane-derived radical reactions (photooxidation schemes involving hydrocarbons in NO oxidation have been discussed by many authors – Refs. 3-37 and 3-38):

$CH_4 + OH \rightarrow CH_3 + H_2O$,	$k \approx 10^{-14}$
$M + O_2 + O \rightarrow O_3 + M$,	$k_2 \approx 10^{-15}$ (M taken as ≈ 0.1 atm)
$CH_3 + O_2 \rightarrow CH_3O_2\cdot$,	$k \approx 10^{-15}$
$CH_3O_2\cdot + NO \rightarrow NO_2 + CH_3O\cdot$,	$k \approx 10^{-13}$
$NO_2 + CH_3O\cdot \rightarrow CH_3ONO_2$,	$k \approx 10^{-12}$
$NO + O_3 \rightarrow NO_2 + O_2$,	$k \approx 10^{-14}$

The steady-state concentrations of $CH_3O_2\cdot$ should be much lower than the ambient ozone that is about 1 ppm at 20 km. Comparison of the first three of these reactions illustrates this, because $(O) \approx (OH)$ and $(O_2) >> (CH_4)$. Proper treatment would of course include all formation and destruction reactions. The third reaction is necessary to convert the slowly formed CH_3 to $CH_3O_2\cdot$; it seems clear that $CH_3O_2\cdot$ will be present only in small concentration. Comparison of the fourth and last of the foregoing reactions shows that oxidation of NO by O_3 should be faster than the hydrocarbon-assisted oxidation.

Attack of the radicals has been discussed previously, making their regeneration and participation in cyclic peroxyl oxidation of NO unlikely. Also, reaction products can form other stable products, as illustrated by the fourth and fifth of the foregoing reactions taken in sequence.

Finally, the energetic reactions lead to degradation of the radicals, removing them from the system, as discussed previously.

3.5.4 Reactions Leading to Stable Hydrocarbon-NO_x Products

Reactions of NO_x that are of interest are given below

$$R\cdot + NO \rightarrow RNO \text{ (nitrosoalkane)} \quad (3.28)$$

$$R\cdot + NO_2 \rightarrow RNO_2 \text{ (nitroalkane)} \quad (3.29)$$

$$RO\cdot + NO \rightarrow RONO \text{ (alkylritrite)} \quad (3.30)$$

$$RO\cdot + NO_2 \rightarrow RONO_2 \text{ (alkylnitrate)} \quad (3.31)$$

$$R\cdot + NO_2 \rightarrow RONO \text{ (alkylnitrite)} \quad (3.32)$$

$$RCO_2\cdot + NO_2 \rightarrow RCO_2NO_2 \text{ (peroxyacetyl nitrate, PAN)} \quad (3.33)$$

Reactions (3.29) and (3.31) give stable, chain ending products. All the reactions result in NO_x being tied up with an organic moiety. Most of these reactions, excluding Eq. (3.33) have been studied in depth by Phillips and Shaw (Ref. 3-39). The products in Eqs. (3.28), (3.30), and (3.32) are not particularly stable to ultraviolet (uv) photolysis, whereas Eqs. (3.29) and (3.31) products are quite stable to uv. They do not absorb much energy above 2,000 Å and can be considered to be stable, long-lived reaction products. Certainly the nitroalkanes should be as stable as PAN. All these reactions are exothermic, based on the thermochemical data given in the treatise by Benson (Ref. 3-35).

Oxygen atom and hydroxyl radicals can react with the nitroalkanes and the nitrates to form nitroalkane radicals. These radical species are relatively unreactive and should not contribute to catalytic chain cycles with ozone. The chemistry of the alkyl nitrate radical ($RCHONO_2$) is quite similar to that of the nitroalkyl radical ($RCHNO_2$).

It is conceivable that high concentrations of hydrocarbons in the exhaust relative to ambient levels might lead to some NO_x capture. As shown previously, $CH_3^{\cdot}$ might be present in the exhaust jet, leading to the following reaction:

$$CH_3^{\cdot} + NO \rightarrow CH_3NO \qquad \Delta H = -39.6$$

However, thermochemical and photochemical stabilities of nitrosoalkanes are not particularly great. The corresponding methyl radical reactions with NO_2 would be limited by the small NO_2 concentrations in the near wake.

Possible NO_x-removing reactions of unburned hydrocarbons in the wake itself are illustrated below for radicals derived from reactions of methane with ambient oxidizing radicals. The rate constants are taken from Niki (Ref. 3-34), and the thermochemical estimates are based on Benson's tables (Ref. 3-35):

$$CH_3^{\cdot} + NO_2 \rightarrow CH_3NO_2 , \qquad k = 2.8 \times 10^{-12} \text{ cm}^3/\text{molecule sec}, \quad \Delta H = -33 \text{ kcal/mole}$$

$$CH_3^{\cdot} + NO_2 \rightarrow CH_3O\cdot + NO , \qquad k = 5.4 \times 10^{-12}, \quad \Delta H = -17$$

$$CH_3O\cdot + NO \rightarrow CH_3ONO , \qquad k = 6.7 \times 10^{-13}, \quad \Delta H = -41$$

$$CH_3O\cdot + NO_2 \rightarrow CH_3ONO_2 , \qquad k = 2 \times 10^{-12}, \quad \Delta H = -41$$

$$CH_3O_2\cdot + NO \rightarrow NO_2 + CH_3O , \qquad k = 2 \times 10^{-13}, \quad \Delta H = -17$$

In the wake, relatively high concentrations of hydrocarbons might promote some of the foregoing reactions, as illustrated below

$$CH_4 + OH \rightarrow CH_3^{\cdot} + H_2O , \qquad k \approx 10^{-14}$$

$$CH_3^{\cdot} + NO_2 \rightarrow CH_3NO_2 , \qquad k \approx 10^{-12}$$

The second step is fast but must compete with

$$CH_3 + O_2 \rightarrow CH_3O_2^{\cdot}, \qquad k \approx 10^{-15}$$

The latter reaction is very fast because of the high O_2 concentration.

It is important to note the high ambient concentrations of methane – i.e., about 5×10^{12} molecule/cm^3 or 1 ppm at 20 km (Ref. 3-40). The total methane contribution from an SST fleet is estimated to add only 0.5 ppb to the background (Ref. 3-41).

Thus, in the long run, the ambient atmospheric reactions should dwarf any effects of the hydrocarbons added from the aircraft exhaust. If ambient methane can be shown to participate in reactions that cause a significant net NO_x depletion the conclusions of H. S. Johnston and others regarding ozone destruction would have to be modified.

3.5.5 Comparison of Roles of NO_x and Hydrocarbons in Urban Atmospheres With Their Possible Roles in Stratosphere

It is well known that nitrogen oxides are a necessary ingredient of photochemical smog, specifically ozone production in urban atmospheres. The question may arise, therefore, as to why NO_x, which helps produce ozone at sea level, should help to destroy it in the stratosphere. Also, it has been indicated that hydrocarbons are not expected to contribute significantly to stratospheric smog even though it is well known that they are of key importance in urban smog formation. The underlying explanation stems from the fact that the intense uv radiation in the stratosphere dissociates molecular oxygen to form O atoms, whereas at sea level this effect is of little significance. However, NO_2 may be photolyzed in both environments thereby providing a potential source of O atoms at sea level when NO_x is added. At sea level, the presence of NO_x alone is insufficient for production of ozone because photolysis of NO_2 also produces nitric oxide, a good oxygen atom scavenger. Since most of the NO_x is added initially as nitric oxide, it is oxidized by any O atoms produced in preference

to oxidation of molecular oxygen to form ozone. It is here that the hydrocarbons added to urban atmospheres play a major role in formation of photochemical smog. They provide a path by which molecular oxygen can be used to oxidize the nitric oxide to NO_2. Once the nitric oxide has been depleted sufficiently, the photolysis of NO_2 and, consequently, production of O atoms leads to ozone formation, since there is now a greatly reduced competition for the O atoms from nitric oxide.

The details of the hydrocarbon role in helping molecular oxygen to convert NO to NO_2 are complicated. The key species in the oxidation steps are organic peroxy radicals. Also, carbon monoxide can play a role through production of hydrogen atoms during its slow oxidation. The hydrogen atoms react with molecular oxygen and these products, in turn, can oxidize carbon monoxide, liberating more hydrogen atoms. The key species in this cycle is the hydroxyl radical, which is currently believed to be the important intermediate in converting molecular oxygen to the organic peroxy radicals.

Figure 3-11 shows some typical chains whereby the hydrocarbon species provide paths for the ground level oxidation of nitric oxide and other species initiated by hydroxyl radicals. It is noteworthy that when the organic peroxy radicals oxidize NO, they are converted to alkoxy radicals. These decompose to stable carbonyl – e.g., formaldehyde and a carbon-centered radical. The reactions continue until degradation of the original hydrocarbon molecule into stable oxidized products is complete.

Thus, in polluted urban atmospheres, there is no ozone until the hydrocarbons have provided a path that converts nitric oxide to NO_2. It is the photolysis of the NO_2 and the lack of competition from nitric oxide, which has been reduced to low concentrations, that liberates and increases the levels of oxygen atoms and, consequently, the ozone level through reaction with molecular oxygen. Eventually, ozone begins to react with unsaturates. The ozonolysis reactions lead to nitrogen-containing products.

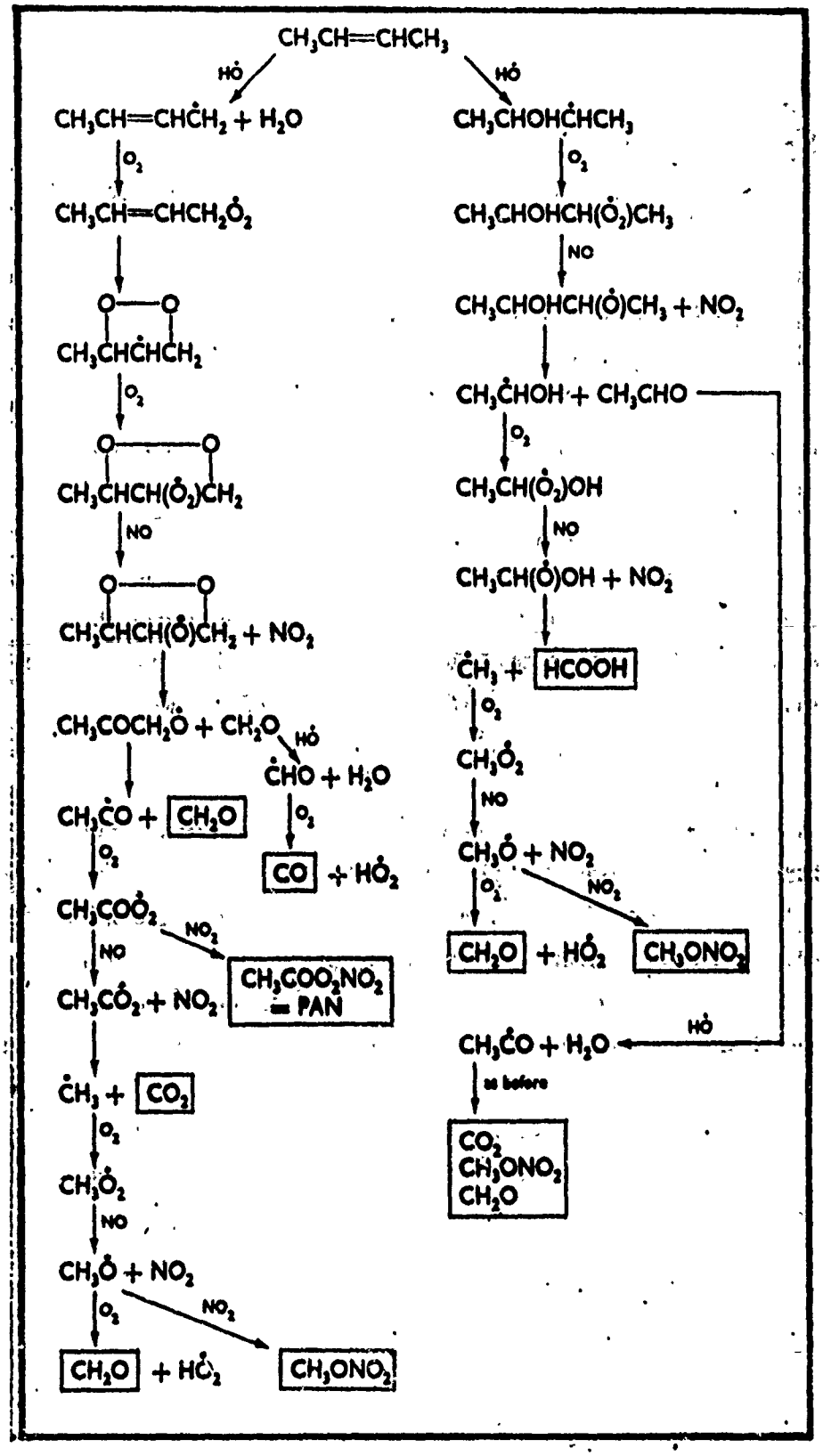

Figure 3-11 Photo-Oxidation of trans-but-2-ene in the Presence of Nitric Oxide and Nitrogen Dioxide: Skeleton Reaction Scheme Involving Hydroxyl Radicals.

(Taken From J. A. Kerr et al., Chemistry in Britain, 8, 252 (June 1972)

The situation in the stratosphere is quite different because the initial ozone and oxygen levels are quite high and the photodissociation of molecular oxygen tends to keep them high. Thus, ample mechanism for oxidizing nitric oxide to NO_2 is already present in the stratosphere. The oxygen atom concentrations are sufficiently high to assist in conversions of NO_2 back to nitric oxide via the reaction

$$NO_2 + O \rightarrow NO + O_2$$

Thus, the production of O atoms from the photolysis of NO_2 in the stratosphere affects the destruction of ozone through the NO_x catalytic cycle. The reasons for this will be seen more clearly in Section 4.

3.6 CHEMICAL REACTIONS IN TURBULENT MEDIUM

3.6.1 Introduction

An important question arising in this and other programs is relative to the effect of turbulence upon the chemistry. To gain some insight into this problem without claiming to have solved it, we will review basic work supported under the Lockheed Independent Research program in connection with missile reentry applications. Derivations and results of this work will be presented elsewhere.

To clarify the discussion, a brief description is given on the effect of turbulence in a fluid on a parcel of contaminating fluid injected into it.

It has long been recognized that turbulence causes concentration fluctuations. The earliest related work on this subject, which is quoted in the recent literature, is over 20 years old. It is credited to the Russian Obukhov (Ref. 3-42) and the American Corrsin (Ref. 3-43). Their work dealt directly with temperature fluctuations. The methodology is not changed significantly when one treats concentration fluctuations, which may be caused by temperature fluctuations.

Concentration fluctuations are modeled in the following manner. A contaminant fluid is added to a background fluid undergoing turbulent motion. Turbulence is defined by an irregular fluctuating component in the velocity field of the background fluid. The additive fluid particles move with the local fluid velocity because of collisions with the fluid background. These particles thereby acquire an overall drifting component of motion, due to the mean flow, and an irregular motion, or jitter, due to the fluctuating velocity field of the background fluid. They behave as a tracer element or dye spot of the background motion. It is assumed that the tracer does not affect the background motion, which is determined by some external energy source. In this sense the tracer is called a dynamically passive additive. Another source of concentration fluctuations is due to a random distribution of the initial concentrations. Much of the recent literature models the turbulent medium in the limit of fast reaction by ordinary differential equations in time, subject to these random initial conditions. We also call such models turbulent, despite the absence of the basic velocity contribution to real turbulence.

The tracing is not precise because of diffusion, which smears the additive concentration and thereby dilutes it. Since no reactions take place in this model, the total number of each smeared additive species is conserved. The model is called the conserved passive additive model.

Experimental verification of this effect is performed most easily when the passive additive is simply a hot gas added to the background fluid. The temperature fluctuation is then observable directly.

It is conceptually important to distinguish turbulent diffusion from other basic processes that appear to have a formal similarity. For example, there is an analog between turbulent diffusion of a single fluid particle and Brownian motion. When the Lagrangian viewpoint is used to follow the fluid particle in a homogeneous turbulent medium, a long-time behavior for the mean distance traveled by the particle is derived as proportional to the first power of time (Ref. 3-44). This dependence is identical with the Einstein result for the mean displacement of a Brownian particle (Ref. 3-45). A Brownian particle such as in an aerosol is larger in mass than the molecules that surround it. The molecular background bombards the Brownian particle in a temporally random manner, causing it to suffer small angle deflections. These deflections are thus statistical in origin and are unimportant for the large fluid parcels considered in the turbulence problem. Thus, Brownian motion per se is not the process underlying turbulent diffusion.

In the work discussed here, the Eulerian or field viewpoint is used throughout. The mean displacement of a particle does not appear in this formalism. This displacement is not to be confused with a characteristic "local" length scale defined in terms of one of the partial differential equations governing the dynamics of the turbulence. One such, for example, is the concentration microscale (Ref. 3-46) which is defined in a manner analogous to the Taylor microscale, or dissipation length, for velocity fluctuation (Refs. 3-47 and 3-48). Finally, a calculation describing the evolution of a contaminant spot size with time, based on the Eulerian viewpoint, shows that when

strain is present the spot area grows much faster than the first power of time (Ref. 3-46). It is this time dependence that characterized the homogeneous turbulence result as well as Einstein's Brownian motion result.

By 1958 Corrsin (Ref. 3-49) had included the case of a single chemical reactant in the preceding model of the dynamically passive additive. Formally, this change requires only a simple modification of the equations governing the passive additive model.

More recently, O'Brien, 1971 (Ref. 3-50) considered the problem of two reactants undergoing a second-order reaction. A significant result of his work (Refs. 3-50 and 3-51) is that the concentration fluctuations can be large compared with mean concentration values.

In a quiescent gas it is the mean concentrations that are measured directly. The equations governing the time and space behavior of the concentration (often assumed to be spatially uniform) are in this case governed by the mean quantities alone. When turbulence is present, the time and space behavior of the mean quantities depends on the correlations between the fluctuating components of the concentration.

Later work by du P. Donaldson and Hilst (Refs. 3-52 and 3-53) includes a discussion of the possibility of fluctuations in the reaction rate constant affecting evolution of the mean concentrations. Although we do not agree with the equations of Ref. 3-52, the concept must be examined because of the exponential dependence of the backward reaction upon temperature.

The idea is as follows. The reaction rate constant is a function of temperature – to a significant degree in the bond-breaking direction. The temperature of a gas is a macroscopic quantity defined by an average over a one-particle distribution for the molecular velocities. (It is presumed that a large number of molecules are involved in this averaging process.) Then the reaction rate constant is itself a macroscopically

defined quantity. Because of the energy put into the fluid system (e.g., in the form of a shearing flow), large local temperature fluctuations can exist in the fluid. These can, in turn, cause the reaction rate constant k to vary from point to point. It may be convenient to express this variation in $k(T)$ as a part due to the mean temperature $\bar{T}$ and a part due to the fluctuations in temperature ΔT.

Then

$$\begin{aligned} k(T) &= k(\bar{T} + \Delta T) \\ &\simeq k(\bar{T}) + \left.\frac{\partial k}{\partial T}\right|_{T=\bar{T}} \Delta T \\ &= \bar{k} + k' \end{aligned}$$

where

$$\bar{k} = k(\bar{T}),$$

$$k' = \left.\frac{\partial k}{\partial T}\right|_{T=\bar{T}} \Delta T$$

At this point, we rename $k(T)$ as k_{turb} to emphasize that, although it contains the ordinary reaction rate constant $k(\bar{T})$, which appears in the chemical kinetics literature, k_{turb} is not this familiar rate constant, and should not be confused with it. Care should be exercised in the literature to avoid confusion.

3.6.2 Discussion of Previous Work

The problem of chemical reaction of two species in a turbulent flow is posed as a set of partial differential equations subject to appropriate boundary conditions. In turbulent flow one measures the average values of quantities that have a fluctuating component. In general, the probability distribution function for the fluctuating field

of velocity, pressure, and concentration is unknown. Thus, the averaged quantities replace the precise dependent variables that are solutions of the set of partial differential equations. Unfortunately, because of the nonlinearity of the convective time derivative and, with second-order chemical reactions, the nonlinear coupling of the concentration variables, the number of averaged equations is less than the number of new unknown dependent variables that are the averaged quantities. The problem of closing the set of equations (known as the closure problem) has beset the theory of the turbulence since its beginning.

The traditional method of resolving the closure problem is to relate averages of products of n-fluctuating quantities to averages of products of (n-1)-fluctuating quantities by means of "mixing length" parameters that are determined experimentally. Donaldson and Hilst (Ref. 3-53) use this approach. O'Brien (Ref. 3-50), on the other hand, assumes a closure hypothesis for the second-order reaction term that contains no arbitrary parameters with which to fit the data. It appears, however, that in treating the diffusion terms for the full diffusion-reaction problem, O'Brien must introduce the traditional mixing length approximation; however, he does not discuss this problem. For his closure scheme, he claims the advantage that it guarantees the required positive definiteness of the mean-square concentration fluctuations.

O'Brien has achieved some numerical solutions for the mean concentration and the root-mean-square (rms) fluctuations in concentration for the case in which diffusion effects are negligible. He finds the rms fluctuations can be large. In his work no consideration is given to the possibility of thermal fluctuation contributions to the reaction rate constant. Donaldson and Hilst discuss briefly the problem of fluctuation contributions to the reaction rate constant, but their formulation does not take into account the fact that the backward and forward reaction constants have significantly different temperature dependencies. They have not yet obtained solutions for the concentration variable.

3.6.3 Characteristic Times

It is possible to estimate the importance of diffusion relative to chemical reaction in determining the behavior with time for the concentration of one of two species reacting in the presence of turbulence. This crude estimate is based on an equation describing the evolution in time of the single space point correlation for the fluctuating components of the two species $\overline{C_1' C_2'}$. Here the subscripts denote the two reactants; the bar denotes an averaging process, and the primed quantities are the fluctuating parts of the respective concentration variables. This equation can be written symbolically in the form

$$\frac{\partial}{\partial t} \overline{C_1' C_2'} = \frac{\delta}{\delta t} \overline{C_1' C_2'}\Big|_d + \frac{\delta}{\delta t} \overline{C_1' C_2'}\Big|_c \tag{3.34}$$

where the first term on the right-hand side (rhs) of the equation denotes the diffusion terms, and the second term denotes the chemistry terms. The diffusion terms are proportional to the diffusion coefficient D, while the chemical reaction terms are proportional to the reaction coefficients k_i ($i = 1, 2$).

The size of the diffusion term in this equation is next compared with that of the chemistry term. For this purpose it is convenient to use Eqs. (15) and (20) of Ref. 3-53 for the rhs of Eq. (3.34). An approximation is sought for the rhs to reduce Eq. (3.34) to the form

$$\frac{\partial}{\partial t} \overline{C_1' C_2'} = - (\tau_d^{-1} + \tau_c^{-1}) \overline{C_1' C_2'} \tag{3.35a}$$

Integrating, one obtains

$$\overline{C_1' C_2'}\,(t) = \overline{C_1' C_2'}\,(t = 0)\, e^{-t/T} \tag{3.35b}$$

where $T = (\tau_d^{-1} + \tau_c^{-1})^{-1}$, τ_d^{-1} is the rate of decay of the correlation due to diffusion, and τ_c^{-1} is the rate of decay due to the chemistry.

The relative importance of the two terms in Eq. (3.35a) is evidently determined by the relative magnitude of the two rates or, equivalently, by the ratio N (Ref. 3-54)

$$N = \frac{\tau_c^{-1}}{\tau_d^{-1}} = \frac{\tau_d}{\tau_c} \tag{3.36}$$

$N >> 1$ implies a diffusion limited reaction, and $N << 1$ corresponds to a reaction controlled by the chemistry, because the slowest process limits the rate at which a reaction can go.

The validity of approximating Eq. (3.34) by Eq. (3.35a) depends on the justification for discarding certain terms in the exact equation. In the case of the chemistry terms, this approximation amounts to a prescription for discarding all the self-correlative terms for the concentration fluctuations. This approximation scheme is not founded on physical grounds. It is to be justified a posteriori by comparison with the results of a more precise calculation. Its usefulness resides in the fact that it leads to a tractable way of obtaining some needed numbers.

Thus, one obtains the approximate equality

$$\left.\frac{\delta}{\delta t}\,\overline{C_1' C_2'}\right| \simeq -(k_2 \bar{C}_1 + k_1 \bar{C}_2)\,\overline{C_1' C_2'} \equiv \tau_c^{-1}\,\overline{C_1' C_2'} \quad , \tag{3.37}$$

where $\tau_c = (k_2 \bar{C}_1 + k_1 \bar{C}_2)^{-1}$, $k_2 = k_1 (M_2/M_1)$, and M_i is the molecular weight of species i.

The expression above for τ_c is identical with the τ_c obtained in Ref. 3-54. In the present work, τ_c was obtained by approximating the chemistry term of Eq. (3.34) $\delta\,\overline{C_1' C_2'}/\delta t$, in the time rate of change of $\overline{C_1' C_2'}$. The authors of Ref. 3-54 obtained τ_c as an approximation to the time rate of change of the quantity $\overline{C_1 C_2}$. Thus,

the τ_c as derived by these authors is not appropriate for comparison of the chemistry term with the diffusion term of Eq. (3.34).

In another article (Ref. 3-53) those authors use a different estimate for τ_c without attempting to justify it [$\tau'_C = (k_1 \bar{C}_1)^{-1}$]. This expression is a nonsymmetrical approximation to Eq. (3.35b). This approximation agrees with Eq. (3.35b) for $M_1 \simeq M_2$ and for mean concentrations such that (a) $\bar{C}_1 \simeq \bar{C}_2$ or (b) where one species is dominant, say, $\bar{C}_2 \ll \bar{C}_1$. For either case (a) or (b) the ratio R of Ref. 3-53 ($R = \tau'_c/\tau_d$) is closely related to N. For $M_1 = M_2$, $k_1 = k_2$. Then $\tau'_c \simeq \tau_c$ and $N \simeq R^{-1}$.

The characteristic time for mixing due to diffusion τ_d is obtained from the same equation as that appearing in Refs. 3-53 and 3-54. Discarding the term with a positive coefficient, one obtains

$$\tau_d = \lambda^2/2D \quad , \tag{3.38}$$

where the microscale λ is called the dissipation length. It is chosen identical with the microscale (Refs. 3-46 and 3-47) one would obtain for a passive additive for the case where only a single species is present.

One finds, therefore, that (Ref. 3-45)

$$N = \lambda^2 \frac{(k_1 \bar{C}_2 + k_2 \bar{C}_1)}{2D} \tag{3.39}$$

To evaluate this expression one must reduce λ to directly measurable quantities. For pure mixing (i.e., without reaction) Corrsin (Ref. 3-49) has shown

$$\lambda \simeq \left(\frac{2}{\sigma}\right)^{1/2} \lambda_T \quad ,$$

where λ_T is the Taylor microscale for turbulence, σ is the Schmidt number ($\sigma = \nu/D$), ν is the kinetic viscosity, and D is the diffusion coefficient.

For molecules of equal mass ($M_1 = M_2$) and approximately equal size, classical kinetic theory shows $D = \nu$ (Ref. 3-53). Thus

$$\lambda \simeq 2^{1/2} \lambda_T$$

Now λ_T is related to the integral or outer scale Λ of turbulence by the relation (Ref. 3-46)

$$\lambda_T/\Lambda \simeq (15)^{1/2} \, Re_\Lambda^{-1/2},$$

where the turbulence Reynolds number for the outer scale is given by

$$Re_\Lambda = \frac{\left(\overline{u'^2}\right)^{1/2} \Lambda}{\nu},$$

and $\left(\overline{u'^2}\right)^{1/2}$ is the observed rms fluctuation velocity. Thus

$$\lambda^{-2} = \frac{1}{30} \frac{\left(\overline{u'^2}\right)^{1/2}}{\nu} \Lambda \cdot \Lambda^{-2} \qquad (3.40)$$

Equation (3.40) is, essentially a result quoted in Ref. 3-53. The expression following Eq. (21) of this reference differs from Eq. (3.40) only by the numerical factor, which they taken as 0.05. Since these results are based on order of magnitude approximations, the present result can be said to agree with their estimate for λ. The numerical value chosen in Ref. 3-53 for quantities on the rhs of Eq. (3.40) are in reasonable agreement with other estimates of atmospheric numbers (Ref. 3-46).

In Ref. 3-53 molecules of approximately equal size and mass ($\nu = D$) are assumed. Their choice for the outer scale is $\Lambda = 10$ m, whereas Ref. 3-46 uses $\Lambda = 100$ m for essentially the same numerical values for the other parameters. Examination of the U.S. Standard Atmosphere, 1962, shows that the Ref. 3-53 choice for kinematic viscosity and atmospheric density corresponds to an altitude of 3 km.

Thus. Eq. (3.39) reduces to

$$N \simeq \Lambda k (\bar{C}_1 + \bar{C}_2)/0.06\left(\overline{u'^2}\right)^{1/2} , \qquad (3.41)$$

where $k_1 = k_2 = k$. This equation is useful in making estimates as to whether or not a reaction is diffusion limited.

3.6.4 Application to Jets and Wakes

It is appropriate to apply Eq. (3.41) to chemical reactions occurring in a high-temperature supersonic exhaust jet. Qualitatively, the following remarks can be made: the reaction rate constant will tend to increase with temperature above atmospheric values; the outer scale, corresponding to energy containing eddies, will be of the order of the diameter of the exhaust jet. At typical stratospheric flight altitudes this length is much less than the atmospheric outer scale. Equation (3.41) shows that these two effects tend to offset each other. Thus, a reaction that is diffusion limited in the atmosphere may tend to remain so in an engine exhaust. Of course, a quantitative statement depends on the specific numbers.

A turbulent jet is considered with mean exhaust velocity of 1,600 m/sec and jet diameter of 1 m, which is set equal to Λ. A nominal value of turbulence intensity for the rms velocity $\left(\overline{u'^2}\right)^{1/2}/(\bar{U}) = 0.01$ is assumed near the exit plane of the nozzle, within the cone of constant properties.

This number is not inconsistent with subsonic data (Refs. 3-53 and 3-57). Equation (3.41) is applied to the supersonic case, recognizing that the theory of this equation was based on an incompressible fluid model. For this case, N reduces to $N \simeq k(\bar{C}_1 + \bar{C}_2)$.

The following thermal reactions will be considered, using the reaction rate constants of Section 3 and exit plane concentrations appropriate to the flow. N can then be calculated readily:

Reactions	k (ppm-sec)$^{-1}$	$\bar{C}_1$ (ppm)	$\bar{C}_2$ (ppm)	N
$\underset{1}{CO} + \underset{2}{OH} \rightarrow CO_2 + H$	0.23	820	197	2.3×10^3
$H + O_2 \rightarrow OH + O$	0.022	380	5.5×10^4	1.2×10^4
$H + NO_2 \rightarrow NO + OH$	19.0	380	3.8×10^{-3}	7.2×10^4

It can be seen that all three reactions are diffusion limited. The first reaction at these near-jet conditions has about ten times the value of N as does this reaction under the atmospheric conditions of Refs. 3-53 and 3-54. Thus, it remains diffusion limited – in agreement with the preceding qualitative remarks. Note that in the far field behind the jet, aircraft-induced fluctuations have diminished to atmospheric levels. (Here results like those of Donaldson and Hilst, Ref. 3-53, Table 1, appropriately modified to stratospheric altitudes, apply.)

A criticism of Eq. (3.41) and of the results of Refs. 3-53 and 3-54 arises from use of a diffusion coefficient corresponding to reactants of equal mass. Because of its small mass, hydrogen for example can be expected to diffuse more rapidly than a heavier molecule.

As a possible candidate for a chemically limited process, a reaction is considered that occurs in the wake of a Mach 2 aircraft. Consider the reaction

$$NO + O_3 \rightarrow NO_2 + O_2 \quad ,$$

where $k = 5 \times 10^{-3}$ (ppm-sec)$^{-1}$, $\bar{C}_{O_3} = 1$ ppm, and $\bar{C}_{NO} = 5$ ppm. The fluctuation intensity is estimated as follows. Measurements on a two-dimensional Mach 3 wake are performed in Ref. 3-49. Longitudinal velocity fluctuations relative to the mean velocity values are about 7 percent in the turbulent wake. It is assumed that the mean flow velocity is given by $\bar{U}(x) \simeq \bar{U}_{body}/10 \simeq 60$ m/sec. Thus, the rms velocity fluctuation is approximately 40 m/sec. An outer scale of about 0.3 m arising from the aircraft turbulent boundary layer is appropriate to this problem. Then $N \simeq 4 \times 10^{-3}$. This regime is clearly chemistry limited.

3.6.5 Conclusions

Turbulence produces measurable effects on a passive additive such as the concentration of a chemical injected into a turbulent medium. Such effects have been observed in measurements made on temperature fluctuations of a hot gas. The importance of such turbulence effects to the time and space behavior of mean concentration of the chemical components is uncertain. Two kinds of effects are envisioned. O'Brien's work (Ref. 3-51) indicates that the concentration fluctuations themselves are large in the presence of chemical reactions. They may, therefore, have a large influence on the mean concentrations one wishes to predict. Further, effective turbulent reaction rates may differ significantly from quiescent laboratory values. Even in a well-mixed gas, turbulence may speed up or slow down reactions relative to the usual rates.

It has been shown that diffusion-limited reactions may exist in a near-jet field, and chemically limited reactions may occur in a wake. One cannot yet say with confidence how these results apply to the supersonic jet aircraft. This statement may appear surprising in view of the following result. In a one-component irreversible second-order reaction modeled in the limit of fast reaction by a purely time dependent equation for the concentration, the reaction is slowed by the mean square random fluctuations of the concentration. For a two-component system, however, the correlation function for the two components can take on negative as well as positive values as it evolves in time. Thus, without numerical analysis of specific conditions it is impossible to predict whether or not turbulence speeds up or slows down the reactions.

The preceding review was based on and supported by ongoing Independent Research at LMSC. Results of this work will be presented in a forthcoming report. Although there has been progress, it is felt that work in this field has not yet reached the stage where attempts to obtain solutions for practical jet engine exhaust kinetics problems are warranted.

3.7 REFERENCE LIST FOR RATE DATA TABLES 3-1 and 3-7

1. Baulch et al., High Temperature Reaction Rate Data, No. 1, School of Chemistry, The University, Leeds, May 1968
2. -----, High Temperature Reaction Rate Data, School of Chemistry, The University, Leeds, Dec 1969
3. -----, High Temperature Reaction Rate Data, No. 5, School of Chemistry, The University, Leeds, Jul 1970
4. Brown et al., Chemical Kinetics Data Survey I. Rate Data for Twelve Reactions of Interest for Stratospheric Chemistry. NBS Report 10-692, Jan 1972
5. W. Braun et al., Chemical Kinetics Data Survey II. Photochemical and Rate Data for Fifteen Gas Phase Reactions of Interest for Stratospheric Chemistry, NBS Report 10-828, Apr 1972
6. D. Garvin and L. H. Gevantman, Chemical Kinetics Data Survey III, Selected Rate Constants for Chemical Reactions of Interest in Atmospheric Chemistry, NBS Report 10-867, Jun 1972
7. Baulch et al., Evaluated Kinetic Data for High Temperature Reactions, Butterworths, London, 1972
8. Simonaitis and Heichlem, "The Kinetics of the Reaction of OH with NO_2," Transactions, American Geophysical Union, Vol. 52, Nov 1971, Abstracts
9. V. N. Kondratiev, Rate Constants of Gas Phase Reactions, Office of Standard Reference Data NBS, Washington, Jan 1972
10. D. Garvin, ed., A Compendium of Evaluated and Estimated Rate Coefficients, NBS Report 9884, Jul 1968
11. H. S. Johnston, Catalytic Reduction of Stratospheric Ozone by Nitrogen Oxides, UCRL-20568, Jun 1971
12. Levy et al., "Mechanisms of Formations of Sulfur Oxides in Combustion," Environmental Science and Technology, 4, Aug 1970

13. Laurendeau, The Thermal Decomposition of Nitric Oxide and Nitrogen Dioxide, Univ. of California (Berkeley), Report TS-72-4, Apr 1972

14. Fletcher et al., The Control of Oxides of Nitrogen Emission From Aircraft Gas Turbine Engines, Vol. 21, The NO_x Formation Process, Report FAA-RD-71-111, 2, 1971

15. D. A. Bittker and V. J. Scullin, General Chemical Kinetics Computer Program for Static and Flow Reactions, With Application to Combustion and Shock-Tube Kinetics, NASA TN D-6586, Jan 1972

16. W. E. Wilson, "A Critical Review of the Gas-Phase Reaction Kinetics of the Hydroxyl Radical," J. Phys. Chem. Ref. Data, Vol. 1, No. 2, 1972

17. H. S. Johnston, Gas Phase Reaction Kinetics of Neutral Oxygen Species, NSRDS-NBS 20, Sep 1968

18. D. D. Davis, Univ. of Maryland, private communications

19. Fletcher et al., The Control of Oxides of Nitrogen Emission From Aircraft Gas Turbine Engines, Vol. 1, Program Description and Results, Report FAA-RD-71-111, 1, 1971

20. P. J. Crutzen, Gas-Phase Nitrogen and Methane Chemistry in the Atmosphere, Report AP-10, Inst. of Meteorology, Univ. of Stockholm, 29 Jun 1972

21. H. Harrison, H. S. Johnston, and E. R. Hardwick, "Kinetics of the Thermal Decomposition of Nitric Acid Vapor, IV. A Shock Tube Study Between 800–1200°K," J. Am. Chem. Soc., Vol. 84, 1962, p. 2478

3.8 REFERENCES FOR SECTION 3

3-1 Fristrom and Westenberg, Flame Structure, Chap. XIV, McGraw-Hill, New York, 1965

3-2 Singh and Sawyer, "CO Reactions in the Afterflame Region of Ethylene/Oxygen and Ethane/Oxygen Flames," 13th Symposium (International) on Combustion, Combustion Institute, Pittsburgh, 1971, p. 403

3-3 Johnson, Caretto, and Starkman, "The Kinetics of CO in Reciprocating Engines," Paper No. WSCI 70-4, presented in Western States Section/The Combustion Institute, Apr 1970

3-4 Baulch et al., High Temperature Reaction Rate Data, No. 1, School of Chemistry, The University, Leeds, May 1968

3-5 Starkman, Mizutani, Sawyer, and Teixeira, "The Role of Chemistry in Gas Turbine Emissions," Trans. ASME, J. Eng. Power, Jul 1971, p. 3.33

3-6 Heywood, "Gas Turbine Combustor Modeling for Calculating Nitric Oxide Emission," AIAA Paper No. 71-712, presented at AIAA/SAE 7th Propulsion Joint Specialist Conference, Salt Lake City, Jun 1971

3-7 Heywood, Fay, and Linden, "Jet Aircraft Air Pollutant Production and Dispersion," AIAA J., Vol. 9, 1971, p. 841

3-8 Caretto, Muzio, Sawyer, and Starkman, "The Role of Kinetics in Engine Emission of Nitric Oxide," Combustion Sci. and Tech., Vol. 3, 1971, p. 53

3-9 Zeldovich, "The Oxidation of Nitrogen in Combustion Explosions," Acta Physicochimica URSS, Vol. 21, 1946, p. 577

3-10 Laurendeau and Sawyer, "General Solution of Reaction Rate Problems Via Combined Integration and Steady State Analysis: Application to Nitric Oxide Formation and Decomposition," Paper No. WSCI 71-27, presented at Western States Section/The Combustion Institute, Oct 1971

3-11 Baulch et al., High Temperature Reaction Rate Data, School of Chemistry, The University, Leeds, Dec 1969

3-12 Baulch et al., High Temperature Reaction Rate Data, School of Chemistry, The University, Leeds, Jul 1970, No. 5

3-13 W. K. McGregor et al., "Concentration of OH and NO in YJ93-GE-3 Engine Exhausts Measured in situ by Narrow-Line UV Absorption," paper present at 2nd Conference on Climatic Impact Assessment Program, Cambridge, Mass., 14 – 17 Nov, 1972

3-14 Bittker and Scullin, General Chemical Kinetics Computer Program for Static and Flow Reactions, With Application to Combustion and Shock Tube Kinetics, NASA TN D-6586, 1972

3-15 G. N. Abramovich, The Theory of Turbulent Jets, MIT Press, 1963

3-16 W. Forstall and A. H. Shapiro, "Momentum and Mass Transfer in Coaxial Gas Jets," J. Appl. Mech. Vol. 17, 1950, p. 399

3-17 SST Powerplant, Exhaust Emission Characterization, SRL-1220-01-0371, Scott Research Laboratories, Plumsteadville, Pa.

3-18 J. Neely and D. L. Davidson, "Emission Level of the YJ93-GE-3 Engine, an SST-Like Engine," paper presented at 2nd Conference on Climatic Impact Assessment Program, Cambridge, Mass., 14 – 17 Nov, 1972

3-19 U.S, Department of Commerce, Environmental Aspects of the Supersonic Transport, No. 0300-0050, May 1972, p. 11

3-20 NASA TMX-2323

3-21 NAPTC-ATD-212

3-22 Starkman et al., "The Role of Chemistry in Gas Turbine Emissions," J. Eng. Power, Jul 1971

3-23 Fletcher et al., Report FAA-RD-71-111, 1

3-24 Caretto et al., "The Formation of NO in Combustion Processes," presented at Central States Section/Combustion Institute, Mar 1968

3-25 G. R. Lazalier and J. W. Gearhart, Measurement of Pollutant Emissions From an Afterburning Turbojet Engine at Ground Level II Gaseous Emissions, AEDC-TR-70-70, Aug 1972

3-26 Mellor et al., Emissions From and Within an Allison J-33 Combustor

3-27 H. S. Johnston, Catalytic Reduction of Stratospheric Ozone by Nitrogen Oxides, UCRL-20568, Jun 1971

3-28 P. J. Crutzen, Gas Phase Nitrogen and Methane Chemistry in the Atmosphere, Report AP-10, Inst. of Meteorology, Univ. of Stockholm, 29 Jun 1972

3-29 Levy et al., "Mechanisms of Formation of Sulfur Oxides in Combustion," Environmental Science & Technology, 4, 8 Aug 1970

3-30 H. T. McAdams, Analysis of Aircraft Exhaust Emission Measurement Statistics, CALNA 5007 K-2, Cornell Aeronautical Laboratory, Nov 1971

3-31 NASA TMX 2323

3-32 E. S. Starkman et al., "The Role of Chemistry in Gas Turbine Emissions," J. Engineering Power, Jul 1971, p. 333

3-33 NAPTC-STD-212

3-34 H. Niki et al., Mechanism of Smog Reactions (Ford Motor Company Scientific Research Staff), 14 Apr 1972 (Appendix: Complete Reaction List)

3-35 S. W. Benson, Thermochemical Kinetics, Wiley, N. Y., 1968

3-36 P. Gray, R. Shaw, and J. C. J. Thynne, "The Rate Constants of Alkoxyl Radical Reactions," Progress in Reaction Kinetics, Vol. 4, Pergamon Press, N. Y., 1967, p. 63

3-37 P. A. Leighton, Photochemistry of Air Pollution, New York, Academic Press, 1961

3-38 L. G. Wayne, "On the Mechanism of Photo-Oxidation in Smog," Archives of Environmental Health, Vol. 7, 1963, p. 229

3-39 Phillips and Shaw, "Reaction of Methyl and Methoxyl Radical With Nitrogen Dioxide and Nitric Oxide," presented at 10th International Symposium on Combustion, Combustion Institute, Pittsburgh, 1965, p. 453

3-40 F. Bortner and A. Kummler, The Daylight Atmosphere, 1969

3-41 U.S. Department of Commerce, Environmental Aspects of the Supersonic Transport, No. 0300-0050, May 1972, p. 11

3-42 A. M. Obukhov, Imv Akad. Nauk SSSR, Geogr. I, Geofiz. Vol. 13, 1969, p. 58

3-43 S. Corrsin, J. App. Phys., Vol. 22, 1961, p. 469

3-44 C. C. Lin in, Turbulent Flows and Heat Transfer, ed. C. C. Lin, Princeton University Press, 1959

3-45 A. Einstein, Ann. Phys., (4) Vol. 17, 1905, p. 549, translation appears in Part 1 of, "Investigations on the Theory of Brownian Motion," Dover

3-46 H. Tennekes and J. L. Lumley, A First Course in Turbulence, MIT Press, 1972

3-47 G. I. Taylor, Proc. Roy. Soc., Vol. A151, 1935, pp. 421 – 478

3-48 G. K. Batchelor, "The Theory of Homogeneous Turbulence," Cambridge, 1960

3-49 S. Corrsin, Phys. Fluids, Vol. 1, 1958, p. 42

3-50 E. E. O'Brien, Phys. Fluids, Vol. 14, 1971, p. 1326

3-51 E. E. O'Brien and C. H. Lin, Phys. Fluids, Vol. 15, 1972, p. 931

3-52 C. du P. Donaldson, AGARD-CP-93, 1971

3-53 C. du P. Donaldson and G. R. Hilst, A.R.A.P. Report No. 166, 1971

3-54 C. du P. Donaldson and G. R. Hilst, Proceedings of the 1972 Heat Transfer and Fluid Mechanics Institute, ed. R. B. Landis and G. J. Hordemann, Stanford University Press, 1972

3-55 J. Jeans, The Dynamical Theory of Gases, Dover

3-56 I. Wygnanski and H. Fiedler, J. Fluid Mech., Vol. 38, 1969, p. 577

3-57 C. du P. Donaldson et al., J. Fluid Mech., Vol. 45, 1971, p. 477

3-58 A. Demetriades, J. AIAA, Vol. 9, 1971, p. 2128

Section 4

PHOTOCHEMISTRY IN THE WAKE REGIME

4.1 TIME-DEPENDENT CATALYTIC REDUCTION OF STRATOSPHERIC OZONE IN A THIN STRIP

Following injection of NO contained in an aircraft wake into the stratosphere, several reactions begin to take place. The two which most affect ambient species concentrations are the oxidation of nitric oxide by ozone, which depletes ambient ozone, and the photolysis of nitrogen dioxide, which increases oxygen atom concentrations. Near the exhaust jet region where the local NO concentration is higher than that of ozone, the reaction is limited by ozone, and there is little nitrogen dioxide formed relative to the nitric oxide level. Thus, there is an initial period of adjustment, during which the wake is diluted, where two things occur: (1) the NO_x concentrations decrease to below the ambient O_3 levels, and (2) the NO/NO_2 ratio increases toward its proper "photochemical steady state" value. As has been shown in Section 3, this period of adjustment is slow with regard to the wake time frame of a few minutes. However, it is relatively fast in comparison with elapsed times of several hours and beyond, so that a convenient starting point for analysis of the progress of photochemical catalytic effects on ambient ozone is suggested, namely, to start with a uniformly mixed thin layer or ribbon of NO_x, irradiated from above, and at concentrations below that of the ambient ozone in the strip. This is the "ozone in a box" problem, or, rather, "ozone in an irradiated ribbon."

Interdiffusion with the surrounding environment does proceed while the photochemical reactions are taking place. However, it is instructive to examine the maximum effects of the catalytic cycle for the case where diffusion times are long compared with reaction times. The analysis can be performed in a relatively simple manner for this artificial "closed system." The results will be useful to show trends and relationships among the variables, and will approach quantitative accuracy for those limited conditions under which the closed system assumption becomes more nearly satisfied.

An analysis has been carried out to determine the ozone concentration as a function of time for injection of a given concentration of NO_x in a thin strip at various altitudes in the stratosphere. The analysis makes use of several justifiable simplifications in order to avoid the complications of integrating the full set of differential equations governing stratospheric photochemistry in the presence of oxides of nitrogen.

4.1.1 Reactions

The important chemical reactions governing catalytic reduction of ozone by oxides of nitrogen have been given by Johnston (Ref. 4-1) and are as follows:

(a)	$O_2 + h\nu$	$\rightarrow 2\,O$
(b)	$O + O_2 + M$	$\rightarrow O_3 + M$
(c)	$O_3 + h\nu$	$\rightarrow O_2 + O$
(d)	$O + O + M$	$\rightarrow O_2 + M$
(e)	$O + O_3$	$\rightarrow O_2 + O_2$
(f)	$NO + O_3$	$\rightarrow NO_2 + O_2$
(g)	$O + NO_2$	$\rightarrow NO + O_2$
(h)	$NO_2 + h\nu$	$\rightarrow NO + O$
(i)	$NO + NO + O_2$	$\rightarrow NO_2 + NO_2$
(j)	$O + NO + M$	$\rightarrow NO_2 + M$
(k)	$NO_2 + O_3$	$\rightarrow NO_3 + O_2$
(l)	$NO_3 + h\nu$	$\rightarrow NO + O_2$

The rate expressions and rate constants for these reactions have also been given by Johnston. Reaction (l) is much faster than (k) so that in daylight NO_3 is in steady state and reaction (l) can be eliminated.

Also, at 20 km and above reactions (i), (j), and (k) are relatively slow compared to (f), (g), and (h) and do not greatly effect either the rate of ozone destruction or the steady-state ozone levels (Refs. 4-1, 4-2). With these simplifications, the above set is reduced to the eight reactions (a) through (h).

For the low altitude (20 to 25 km) regions of the stratosphere of interest here, the ozone destroying reactions (d) and (e) are very much slower than the catalytic destruction reactions (f) and (g) and are therefore neglected in the present analysis. Thus, the set of governing reactions is reduced to the following six:

$$\begin{aligned}
&\text{(a)}\quad O_2 + h\nu \rightarrow 2\,O\\
&\text{(b)}\quad O + O_2 + M \rightarrow O_3 + M\\
&\text{(c)}\quad O_3 + h\nu \rightarrow O_2 + O\\
&\text{(f)}\quad NO + O_3 \rightarrow NO_2 + O_2\\
&\text{(g)}\quad O + NO_2 \rightarrow NO + O_2\\
&\text{(h)}\quad NO_2 + h\nu \rightarrow NO + O
\end{aligned}$$

4.1.2 Steady-State Simplifications

In complex chemical kinetic analyses, the steady-state assumption is often applied to minor species with fast reaction rates. Basically, what is assumed is that such a species can, by virtue of its fast production and destruction rates, instantly adjust its concentration level to any changes of major species. The explicit dependence of concentration upon time for a steady-state species is thus eliminated in favor of an implicit dependence through the major species.

In the above reaction scheme, it is found that the O atoms can rapidly adjust to changes in the ozone or NO_x levels and thus qualify as a steady-state species. Also, the NO and NO_2 may be taken to be in steady state provided that $[NO]_x \ll [O_3]$. Thus, the further simplification that both O and NO/NO_2 are in steady state is made here.

The steady-state assumption has been confirmed by numerical integration of the reaction set (a) through (h) using the rates given by Johnston. It has been found that $[O]$ and $[NO]/[NO_2]$ reach their steady-state values before significant O_3 depletion occurs, provided that $[NO_x] \ll [O_3]$.

4.1.3 Governing Equations

The set of reactions (a) through (h) leads to the following rate expressions

$$\frac{d[O_3]}{dt} = k_b[O_2][O][M] - k_f[NO][O_3] - j_c[O_3]$$

$$\frac{d[O]}{dt} = 2j_a[O_2] - k_b[O_2][O][M] + j_c[O_3]$$
$$k_g[O][NO_2] + j_h[NO_2]$$

$$\frac{d[NO_2]}{dt} = k_f[NO][O_3] - k_g[O][NO_2] - j_h[NO_2]$$

The steady state condition on O and NO_2 gives

$$\frac{d[O]}{dt} = \frac{d[NO2]}{dt} = 0$$

Setting these two rates equal to zero and adding

$$\frac{d[O]}{dt} + \frac{d[NO_2]}{dt}$$

gives

$$k_b[O_2][O][M] - j_c[O_3] - k_f[NO][O_3] = 2j_a[O_2] - 2k_g[O][NO_2]$$

Substituting this result into the ozone rate gives:

$$\frac{d[O_3]}{dt} = 2j_a[O_2] - 2k_g[O][NO_2] \qquad (4.1)$$

With the exception of the small contribution from reaction (e) which has been neglected here, this expression is the same as given by Johnston. (See Ref. 4-1.)

It now remains to write the above rate as a function of ozone only so that a simple numerical integration will give ozone as a function of time.

From

$$\frac{d[O]}{dt} = 0 \tag{4.2}$$

$$[O] = \frac{j_c[O_3] + j_h[NO_2]}{k_b[M][O_2]}$$

and from

$$\frac{d[NO_2]}{dt} = 0 \quad \text{using} \quad [NO] = [NO_x] - [NO_2]$$

$$[NO_2] = \frac{k_f[O_3][NO_x]}{k_f[O_3] + k_g[O] + j_h}$$

Here $k_g[O] \ll (k_f[O_3] + j_h)$ so that

$$[NO_2] \approx \frac{k_f[O_3][NO_x]}{k_f[O_3] + j_h} \tag{4.3}$$

Substitution of Eq. (4.3) into (4.2), and Eqs. (4.2) and (4.3) into (4.1) gives the final expression for the above rate

$$\frac{d[O_3]}{dt} = F(j_a, j_c, k_b, k_f, k_g, [O_2], [M], [O_3][NO_x])$$

For a given altitude, all parameters are constant except $[O_3]$, and the above expression can be numerically integrated to give $[O_3]$ as a function of time

$$\int_{[O_3]_o}^{[O_3]} \frac{d[O_3]}{F} = \int_o^t dt$$

4.1.4 Results

The curves of $[O_3]$ as a function of time for various $[NO_x]$ levels and altitudes are presented in Figures 4-1 and 4-2. The rate constants and atmospheric properties for these calculations have been taken from Johnston and are given in Table 4-1. The photolysis rate constants are 24-hour averages as computed by Johnston for $\alpha = [NO_x]/[M] = 0$. The values for $\alpha = 0$ have been used since, for a thin strip of NO_x, the incident radiation is that of an unperturbed stratosphere. Some results for daytime 12-hr average radiation are also shown. The effect of the addition of NO_x

Table 4-1

PARAMETERS FOR PHOTOCHEMICAL CALCULATIONS

Parameters	20 km Altitude	25 km Altitude
j_a	$10^{-14.49}$	$10^{-12.09}$
k_b	$10^{-32.58}$	$10^{-32.63}$
j_c	$10^{-3.73}$	$10^{-3.72}$
k_f	$10^{-15.10}$	$10^{-15.01}$
k_g	$10^{-14.40}$	$10^{-14.34}$
j_h	$10^{-2.35}$	$10^{-2.35}$
$\log_{10}[M]$	18.27	17.93

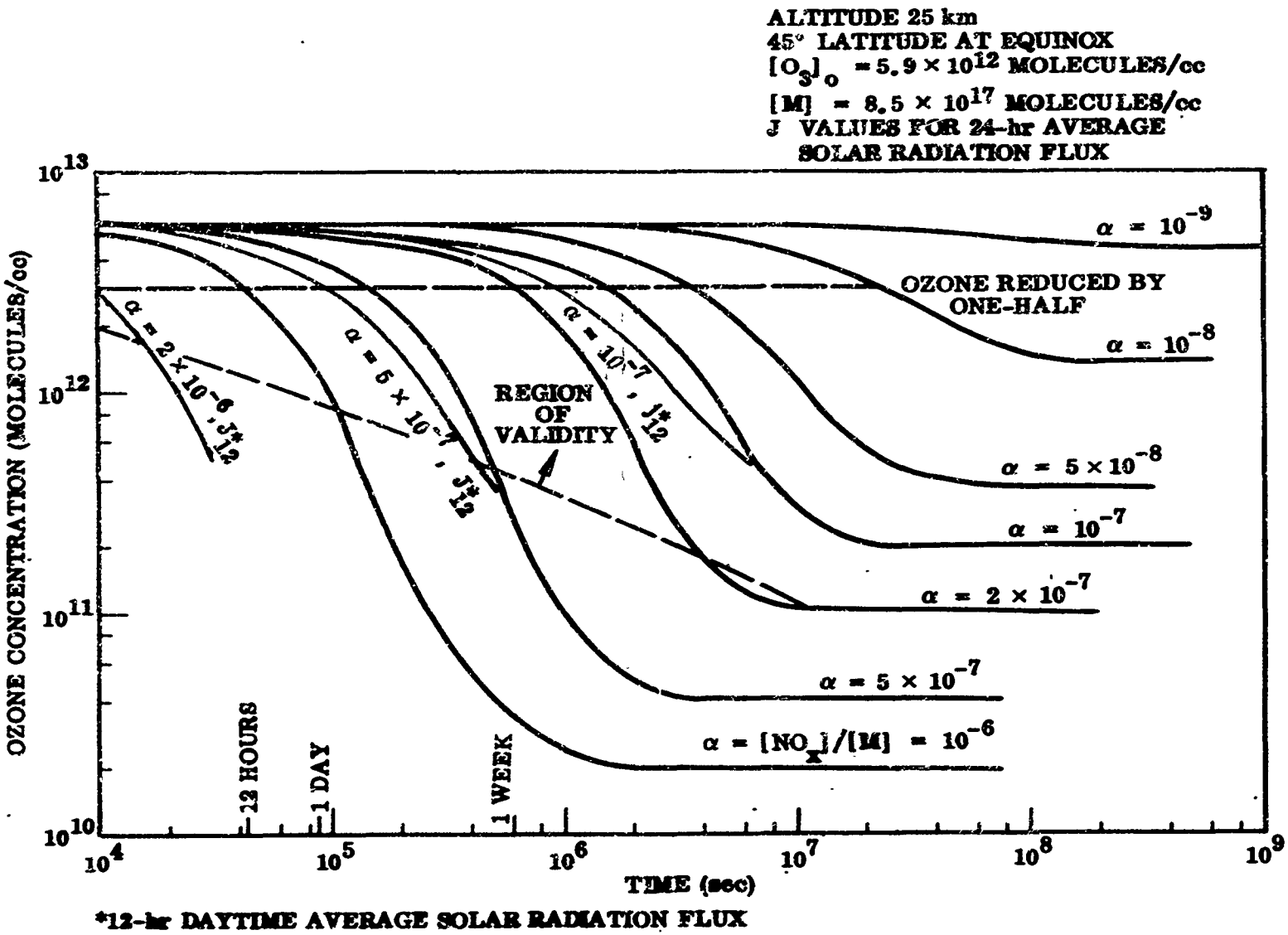

Figure 4-1 Ozone Reduction at 25 km

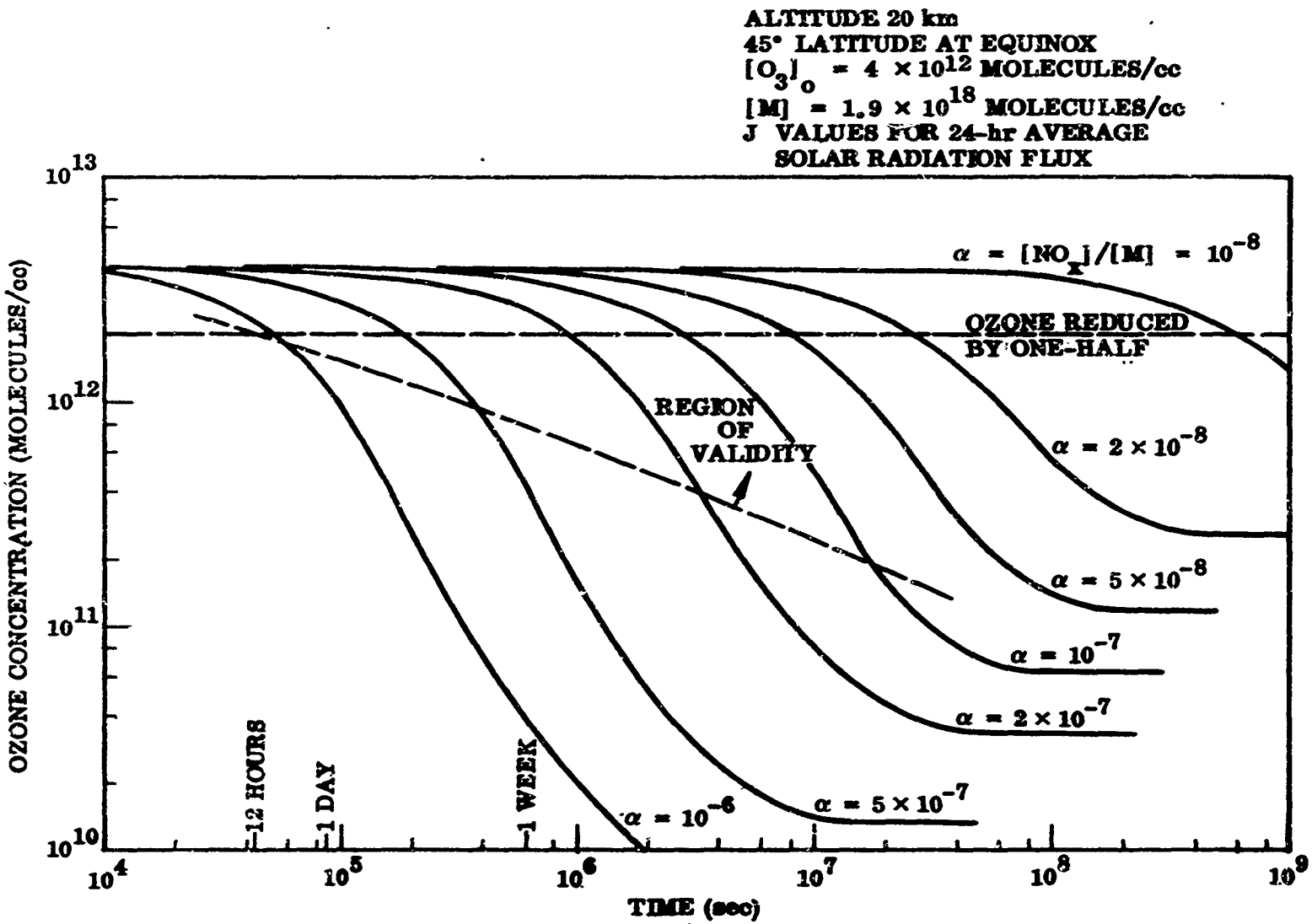

Figure 4-2 Ozone Reduction at 20 km

is to reduce the O_3 concentration in the narrow strip to a new steady-state value. Higher concentrations of NO_x reduce the ozone faster and to lower steady-state concentrations. The dashed curves of "validity" simply marks the concentration regions where ozone falls below the NO_x levels, and the analysis becomes invalid.

The main conclusion to be drawn from Figures 4-1 and 4-2 is that the ozone level is not reduced in the wake time frame O (10^3 sec). The characteristic times for the catalytic reduction cycle to have a significant effect are much longer. It would take very large changes in the rate constants to invalidate this conclusion.

The ozone half-times (time for $[O_3]$ to be reduced to one-half its initial value) are presented in Figure 4-3 for 20- and 25-km altitudes. The half-times have been computed by two different methods. The curves marked ambient [O] have been taken from the half-time data given by Johnston and are based on initial steady-state $[NO_2]$ levels. The curves marked steady-state [O] are the half-times taken directly from the ozone versus time curves of Figures 4-1 and 4-2.

The half-times for steady-state [O] are considerably shorter than those for ambient [O], especially at higher $[NO_x]$ levels. The reason for this is that the initial effect of adding NO_x is to raise the steady-state level of O atoms by virtue of the $j_h [NO_2]$ term. This new steady-state [O] level is reached quite rapidly before any depletion of O_3 begins. The effect of this higher [O] is, of course, to speed up the catalytic destruction of ozone -- hence, the shorter half-times. It is felt that the steady-state [O] half-times are the appropriate ones for the present discussion.

It should also be noted that the steady-state [O] half-times presented here closely agree with those calculated by Johnston's method if the initial steady-state [O] level is used in Johnston's half-time relationship. This may seem fortuitous because the half-time relationship given by Johnston is for constant [O] and constant [NO], while these quantities vary with time in the present analysis. However, Johnston's half-time depends upon the product [O] [NO] which does tend to remain constant during the initial ozone depletion since [O] is decreasing while [NO] is increasing.

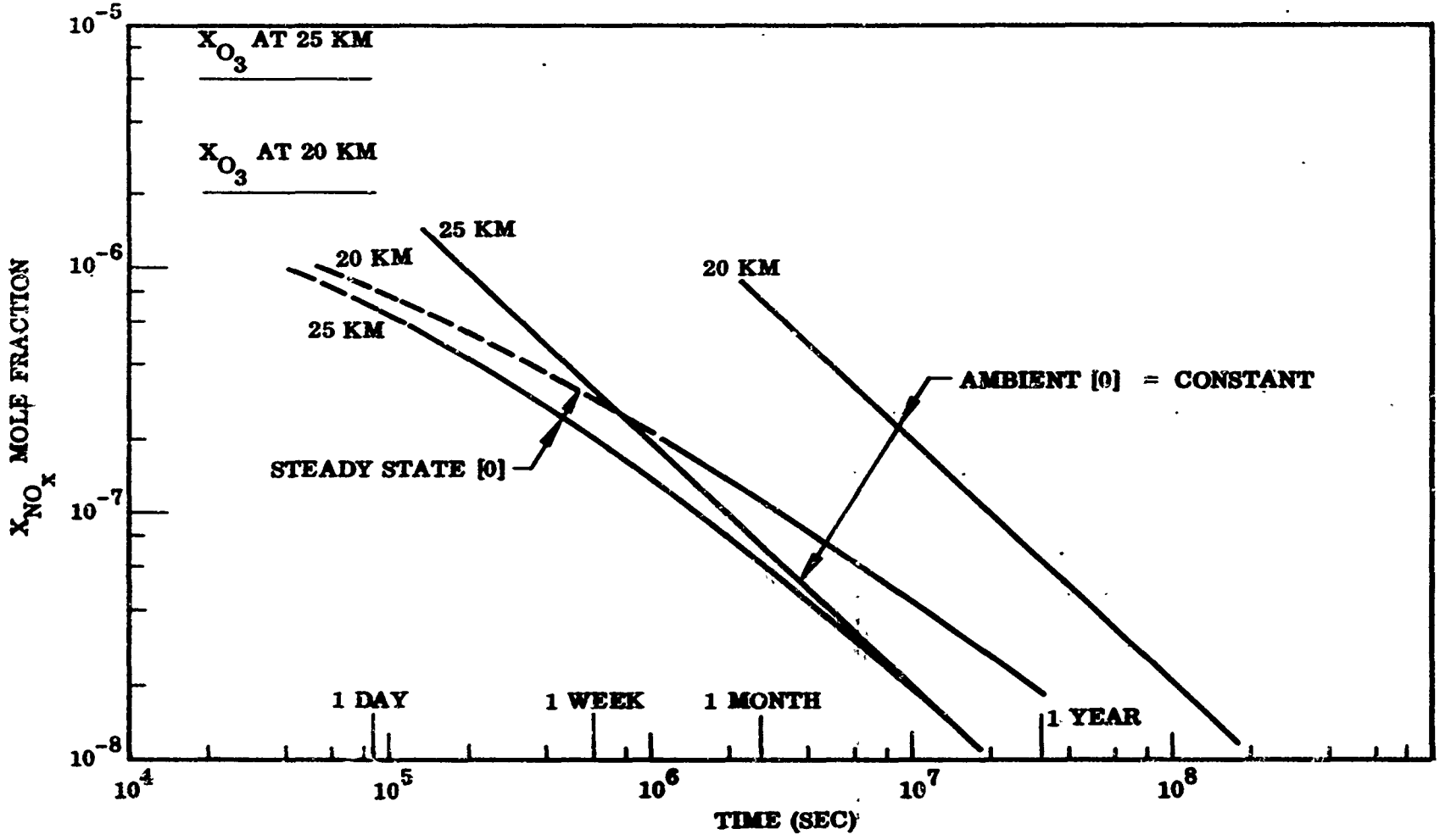

Figure 4-3 O_3/NO_x Catalytic Half-Times

4.2 PARTICULATE FORMATION

4.2.1 General Considerations

In the H, C, N, O, S, $h\nu$ system, there are many possible reactions that can lead to formation of particulates. These are reviewed below.

It is concluded that many of these reactions must be regarded as "unknown" in light of present knowledge. Except for these "unknown areas" it is not anticipated that heterogeneous chemical effects attributable to the presence of particulates in the wake regime will significantly modify the results that have been obtained on the basis of homogeneous gas-phase kinetics. This is largely a consequence of the relatively short residence times in the wake – i.e., less than 20 min.

The possible significance of particulates and aerosols in stratospheric chemistry has been discussed briefly by Harrison (Ref. 4-3). The two types of mechanism through which particulates can affect the chemistry are (1) adsorption, which simply removes species from the gas phase and (2) surface catalysis through which the rates of homogeneous gas processes can be greatly accelerated. Harrison concludes that heterogeneous chemistry may affect the stratospheric kinetics significantly because characteristic times for gas diffusion to an aerosol's surface may be comparable to or shorter than those for many important homogeneous reactions. He further concludes that catalytic effects appear to be potentially more significant than removal by adsorption.

Harrison's remarks are based on ambient stratospheric concentrations of particulates. Therefore, the competition between homogeneous and heterogeneous kinetics may be expected to become even more important if additional particulates are injected in the stratosphere from jet regime exhaust. A start has been made at treating the whole subject of stratospheric aerosols in the context of their potential climatic modifications (Ref. 4-4).

The present discussion focuses on photochemical development of new aerosols within the aircraft wake. Particulates added to the flow at the engine exit plane, such as solid carbon, and formation of new aerosols at late times in the stratosphere will be covered by other portions of the CIAP program.

Formation and growth of new aerosols in the wake, regime, as in any regime, depends on an excess vapor pressure condition, i.e., there must be supersaturation with respect to the species which is to be condensed. In other words, the equilibrium vapor pressure of species in condensation with the condensed aerosol must be exceeded. There is a body of literature that refers to the growth of aerosols in "unsaturated" conditions. This refers to the fact that new species with higher molecular weights are formed in the irradiated gas, and that the vapor pressure of these species with respect to the various groups it contains is quite low. Thus, in an environment that is highly unsaturated with regard to water – i.e., when the vapor pressure of water is far below the saturation vapor pressure – photochemical formation of new species with low vapor pressure may still be possible. In this case, the growth of aerosols from the vapor phase is still possible, akin to photochemical synthesis, and this type of process is sometimes referred to as particle formation under unsaturated conditions (Ref. 4-5).

For consideration of normal aerosol formation under saturated or supersaturated conditions, condensation of water vapor from the engine exhaust is the most obvious potential process.

Here ther are ample condensation nuclei to serve as condensation sites if condensation favoring conditions exist. These nuclei include ambient particulate species taken into the engine, soot and ions (exhaust plasma levels correspond to approximately 10^7 ions/cm^3). On the other hand, the rates of condensation in relation to the time scales of interest are highly uncertain. It is noteworthy that the nucleation and growth of water particles to visible size within the wake regime is unlikely because visible contrails are almost never observed in stratospheric flight.

A simple exercise will demonstrate that a saturated condition for H_2O vapor exists only briefly in the wake. Assuming complete homogeneity, a wake energy balance yields the following relation between water concentration and temperature:

$$[H_2O]_w = [H_2O]_e \frac{(T_w - T_a)}{(Z T_e - T_w)}$$

where: subscript w denotes the wake, subscript a the ambient, and subscript e the engine exhaust conditions; Z is the ratio of the specific heat of the exhaust products to that of air. Because of its very low 2-ppm level (Ref. 4-6) the ambient stratospheric water vapor can be neglected.

The above relationship has been plotted in Figure 4-4 for the GE-4 engine with afterburning – $T_e = 950°K$, $[H_2O]_e = 10^5$ ppm, and $Z = 1$. The curve for cruise operation would not be greatly different because the effect of the lower water concentration would be cancelled by a lower exhaust temperature. Also included in Figure 4-4 are curves representing saturated conditions at 15, 20, and 25 km altitude.

The figure shows there is no condensation to be expected at 25 km, but there is a brief period when slightly supersaturated conditions exist in a 20-km wake. This period encompasses the region between 2300 ppm and 550 ppm water concentration, which implies the range of air dilution factors from 45 to 180. At 15 km the wake becomes saturated at a dilution factor of 25, and the condition continues until a dilution of 550 is reached. The time scale for the wake to grow through this range of dilution is of the order of 1 to 10 sec. Therefore, at lower altitudes the extent of water condensation in the wake will depend on the rates of nucleation and droplet growth. There should be ample nuclei in the engine exhaust. The lack of contrail formation in the stratosphere must therefore be due to the failure of the particles to grow to visible size during the brief period of saturated conditions.

In reviewing the many possible reactions capable of forming particulates, the objective has been to identify those reactions in the wake of a GE-4 engine operating at 20-km altitude which, in the process of particulate formation, will lead within 20 minutes to significant changes (e.g., 10 percent) in the appropriate exhaust species composition.

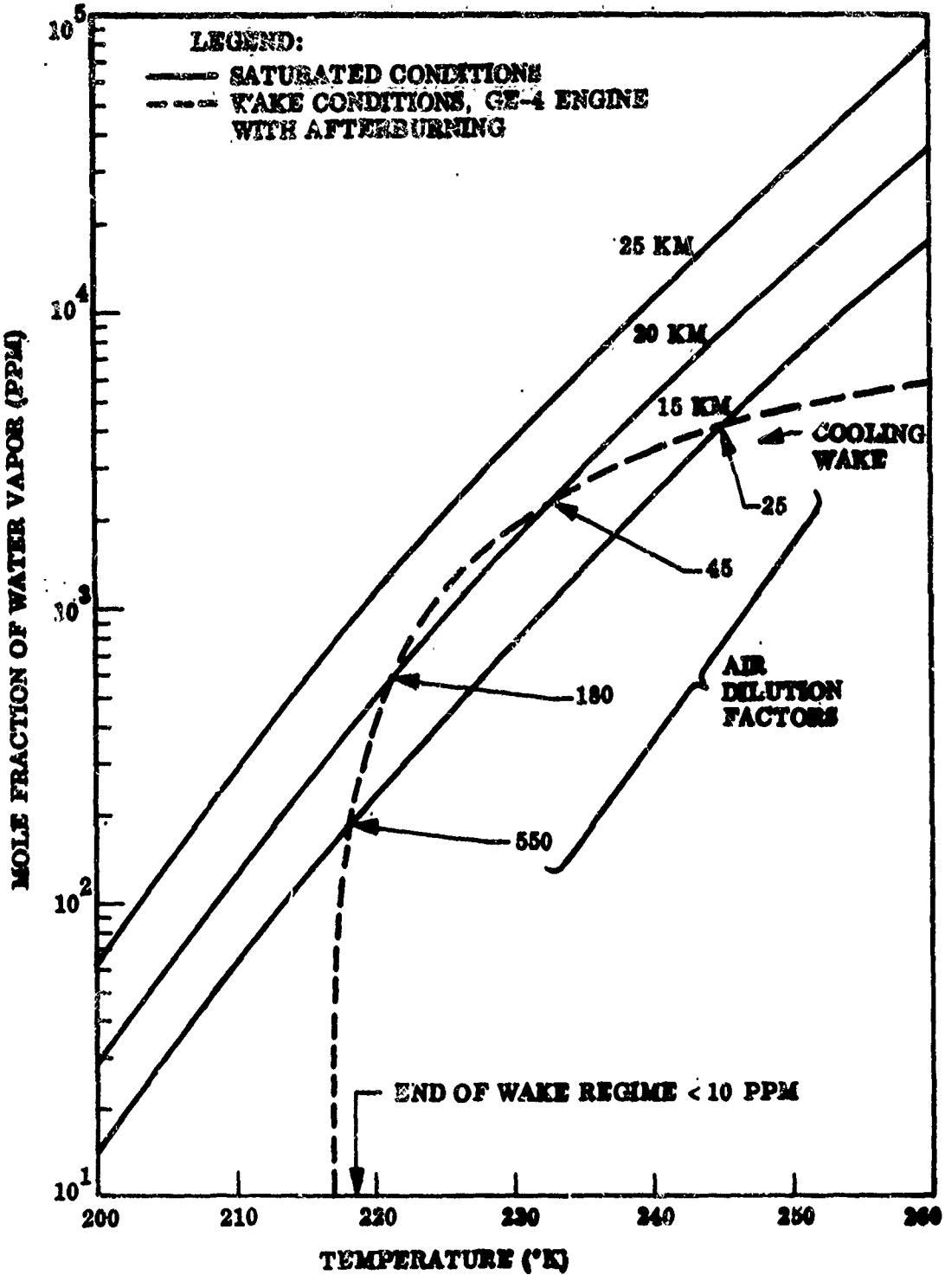

Figure 4-4 Water Condensation Regimes in the Wake

Additionally, reactions with half times of up to about a week are identified to aid in analysis of the diffusion regime. For initiation of the latter, a dilution of the exhaust by a factor of 3,000 is assumed. To provide a basis for kinetic analysis, an estimate of the engine exhaust characteristics must be made. Additional information is required relative to the ambient chemical species, particulates, and light intensity and spectrum.

From an analysis of aircraft engines without afterburners, it has been found that the concentrations of unburned hydrocarbons are extremely low (Ref. 4-7). With afterburners in operation, however, the hydrocarbon concentration generally increases drastically (Refs. 4-8 to 4-10). The concentration of hydrocarbons may be as much as 10 percent of the carbon monoxide formed. The maximum concentration of sulfur in the JP-5 fuel is specified as 0.1 weight percent. With an overall equivalence ratio of 0.8, a maximum sulfur dioxide content of about 100 ppm is calculated. Other exhaust species concentrations are taken from the previous sections. These are summarized in Table 4-2. It should be noted that the nitric oxide and SO_2 concentrations are considerably higher than those employed in atmospheric pollution studies which have been the principal source of photochemical kinetic data for this analysis.

Table 4-2

ENGINE EXHAUST CONCENTRATIONS

Component	Concentration	
	Mol Fraction	PPM by Volume
N_2	0.747	
H_2O	0.102	
CO_2	0.093	
O_2	0.055	
CO	0.001	
H, H_2, NO, O		400
OH		200
Hydrocarbon		250
SO_2		<100

Since many of the reactions which might lead to the formation of particulates are photochemical in nature, the light intensity at 20-km altitude is relevant to the problem. Attenuation of the solar spectrum will result principally from Rayleigh scattering, aerosol scattering, and ozone absorption. The relative importance of each will vary as a function of the wave length. Tabulations of extinction coefficients and optical thickness (Ref. 4-14) plus subsequent modifications (Ref. 4-15) were used as a basis for the relative intensities given in Table 4-4. The intensities are expressed as relative amounts reaching 20 km from outer space and relative amounts reaching sea level from 20 km. Attenuation coefficients are included to show the relative importance of each of the mechanisms.

Laboratory light intensities, when given in the aerosol literature, are usually related to sunlight at sea level. The increased intensities at 20 km must therefore be taken into account. From Table 4-4, this factor may vary from 2 at 4,000 Å to 16 at 3,000 Å. Short wave lengths are absorbed by ozone.

The effect of increased light intensity is often roughly compensated for by the effect of reduced temperature at 20 km. For example, in the laboratory photo-oxidation of nitric oxide in the presence of trans-2-butene, Altshuller and Bufalini found that an increase of 20°C caused the same increase in the rate of oxidation as a 2-fold increase in light intensity (see Ref. 4-16). Since the temperature at 20 km is roughly 80°C below laboratory temperatures, a reduction in rate of 2^4, or 16, is indicated for a process of the same activation energy. At wave lengths above 3000 Å, therefore, the net effect of the increased altitude may actually be a reduction in the rate observed under laboratory conditions.

The reactions of the engine exhaust species with each other and with ambient species to form particulates may be grouped as sulfur dioxide reactions, nitrogen oxide reactions, and combinations of both. Finally, consideration is given to heterogeneous reactions between particulates and gaseous species.

Table 4-4

ATMOSPHERIC ATTENUATION

Wave Length A	Attenuation Coefficients, 10^3 km^{-1}			Relative Intensities	
	Rayleigh	Aerosol	Ozone	I_o km/I_{20} km	I_{20} km/I_∞
6000	0.6	1.4	2.2	0.73	0.96
4000	3.1	1.9	0	0.52	0.97
3400	6.2	2.3	1.1	0.35	0.94
3200	8.0	2.4	14.7	0.25	0.78
3000	11	2.5	166	0.06	0.11
2800	14	2.6	1740	3.2×10^{-7}	1.12×10^{-10}

4.2.2 Sulfur Dioxide Reactions

As discussed previously in section 3.4.13 the oxidation of SO_2 by O atoms in the wake is negligible. In the rapidly cooling mixing region, function of SO_3 is forestalled by the faster removal of O atoms by $O + O_2 + M \rightarrow O_3 + M$.

SO2 Photolysis (dry). Widely varying rates of photolysis of SO_2 in air have been published. Hall found that SO_2 (56 to 230 mm) and O_2 (5 to 200 mm) reacted in sunlight with a first-order rate constant of 8×10^{-6} min^{-1} (see Ref. 4-17). Sethi et al. claimed a quantum yield of 2×10^{-3} over the wave length range of 2800 to 4200 Å (see Ref. 4-18). Renzetti and Doyle (Ref. 4-19) found a photolysis rate of 0.45 percent/min. Urone et al. (Ref. 4-20) cite a rate 0.1 percent/hr in the equivalent of a noonday sun. In the 0.14 to 1.0 ppm sulfur-dioxide range, Cox and Penkett (Ref. 4-21) found a first-order rate constant of 2×10^{-3} hr^{-1}, essentially independent of SO_2 concentration. Gerhard and Johnstone (Ref. 4-22) worked in the 2950 to 3650 Å range with SO_2 (5 to 50 ppm) in air and found a first-order conversion of 0.1 to 0.2 percent/hr in intense sunlight (3× sun). The short-term (20 min) conversion to SO_3 will be insignificant based on most of the above rates. However, in one week the conversion should exceed 10 percent.

SO_2 Photolysis (moist). The effect of moisture on the oxidation reaction rate is debatable. Water vapor was found to have no effect on the rate of less than 0.1 percent/hr except at 100 percent relative humidity, where the rate was slightly greater (Ref. 4-22).

Gartrell et al. found (Ref. 4-23) that the oxidation of SO_2 increased from 1/6 percent/min to about 2 percent/min in passing from low to high humidity.

The conclusion is drawn that the somewhat moist SO_2 oxidation probably falls in the same category as the dry reaction – of minor significance for 20 min, but significant over a 1-wk period. The significant aspect is that the subsequent formation of aerosol is always fast compared to the oxidation rate. Thus, $SO_3 + H_2O \rightarrow H_2SO_4$ is fast – i.e., $H_2SO_4(\ell)$ droplet formation is much faster than the 2%/min SO_3 maximum formation rate.

SO_2 + Ozone. This reaction is slower than the irradiation oxidation (Ref. 4-24) and is also considered to be too slow to be significant at atmospheric concentrations (see Ref. 4-25). It therefore would probably not be significant in 20 min in the stratosphere. It is possible, however, that a significant amount could react in a week, because of the much higher ambient concentration of ozone relative to oxygen atoms.

SO_2 + O + Third Body. A third-body reaction rate constant of 8×10^{-32} cm^6 $molecule^{-2}$ sec^{-1} was published by Cadle (see Ref. 4-26). This leads to an initial rate of 6×10^{-4} percent/min with oxygen atoms in the stratosphere, but the rate is eight orders of magnitude greater in the exhaust due to the vastly higher concentration of O-atoms. A rate constant of 1.5×10^{15} cm^6 $mole^{-2}$ sec^{-1} at 784°K has been calculated by Levy et al. (see Ref. 4-27). This is actually somewhat smaller than other values reported in the same paragraph for the reaction at 300°K and an order of magnitude lower than the estimate of Webster and Walsh (Ref. 4-28) for 784°K. With respect to the reaction rate near the exhaust jet, high O-atom levels and oxidation rates have been discussed previously.

SO_2 + Ozone + Olefins. High concentrations of ozone and olefins have been observed (Ref. 4-29) to produce a dense smoke, particularly with cyclic olefins, and the

addition of SO_2 did not significantly affect the rate of aerosol formation or the amount obtained. However, the aerosol appeared rapidly and the maximum amount formed within 5 min. Leighton has tabulated (Ref. 4-30) second-order rate constants for ozone-olefin reactions. Most are in the 2000 to 20,000 1 $mole^{-1}$ sec^{-1} range with a maximum of 10^5 1 $mole^{-1}$ sec^{-1} for trans-2-butene. If the latter rate is applied to the exhaust (O_3 = 1.6×10^{-9} mole/l and assuming 10 percent of the exhaust hydrocarbon is trans-2-butene = 1.8×10^{-8} mole/l) it yields an initial maximum rate of 1.0 percent/min. Both the rate constant and olefin concentration are likely to be much lower. In addition, a volume dilution factor of about 3000 in the wake is anticipated.

Kinetic data are also given by Cox and Penkett (Ref. 4-25) for low concentrations. It is suggested that the mechanism involves the formation of a peroxide zwitterion during the ozone-olefin reaction. Although the SO_2 did not have any significant effect on the rate of disappearance of ozone or hydrocarbon, large amounts of aerosol were produced when SO_2 was added to the mixture. At ozone and olefin concentrations of 0.05 ppm, the oxidation rate of 0.1 ppm SO_2 is estimated to be about 3 percent/hr for cis-2-pentene and 0.4 percent/hr for propene.

Based on the foregoing discussion, it is concluded that this reaction will not be significant within 20 min, but that the olefin concentration may be reduced by reaction within a 1-wk period. However, if the rate of SO_2 removal is proportional to the olefin concentration, dilution by more than three orders of magnitude will reduce the rate to insignificance for a 1-wk period.

Photolytic SO_2 + Organic. Irradiation at 2400 to 3340 Å of saturated and unsaturated hydrocarbons in the presence of SO_2 has been found by Dainton and Ivin to produce sulfinic acids (see Ref. 4-31). To the extent that the aerosol is organic it may experience instability by evaporation or oxidation (see Ref. 4-32). Harkins and Nicksic (Ref. 4-33) found that SO_2 consistently formed an aerosol in contact with hydrocarbons, that heavy hydrocarbons produced aerosols without irradiation, and that very little SO_2 actually oxidized. Another interesting observation was that an inverse correlation

exists between chamber temperature and aerosol formation. Johnston and Dev Jain (Ref. 4-34) irradiated 50 mm each of n-butane and SO_2 in 400 mm air and produced heavy fogs within 2 min.

Although aerosols containing sulfinic acids are produced, the rate of aerosol formation is negligible when the reactants are at concentrations of 100 ppm or less (see Ref. 4-35). Kopcynski and Altshuller also found that saturated hydrocarbons did not contribute significantly to aerosol production when compared to olefins. They concluded that the rate of photochemical reaction of paraffins or olefins with SO_2 was very slow in the 100 to 1000 ppm range. It is therefore concluded that the reaction will be insignificant in the wake regime. There is insufficient information to indicate its possible importance in the diffusion and transport regime.

4.2.3 Nitrogen Oxide Reactions

The exhaust is estimated to contain 300 ppm NO with almost no NO_2 present initially. The relative amounts of NO and NO_2 are very significant in the reaction rates of organic compounds. This influence is believed to be dependent on the fact that NO is more rapidly oxidized than hydrocarbons by reactive oxygen species. In general, the presence of NO retards the organic oxidation processes.

Photolytic NO + Organic. Methane, ethane, propane, and 2, 2-dimethyl propane are relatively unreactive in the photo-oxidation of NO. However, NO photo-oxidation rates appear to correlate with aerosol formation (see Ref. 4-36). Di-substituted internal olefins (2, 3 dimethyl-2-enes) have the highest NO photo-oxidation rate. For example, 2, 3 dimethyl-2-butene (1 ppm) and NO (0.4 ppm) provided a photo-oxidation rate of 0.059 ppm min^{-1}. The majority of some 40 other olefins evaluated by Glasson and Tuesday reacted in the range of 0.002 to 0.012 ppm min^{-1}. Stephens and Schuck (Ref. 4-37) irradiated NO plus auto exhaust and obtained aerosols after 30 to 60 minutes.

It is concluded that certain olefins could react significantly within a 20-min period; most will not. Since the special olefins will constitute only a very minor part of the total exhaust hydrocarbons, the total hydrocarbon content will not change significantly during this period.

Photolytic NO + Olefin + CO. According to Westberg et al., the presence of CO markedly accelerates the disappearance of olefin, the conversion of NO to NO_2, and the appearance of ozone (Ref. 4-38). However, from the published curves, the presence of 100 ppm CO had little effect in 20 min on the photo-oxidation of NO (1.5 ppm) in the presence of isobutene (3 ppm) and 70 percent relative humidity. The mechanism is dependent upon a hydroxyl carrier, as follows:

$$OH + CO \rightarrow CO_2 + H$$
$$H + O_2 + (M) \rightarrow OOH + (M)$$
$$OOH + NO \rightarrow OH + NO_2$$

The more rapid reactions of ozone and O-atoms with NO would probably override this reaction.

The reaction does not appear to be of concern in the 20-min picture, since dilution by 3000 will reduce the CO concentration from 1000 to less than 1 ppm. From the data in Ref. 4-38, it appears that changes in the olefin and NO concentrations could be significant in the diffusion regime although in this case the CO would tend to reduce the amount of NO_2 formed.

Photolytic NO_2 + Organic. The photolysis of NO_2-hydrocarbon mixtures in air has been examined by Schuck and Doyle (see Ref. 4-39). The maximum rate constant for 3-methyl pentane (6ppm) and NO_2 (2ppm) corresponded to 0.15 percent/min. The olefins produced much greater rates. For example, trans-2-butene (~ 3 ppm) and NO_2 (~ 1 ppm) yielded a rate corresponding to 13.6 percent/min. Other olefins were in the 1.5 to 3.5 percent/min category.

From these data, it is concluded that the total hydrocarbons will not be significantly reduced in the 20-min period when the 3000-fold volume dilution is taken into account. However, the occurrence of significant photolytic reactions with olefins, even with dilution, is conceivable over a one-week period.

Inorganic Nitrates and Nitrites. Nitric acid is not sufficiently hygroscopic to form aerosols in the stratosphere (see Ref. 4-40). There are many possible reactions for formation and destruction of nitrous acid, for example:

$$M + NO + OH \rightarrow HNO_2 + M$$
$$NO_2 + OH \rightarrow HNO_2 + O$$
$$NO_2 + H_2O \rightarrow HNO_2 + OH$$
etc.
$$H + HNO_2 \rightarrow H_2 + NO_2$$
$$OH + HNO_2 \rightarrow H_2O + NO_2$$
etc.

The first reaction in each set utilizes readily available species, i.e., NO, OH, and H from the exhaust jet.

Rate data are not available for some of these reactions (Ref. 4-41), but it seems unlikely that aerosol formation will result, even if HNO_2 is present. In moist air, nuclei may form by hydration of HNO_2 or HNO_3, but the aerosol formation rate is very slow according to Vohra (see Ref. 4-42).

Ammonium nitrate could easily form particulates, for example:

$$NH_3 + HNO_3 \rightarrow NH_4NO_3$$

However, as discussed in Section 3, very little HNO_3 is anticipated in the exhaust and wake, and there is no evidence that significant quantities of NH_3 may be expected. In general, inorganic nitrate particulate formation in the wake is not anticipated.

4.2.4 Combinations of Nitrogen and Sulfur Oxide Reactions

SO_2-NO. The combination of SO_2 and NO produces no aerosol according to Prager et al. (see Ref. 4-43).

Photolytic SO_2 + NO + Organic. Haagen-Smit (Ref. 4-29) found that the irradiation of cyclohexene, NO, and SO_2 did not produce any aerosol in the first half hour.

In the irradiation of propylene (2 ppm), NO (0.5 ppm), and SO_2 (1.2 ppm) Altshuller et al. (Ref. 4-44) found that the rate of consumption of propylene was independent of the amount of SO_2. With essentially the same concentration of reactants, Cox and Penkett obtained a 7 to 10 percent conversion of SO_2 to sulfate aerosol in a 2-hr irradiation (see Ref. 4-21). With cis-2-pentene (0.98 ppm), NO (0.73 ppm), and SO_2 (0.07 to 0.25 ppm), the same experimenters obtained an SO_2 reaction rate of 0.64 percent/min. In the latter case, the chamber intensity was only one-fourth that of sunlight. Aerosol appeared after 100 min (Ref. 4-45) in the system 1-butene (4 ppm), NO (1 ppm), and SO_2 (0.72 ppm). Ozone does not appear until almost all the NO is converted to NO_2 (see Ref. 4-43).

Since the induction period for particulate formation with 5 ppm NO approaches 20 min a significant concentration change is not anticipated within this time interval. Over the period of 1 wk however, certain olefins may undergo significant changes although a 3000-fold dilution will tend to offset this possibility. Except for independence of SO_2 concentration, not enough details of the mechanism are known to predict the effect on NO and SO_2 concentrations.

Photolytic SO_2 + NO_2. The irradiation of SO_2 and NO_2 has been studied by Jaffee and Klein (see Ref. 4-46). They obtained an overall rate constant which was a function of the third body concentration. For the conditions in the exhaust and in the ambient stratosphere, $k = 1.4 \times 10^{10}\ l^2\ mole^{-2}\ sec$. The overall rate at the exit plane of the exhaust is

$$\text{Rate} = 1.4 \times 10^{10}\,[O]\,[SO_2]\,[M]\,60 = 5.1 \times 10^{-5}\ mol\ l^{-1}\ min^{-1}$$

or 1.8×10^4 percent/min, a rate reasonably close to the earlier estimates for the three-body SO_2-O reaction. Gerhard and Johnstone (Ref. 4-22) irradiated SO_2 (5 to 30 ppm) and NO_2 (2 ppm), and found no effect of salt or moisture on the rate.

Renzetti and Doyle found (Ref. 4-19) that NO_2 enhanced aerosol formation whereas NO suppressed it.

This reaction may be presumed similar to the three-body SO_2-O reaction previously discussed.

Photolytic SO_2 + NO_2 + Organic. The addition of 12 ppm n-hexane to SO_2 (16 ppm), NO_2 (15 to 410 ppm), and air containing 0 to 100 percent relative humidity showed that the reaction rate was independent of moisture content except at 100 percent humidity (see Ref. 4-20). The highest rate observed, 0.4 percent/min was found at the highest moisture and NO_2 levels. In most cases less than 10 percent of the SO_2 reacted over extended periods of time. Aerosol was not produced (Ref. 4-43) with n-butane or 2-methyl pentane.

A considerable amount of work has been devoted to examining the increased aerosol production rate obtained by adding olefins to the NO_2-SO_2 system. All types of olefins produced particulates. The induction period for conversion of NO to NO_2 was again noted during the irradiation of engine exhaust (see Ref. 4-39). Diolefins were found (Ref. 4-43) to increase the reaction rate less than straight-chain mono-olefins. Cyclic olefins formed particulates more rapidly than straight-chain olefins (see Ref. 4-29). The reaction was completed in 0.5 hr or less, according to Haagen-Smit.

The photolysis of 1-hexene (1.5 ppm), with 1 ppm each of SO_2 and NO_2 in air, removed SO_2 at up to 15 percent/hr (see Ref. 4-17.). Endow et al. found that sulfuric acid was a major component of the resulting aerosols and that aerosols formed at 10 to 20 percent relative humidity contained more inorganic nitrogen than those formed at 50 percent relative humidity (see Ref. 4-47). Goetz and Pueschel (Ref. 4-48) determined that the growth rate of the aerosol was proportional to the hydrocarbon concentration. They also found that the sequence of addition of reactants influenced the aerosol. When Stevenson et al. added less than 1 ppm SO_2 to systems containing 10 to 20 ppm unsaturated hydrocarbons and 3 ppm NO_2, the photolytic aerosol production increased (see Ref. 4-49).

It is concluded that the occurrence of a significant degree of hydrocarbon reaction with SO_2 and NO_2 within 20 min would not be expected; further, little or no NO_2 is initially present. The importance of the reaction will depend on the speed with which NO is converted to NO_2. Certain olefins may react substantially over a 1-wk period. This indication is based upon the observed rates in the SO_2-free system and the increased aerosol production observed when SO_2 was added to the system. Here again, the overall hydrocarbon concentration would not decrease significantly, since a major portion of the composition is saturated.

4.2.5 Heterogeneous Reactions

The potential effect of recently-formed or existing particulates on chemical reactions forming aerosols may be explored. First, it has already been shown that the ambient concentration of particles at 20 km altitude is extremely low (100 particles/liter) and is therefore not likely to significantly affect the reactions of the exhaust species. The potentially catalytic nuclei which result from the exhaust itself may be classified as aqueous sulfate systems or basic oxides.

Aqueous Sulfate Systems. The rate of oxidation of SO_2 in 30 percent sulfuric acid (Ref. 4-22) is said to be negligible compared to the rate of photochemical oxidation. In the presence of ammonia, however, Van der Hemel and Mason (ammonia-SO_2-water-air system) found (Ref. 4-50) that oxidation of SO_2 in cloud droplets may be more efficient than the photochemical conversion.

Scott and Hobbs (Ref. 4-51) observed that the concentration of sulfate in a droplet after 24 hr is about two orders of magnitude greater when ammonia is present than when it is absent. By assuming that the rate of formation of sulfate is proportional to the sulfite ion concentration and considering the several equilibria involved, the following rate expression is developed:

$$\frac{d[SO_4^{=}]}{dt} = K\,[SO_3^{=}] = 9.84 \times 10^{-11}\,\frac{[P_{SO_2}]}{[H^+]^2}$$

where H^+ is related to P_{NH_3}.

Information on stratospheric ammonia was not found. An average sea-level atmospheric concentration of 7×10^{-9} atm, together with the estimated exhaust SO_2 partial pressure of 4.7×10^{-6} atm, would yield an initial conversion rate of 1580 percent/min.

Certain salts, notably those of iron, copper, and manganese, are known to catalyze the conversion of SO_2 to sulfate. Johnstone and Coughanowr (Ref. 4-52) estimated that 1 ppm SO_2 oxidized at 1 percent/min. Manganese sulfate produced the highest rate among the salts tested. Johnstone and Moll found, when manganese or ferrous sulfates were present in the 250-ppm SO_2 – moist air system, that about 1 percent/min of sulfuric acid formed in fogs (Ref. 4-53).

It has not been established to what extent ammonia, iron, or manganese are present either in the engine exhaust or in the ambient stratosphere. At this time, it can only be stated that if any or all are present, significant reductions in SO_2 concentration could occur in the dispersion regime. In the wake region, diffusion to the catalytic nuclei would probably limit the SO_2 concentration reduction rates.

Basic Oxides. Although sodium chloride showed relatively little effectiveness in oxidizing SO_2 (Refs. 4-20, 4-53), certain basic oxides have demonstrated great efficiency in scavenging SO_2. Forty percent of the SO_2 (1 ppm) in air (46 percent relative humidity) was quickly absorbed by 1.8×10^8 nuclei per liter. Oxidized lead aerosols removed SO_2 completely in less than 5 min according to Smith (See Ref. 4-54). Dried hydrous iron-oxide particles were successful in removing SO_2 within seconds (Ref. 4-20), but this result was obtained with high powder/SO_2 ratios. Oxides of aluminum, calcium, and lead also yielded high absorption rates.

It is unlikely that these oxides would be found in either the wake or dispersion areas in sufficient concentration to significantly alter the SO_2 concentration.

4.3 REFERENCES FOR SECTION 4

4-1 H. S. Johnston, Calalytic Reduction of Stratospheric Ozone by Nitrogen Oxides, Report UCRL-20568, Jun 1971

4-2 H. S. Johnston, "The Effect of Supersonic Transport Planes on the Stratospheric Ozone Shield," Environmental Affairs, 1972

4-3 H. Harrison, "Aerosols, An Influence Upon Stratospheric Chemistry," Proceedings of Climatic Impact Assessment Program Workshop on Computational Modeling of the Atmosphere," DOT-TST-90-1, Apr 1972

4-4 "Stratospheric Aerosols," (Nov 1972) Report of an Informal Meeting Held at Dept. of Transportation, Washington, D.C., 5–6 Oct 1972

4-5 I. D. Clark, and T. F. Noxon, "Particle Formation during Water-Vapor Photolysis," Science, Vol. 174, 26 Nov 1971, p. 4012

4-6 N. Sissenwine, et al., How Dry is the Sky? A Decade Later and the SST, AFCRL-72-0294, Apr 1972

4-7 H. T. McAdams, Analysis of Aircraft Exhaust Emission Measurements Statistics, Cornell Aeronautical Laboratory, CAL NA 5007 K-2, Nov 1971

4-8 NASA TMX 2323

4-9 NAPTC-ATD-212

4-10 E. S. Starkman et al., "The Role of Chemistry in Gas Turbine Emissions," J. Eng. Power, Jul 1971, pp. 333–341

4-11 J. Geophys. Res., Vol. 68, 1963, p. 3977

4-12 J. Meteorology, Vol. 18, 1961, pp. 746 – 752

4-13 J. Meteorology, Vol. 18, 1961, pp. 8[illegible] – 101

4-14 L. Elterman, Atmospheric Attenuation Model to 50 km, AFCRL 64-740

4-15 -----, Atmospheric Attenuation Model to 50 km, AFCRL 68-0153

4-16 Int. J. Air and Water Poll., Vol. 7,1963, pp. 669–671

4-17 Envir. Sci. Tech., Vol. 2,1969, p. 438

4-18 Fifth International Conference on Photochemistry, Yorktown Heights, New York, Sep 1969

4-19 Int. J. Air Poll., Vol. 2, 1960, pp. 327–345

4-20 Envir. Sci. Tech., Vol. 2, 1968, pp. 611-8

4-21 Nature, Vol. 229, 1971, pp. 486–488

4-22 Ind. Eng. Chem., Vol. 47, 1955, pp. 972–976

4-23 Envir. Sci. Tech., Vol. 3, 1969, p. 437

4-24 Nature, Vol. 188, 1960, pp. 51–52

4-25 Nature, Vol. 230, 1971, pp. 321–322

4-26 J. Geophys. Res., Vol. 68, 1963, p. 3977

4-27 Envir. Sci., Tech., Vol. 4, 1970, p. 661

4-28 Tenth Symposium (International) on Combustion, The Combustion Institute, Pittsburgh, Pa., 1965, p. 463

4-29 Ind. Eng. Chem., Vol. 44, 1952, p. 1342

4-30 P. A. Leighton, Photochemistry of Air Pollution, New York, Academic Press, 1961, p. 160

4-31 Trans. Far. Soc., Vol. 46, 1950, pp. 374 – 394

4-32 Staub (Dusseldorf), Vol. 28, 1960, p. 303

4-33 J. Air Poll. Cont. Assoc., Vol. 15, 1965, pp. 218 – 221

4-34 Science, Vol. 131, 1960, pp. 1523 – 1524

4-35 Int. J. Air and Water Poll., Vol. 6, 1962, pp. 133 – 135

4-36 Envir. Sci. Tech., Vol. 4, 1970, pp. 916 – 924

4-37 Chem. Eng. Prog., Vol. 54, 1958, p. 71

4-38 Science, (3975), Vol. 171, 1971, pp. 1013 – 1015

4-39 Air Pollution Foundation, Report No. 29, San Marino, Calif., 1959

4-40 Massachusetts Institute of Technology, Study of Critical Environmental Problems, (Summer Study Program, Williams College), 1970

4-41 NBS 10867 and, Environmental Aspects of the Supersonic Transport, U.S. Department of Commerce, No. 0300-0050, May 1972, p. 34

4-42 J. Geophys. Res., Vol. 75, 1970, p. 2951

4-43 Ind. Eng. Chem., Vol. 52, 1960, pp. 521 – 524

4-44 Envir. Sci. Tech., Vol. 1, 1967, p. 899

4-45 J. Air Poll. Cont. Assoc., Vol. 20, 1970, pp. 385 – 390

4-46 Trans. Far. Soc., Vol. 62, 1966, pp. 2150 – 2157

4-47 J. Air Poll. Cont. Assoc., Vol. 13, 1963, pp. 141 – 147

4-48 Atmos. Environ., Vol. 1, 1967, pp. 287 – 306

4-49 Int. J. Air and Water Poll., Vol. 9, 1965, pp. 368 – 375

4-50 Roy. Met. Soc. J., Vol. 89, 1963, p. 271

4-51 J. Atmos. Sci., Vol. 24, 1967, pp. 54 – 57

4-52 Ind. Eng. Chem., Vol. 50, 1958, pp. 1169 – 1172

4-53 Ind. Eng. Chem., Vol. 52, 1960, pp. 861 – 863

4-54 Envir. Sci. Tech., Vol. 3, 1969, pp. 558 – 562

Section 5

RADIATIVE COOLING AND RADIATIVE INDUCED BUOYANCY

In this section we address ourselves to two questions. One, does the energy loss rate due to radiative emission of the hot exhaust gases at the exit temperature have a significant effect on the initial wake cooling? Second, does radiative heating or cooling in the long-time dispersion wake result in a slight temperature change (of a few degrees) which would induce buoyancy effects?

In answering the first question, the proper perspective is obtained by recognizing that the initial wake mixing with cool air results in a 500°K temperature drop in a few milliseconds. At typical exit temperatures around 2000°K the primary source of radiative emission is the intense 4.3-μ band of CO_2. An upper estimate to the radiative cooling rate was determined by assuming an optically thin model, i.e., one in which all energy emitted by the CO_2 molecules escapes from the wake.

The energy loss per unit mass of CO_2 is

$$(Q_{rad})_{CO_2} = 4\pi\, \alpha_{band}\, B_{\omega_o}(T) \left(\frac{erg}{gm_{CO_2}\, sec}\right)$$

when α_{band} is the integrated band absorption for the 4.3-μ CO_2 band, and $B_{\omega_o}(T)$ is the Planck function evaluated at the band center frequency ($\omega_o = 2,350\ cm^{-1}$) and at the exhaust gas temperature. The energy loss due to CO_2 is shared by all of the exhaust species. The energy loss per unit mass of exhaust gases is

$$(Q_{rad})_{exhaust} = C_{CO_2} (Q_{rad})_{CO_2} \quad \left(\frac{erg}{gm\text{-}sec}\right)$$

where C_{CO_2} is the mass fraction of CO_2 species for which we assumed a value of 0.25. The temperature rate of change is simply $(Q_{rad})_{exhaust}$ divided by the specific heat of the high-temperature exhaust gases. At an exhaust temperature of 2000°K, radiative cooling will produce a rate of temperature decrease of about 13°K per millisecond. At an exhaust temperature of 1000°K, the cooling rate has dropped by a factor of six. It is clear from this straightforward upper-bound estimate that the radiation cooling rates are inconsequential when compared with the temperature decrease due to gas dynamic effects.

The question of radiative cooling or heating in the long-time dispersion wake regime is much more difficult to assess. Considered on a global basis, a parcel of air in the middle and upper stratosphere (altitude $\gtrsim$ 30 km) cools by infrared radiative transport. This cooling results primarily from energy lost to space via emission in the CO_2 15-μ band.* In the lower stratosphere, cooling due to 15-μ band CO_2 emission disappears as the parcel of air can no longer "see" the cool space background. Rather, at these lower altitudes a parcel of air is surrounded by an atmosphere that is nearly isothermal over the mean free path for photons emitted in the 15-μ band. A similar situation holds for CO_2 amounts due to exhaust gases at the SST wake altitude.

The situation with respect to water vapor in the SST exhaust is quite different. There will be an imbalance of H_2O molecules above the atmospheric ambient level due to the SST wake. In the long-time dispersion wake the CO_2 level will be only slightly perturbed from the ambient level of about 3×10^{-4} mass fraction. The H_2O imbalance will produce two counterposed effects: (1) absorption of solar radiation in the 2.7-μ band and (2) emission in the H_2O rotation band which starts at approximately 20 μ. An examination of these two effects shows that the far-infrared cooling dominates. A highly accurate determination of the amount of cooling would necessitate a detailed

*W. R. Kuhn and J. London, "Infrared Radiative Cooling in the Middle Atmosphere (30-110 km)," J. Atmos. Sci, Vol. 26, p. 189 – 204, 1969.

numerical solution of the equation of radiative transfer over a number of wavelength intervals sufficient to account for the spectral dependence of the H_2O rotational band. Rather than attempt such a laborious calculation, the following approximate analysis based on an optically thin model was performed. We assume that photons emitted upward, i.e., over a 2π steradian view factor represented by emission to free space, participate in the cooling. Then the cooling rate becomes

$$(Q_{rad})_{H_2O} = 2\pi \int_0^\infty \mu(\omega)\, B(\omega, T)\, d\omega \qquad \frac{erg}{gm_{H_2O}\,sec}$$

It is inadequate to make the approximation that $B(\omega, T) \approx B_{\omega_0}(T)$, since the pure rotational band extends over a large wave-number range. Rather, we approximate the spectral absorption coefficient variation as

$$\mu(\omega) \approx \frac{\alpha_{band}}{\sqrt{\pi}\,\Gamma} \left(\frac{\omega}{T}\right) e^{-(\omega/T)^2}$$

with

$$\Gamma = \left(\frac{4\,kT\,B_e}{hc}\right)^{1/2}$$

and where B_e is the rotation constant which we take as 30 cm^{-1}. Performing the above integration at a wake temperature of 220°K we arrive at a cooling rate of

$$(Q_{rad})_{H_2O} = 2.7 \times 10^8 \frac{erg}{gm_{H_2O}\,sec}$$

Again, the energy loss is shared by all of the exhaust species. Hence the energy loss per unit mass of exhaust gases is

$$(Q_{rad})_{cooling} = (Q_{rad})_{H_2O} \cdot C_{H_2O}$$

where C_{H_2O} is the mass fraction of water vapor. The mass fraction (i.e., mixing ratio) of water vapor in the ambient atmosphere is about 10^{-6}. In a time on the order of a few minutes, the wake is dispersed to an extent that the wake water vapor level is only one order of magnitude above ambient so that $C_{H_2O} = 10^{-5}$. The radiative cooling rates are sufficiently low that negligible cooling occurs over the short time interval where C_{H_2O} exceeds 10^{-5}. At a level of water vapor of 10^{-5} (equal to 10 times ambient) the cooling rate yields a rate of temperature drop of

$$\frac{\Delta T}{\Delta t} = \frac{(Q_{rad})_{cooling}}{\text{heat capacity of air}} \sim 1\ ^\circ K/hr$$

Because of the optically thin model, the above rate of temperature decay is a conservative upper bound. From an examination of the strengths of the lines in H_2O rotational band,* we estimate that only those lines which are located at wavelengths shorter than about 25 μ would emit to free space. This would lower the cooling rate by about one order of magnitude. Furthermore, the mixing of the wake gases with the atmosphere will reduce the wake water vapor concentration to further reduce the cooling rate.

The rate of temperature drop does not persist indefinitely. As soon as the wake drops below ambient temperature, absorption in the 15-μ band of CO_2 occurs. The final temperature reached is such that the absorption by CO_2 balances the loss of H_2O, i.e.,

$$(Q_{rad})_{\substack{heating \\ CO_2}} = (Q_{rad})_{\substack{cooling \\ H_2O}}$$

*See Table 5.5 of R. M. Goody, Atmospheric Radiation, Oxford Press New York, 1964.

The CO_2 15-μ band heating rate is

$$(Q_{rad})_{\substack{\text{heating} \\ CO_2}} = 4\pi \alpha_{band} [B_{\omega_o}(T_{amb}) - B_{\omega_o}(T_{wake})]$$

which yields a final temperature about 2 percent below ambient based on the upper-bound optically thin model and if the water vapor concentration remained at 10 times ambient. It is estimated that self-absorption in the water vapor bands and wake mixing will reduce the final temperature to about 0.2 percent below ambient.

Section 6
EXHAUST PARTICULATE TRANSPORT

The need to include the particulate fallout process as part of the wake model has been investigated. If hours are required for the particles to fall an appreciable distance, say a thousand feet, then this process need not be included. In the study, particle sizes ranging from one micron in diameter to a tenth of a micron were considered. This range of particle sizes is in agreement with that measured in the Naval Air Propulsion Center.* The sinking velocity of the particles was determined from Newton's Second Law where, in this case, the vertical force component was the difference between the gravitational force and the drag force:

$$mg - D = m\,(dV/dt)$$

Because of the relative size of the particle as compared to the mean free path at typical SST cruise altitudes, a free-molecular drag force was assumed:

$$D = C_D qA = C_D\left(\frac{1}{2}\rho V^2\right)\left(\frac{1}{4}\pi d^2\right)$$

where it can be shown to the first order of accuracy that the drag coefficient for a sphere in the free molecular flow regime is:**

$$C_D = \frac{}{\sqrt{\pi}}\frac{35}{6}\frac{1}{S} + O(S) = \frac{35}{6}\sqrt{\frac{2RT}{\pi}}\frac{1}{V}$$

---

*"Study of Altitude and Mach Number Effects on Exhaust Gas Emissions of an Afterburning Turbofan Engine," NAPTC-ATD-212, December 1971.

**Princeton Series on High Speed Aerodynamics and Jet Propulsion, Volume III: Fundamentals of Gas Dynamics, p. 704.

In these expressions ρ is the ambient density; V is the vertical component of the particle velocity; d , the particle diameter; R , the gas constant; and T , the ambient temperature. The parameter S is defined by

$$S = \frac{V}{\sqrt{2\,RT}}$$

For known ambient conditions, the drag force becomes

$$D = \frac{35}{48}\sqrt{2\pi\,RT}\,\rho\ (Vd^2) = (\text{constant})\ (Vd^2)$$

Substituting this expression for D into Newton's law yields a first order differential equation for the velocity V . Assuming as initial conditions zero velocity and zero distance traveled, the first order differential equation is readily integrated yielding

$$v(t) = \tau g\ (1 - e^{-t/\tau})$$

and

$$x(t) = \tau g\ [t + \tau\ (e^{-t/\tau} - 1)]$$

where the characteristic time τ is defined as

$$\tau = \frac{m}{\left(\frac{35}{48}\sqrt{2\pi\,RT}\,\rho\right) d^2} = \frac{m}{(\text{constant})\ (d^2)}$$

For carbon particulate matter deposited at 65,000 feet, these expressions show, Figure 6-1, that 2.5 weeks are required for the one micron particle to fall a thousand feet, and 176 days (approximately six months) are required for the one-tenth micron particle to fall the same distance. From this it can be concluded that the transport of particulate matter in the engine exhaust jet and in the vortex field need not be treated separately from the gas transport since the particles will follow the gas motions closely.

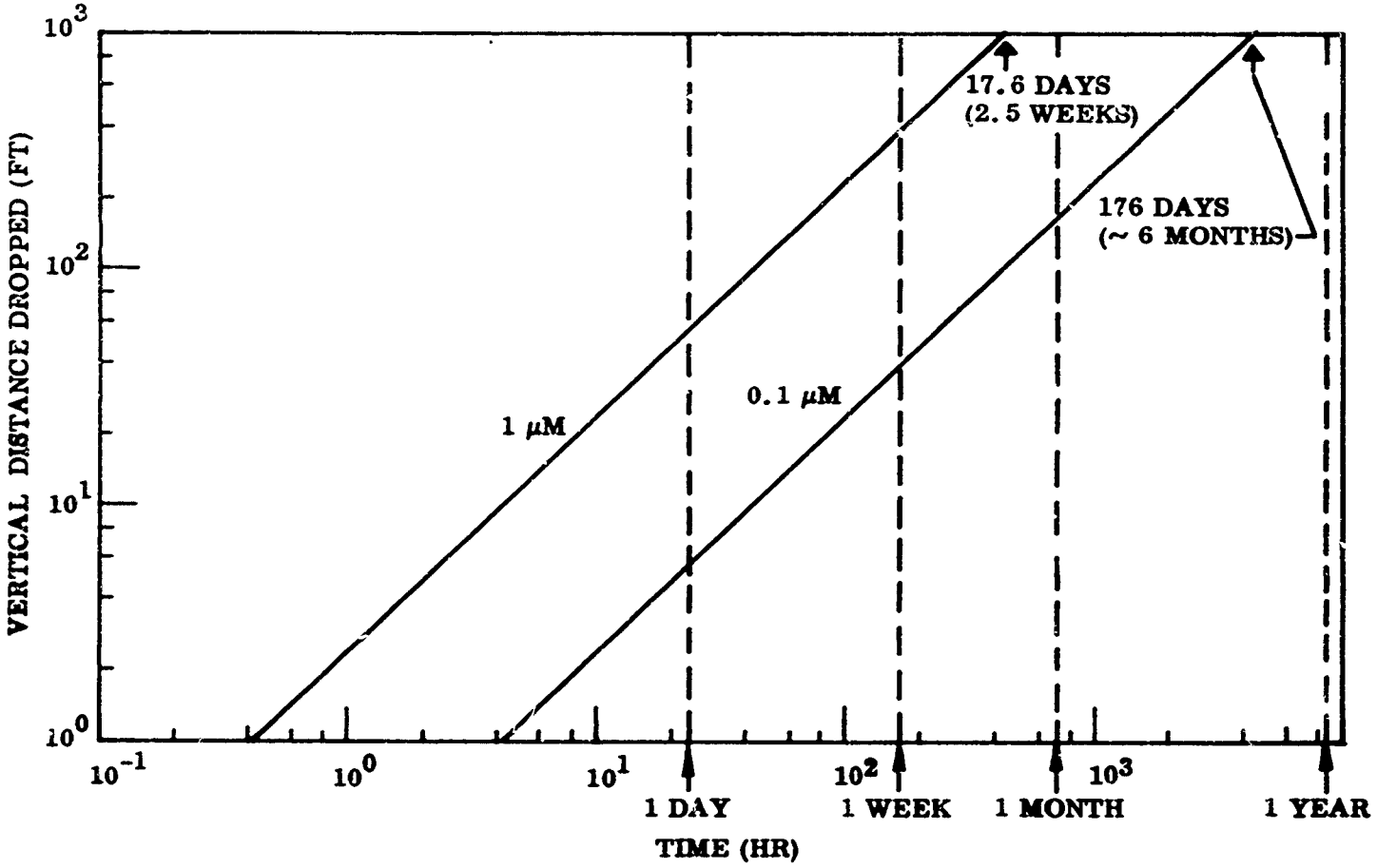

Figure 6-1 Particulate Transport Times

Section 7

INTERFACE BETWEEN WAKE MODEL AND DIFFUSION AND TRANSPORT MODEL

In this section the fluid mechanical and chemical interface between the wake model and the diffusion and transport model under development by the Lawrence Livermore Laboratory is discussed. The interface defines the time interval after passage of the aircraft over which the wake model will predict the fluid mechanical and chemical behavior of the aircraft wake. The interface will also include definition of the output quantities of the wake model which will be used as input quantities to the diffusion and transport model. Also included in this section is a discussion of requirements imposed on the wake model by the basic objectives of the diffusion and transport model.

7.1 INTERFACE DEFINITION

The basic definition of the wake model and the diffusion and transport model interface is that the wake model must describe the aircraft wake for a sufficient distance behind the aircraft until the aircraft-induced perturbations in the atmosphere become small relative to naturally occuring perturbations in the atmosphere. In other words the wake model must extend a sufficient distance behind the aircraft until the aircraft-induced perturbations no longer affect the fluid mechanics and chemical kinetics of the wake.

The fluid mechanical interface can be best defined by considering the wake growth data and theoretical estimates shown in Figure 2-19. The most persistent dispersion mechanisms are those associated with the wake height – namely, wind shear and gravitational collapse. Wind shear is dependent on the height since the difference in advection between the top and bottom of the wake volume is a function of the wake height, vertical wind shear, and angle between the wind vector and the wake axis. Gravitational collapse is height dependent, since the driving potential for collapsing the wake is a function of the density difference between the wake fluid and the atmospheric air, which in turn is directly dependent on the wake height.

The interface between the wake regime and the transport and dispersion regime, can then be defined by the point in time when the wake height is no longer affected by the aircraft flow field. This point is when the gravitational wake collapse is completed, which is at a wake age of about 20 min for the B-52 and about 10 to 15 min for the Convair 990. At the present time, a method for scaling the point at which the gravitational collapse is completed has not been developed. It is hoped that a scaling method will be developed in the near future. The fluid mechanical interface can only be defined in terms of the physical phenomenon at this time.

The output quantities from the wake model will be the width and height of the wake and the concentration of the engine exhaust emission. Although the chemical interface has not been firmly established, it is expected that the species concentrations to be defined at the model interface will include NO, NO_2, O_3, OH, SO_2, SO_3, and, perhaps, hydrocarbons. The solid particulate concentration will also be included which, in the present chemical model, is assumed to be inert.

7.2 DIFFUSION AND TRANSPORT MODEL REQUIREMENTS ON WAKE MODEL

The requirements imposed on the wake model are dictated by the impact errors in the wake model outputs will have on the diffusion and chemistry in the long-term wake, as predicted by the diffusion and transport model. For present purposes, it is assumed that the time frame of the diffusion and transport model is of the order of days. If longer time periods are considered, the requirements on the wake model are considerably relaxed. The requirements on the wake model are discussed in relationship to the NO_x/O_3 photochemistry, wake diffusion, and particulate formation in the diffusion and transport regime.

The half-times for catalytic reduction of ozone by the oxides of nitrogen according to the analysis discussed in Section 4 (Photochemistry in the Wake Regime) are presented in Figure 7-1. Note that the half-times are strongly dependent on the NO_x concentrations. The NO_x concentration is given by the total mass of NO_x in the wake and the total volume over which it is distributed (assuming no NO_x sinks). The total quantity of NO_x in the wake should therefore be given as accurately as possible

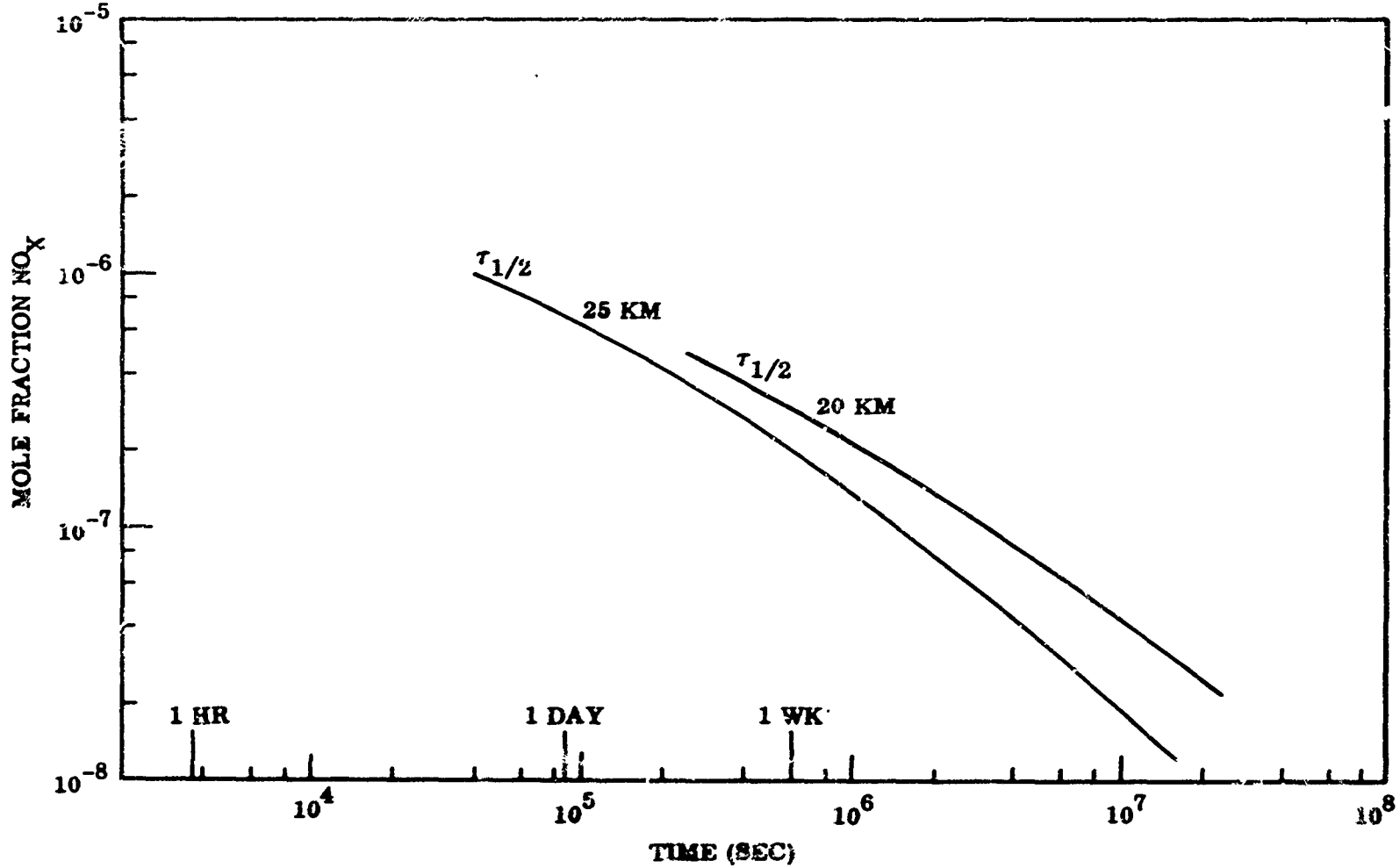

Figure 7-1 Half-Times for Catalytic Reduction of O_3 by NO_X

even though significant NO_x/O_3 photochemical reactions may not occur in the diffusion and transport regime as indicated by Figure 7-1. The NO_x requirement is probably the most important requirement on the wake model.

The dependence of long-term wake diffusion in the diffusion and transport regime on the initial wake size is illustrated in Figure 7-2. These solutions to the diffusion equations were obtained from Ref. 7-1 where the diffusion coefficient is taken to be of the form

$$k \sim \epsilon^{1/3} \sigma(t)^{4/3}$$

where ϵ is the dissipation rate (cm^2/sec^3) and σ is the standard deviation of the concentration. For present purposes, the standard deviation σ is equated to the wake width. At early times, there is some effect of the initial wake size on the wake width but at times of the order of a day, the wake width is weakly dependent on the initial wake size. These results indicate that the initial wake size is not a critical input parameter to the diffusion and transport model.

The chemistry related to the formation of particulates was discussed in detail in Section 4 (Photochemistry in the Wake Regime). The results presented in Section 4 indicate that sulphuric acid particulates may be formed in the wake regime due to the relatively high concentration of oxygen atoms. If it is desirable to trace the formation of particulates in detail, it will be necessary to include the percentage conversion of sulphur dioxide to sulphuric acid as a wake model output quantity. If only the long-term formation of sulphuric acid particulates is of interest, the relatively small degree of conversion in the wake can be ignored.

The time rate of diffusion of engine effluents into ambient air as a function of final wake concentration distribution and diffusion coefficient was investigated to determine the necessity of including concentration gradients as a wake output parameter. The distributions considered were those shown in Figure 7-3. To obtain the Gaussian, it has been assumed that all of the aircraft-generated turbulent mixing has died out, leaving a

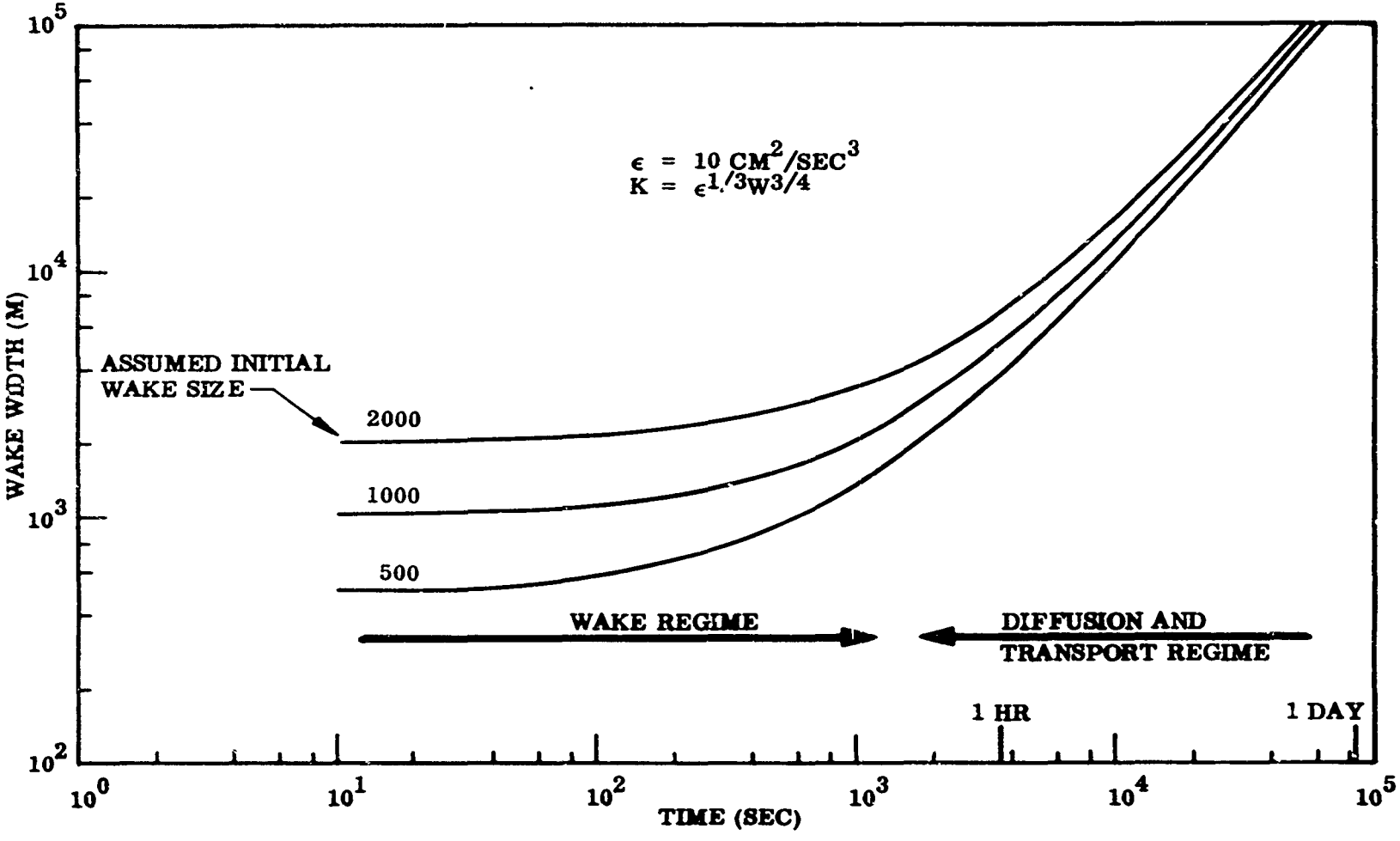

Figure 7-2 Effect of Initial Wake Size on Wake Width in Diffusion and Transport Regime

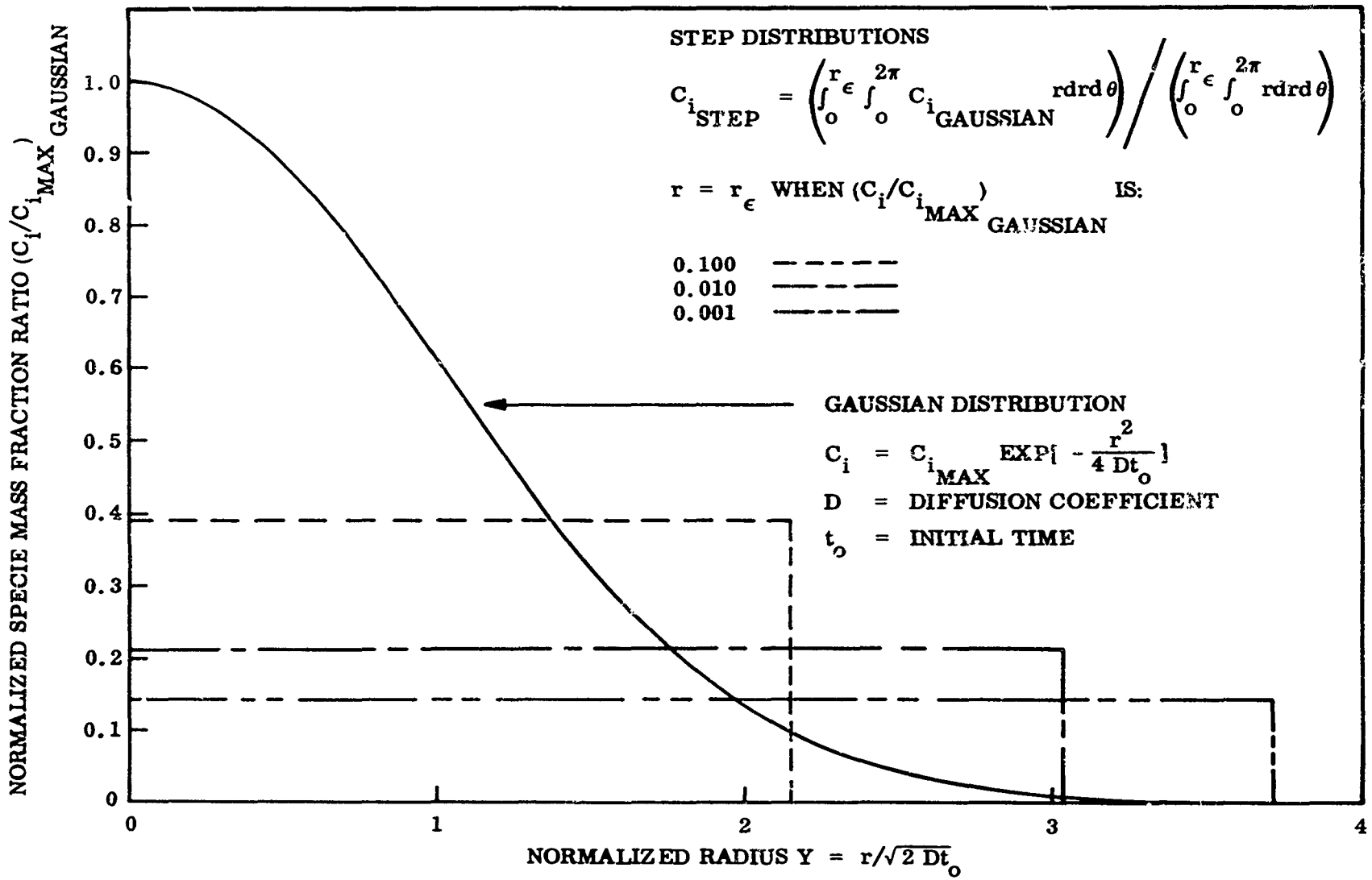

Figure 7-3 Initial Gaussian and Step Distributions

cylindrically diffusing line trail. This, in turn, has been made equivalent to a line source of heat where a certain quantity of heat is deposited instantaneously per unit length. For the line source of heat, the radial distribution of temperature is given by

$$cT = \frac{Q_m}{4\pi\rho kt} \exp\left(-\frac{r^2}{4kt}\right)$$

where

- c = specific heat
- T = temperature
- Q_m = source strength
- ρ = density
- k = coefficient of conductivity
- t = time

The equivalent for the diffusion of species is

$$C_i = \frac{M_m}{4\pi\rho D t} \exp\left(-\frac{r^2}{4 D t}\right)$$

where

- C_i = mass fraction of the ith species
- M_m = original mass deposited per unit length
- D = diffusion coefficient

For convenience in the computation, the Gaussian was normalized, i.e.:

$$\frac{C_i}{C_{i_{max}}} = \exp\left(-\frac{Y^2}{Z}\right)$$

where

$$C_{i_{max}} = \frac{M_m}{4\pi\rho D t}$$

and

$$Y = \frac{r}{\sqrt{2Dt}}$$

The species mass fractions defining the height of the three step distributions are the mean of the Gaussian as obtained by integrating the area under the curve to a radius where the concentration is, respectively, 10, 1, and 0.1 percent of the initial centerline value. When studying the relative diffusion rates of the Gaussian and step, the two were in all cases terminated at the same radius.

To compute the time rate of change of the distributions, the species conservation equation for diffusion was solved numerically. In cylindrical coordinates, this expression is given as

$$\frac{\partial c_i}{\partial t} = \frac{1}{r}\frac{\partial}{\partial r}\left(\rho D r \frac{\partial c_i}{\partial r}\right)$$

For simplicity, a two-component gas mixture was assumed. The distributions shown in all figures are for nitric oxide, whereas its complement was a species with characteristics the same as that of air. At all times, the sum of the species mass fractions was equal to one.

If the time required for the Gaussian and step distributions to converge is short, say in terms of hours rather than several days, then the diffusion and transport regime can be assumed to be independent of the final wake concentration gradients. In the first case studied, the time rates of decay of Gaussian (terminated at a radius

where the concentration was 1 percent of the centerline value) and step distribution whose areas were equal to that of the truncated Gaussian were computed for three constant diffusion coefficients: 10^3, 10^4, and 10^5 cm^2/sec. Figure 7-4 shows the time variation for the ratio of the centerline mass fractions. For 10^3 cm^2/sec, little more than 4 hr were required for the centerline values of the two distributions to decay to within 20 percent of each other, while 30 min and 3 min, respectively, were required for the diffusion coefficients of 10^4 and 10^5 cm^2/sec. A diffusion coefficient of 10^5 cm^2/sec^3 is probably a lower limit for the diffusion and transport regime.

The effects of locating the "edge" of the Gaussian at other than 1 percent were studied for a diffusion coefficient of 10^3 cm^2/sec. The results of the computations are shown in Figure 7-5. For the case where the centerline values of the Gaussian and the step distribution of equal area were initially the most divergent, a 9-hr period was required for the two to converge to within 20 percent of each other. For the other two cases, 4 hr or less were required for this same degree of convergence. Thus, it seems that wake concentration gradients diffuse rather quickly, within a matter of hours for very low values of the diffusion coefficient and within a matter of minutes for more realistic values of the diffusion coefficient, regardless of the diversity of the distributions. Hence, concentration gradients need not be included in the description of the wake model output.

7.3 REFERENCE FOR SECTION 7

7-1 J. J. Walton, Scale Dependent Diffusion, VCRL-74134, Lawrence Livermore Laboratory, 25 Aug 1972

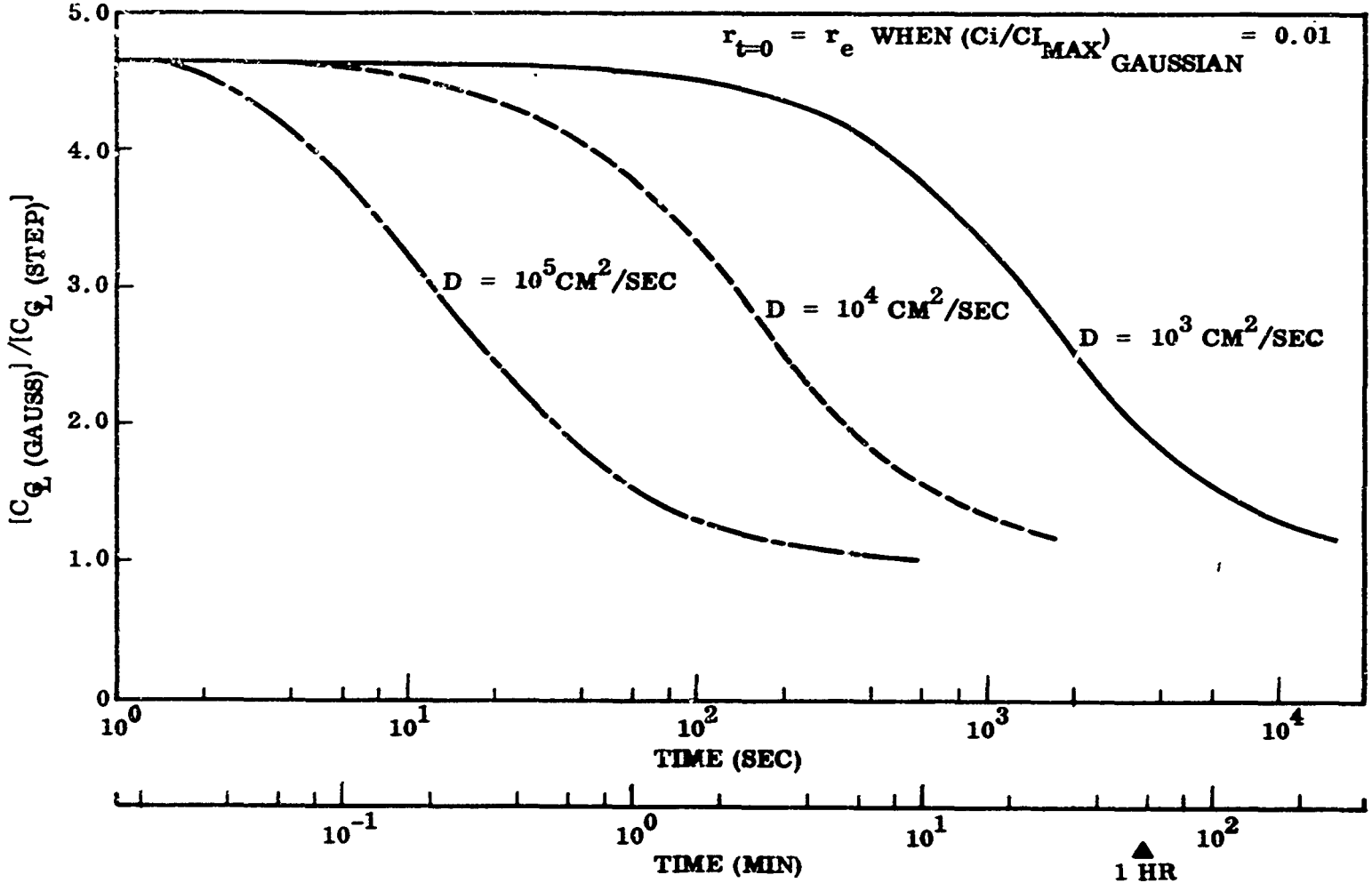

Figure 7-4 Diffusion Coefficient Influence on Relative Decay of Gaussian and Step Distribution – Centerline Mass Fraction

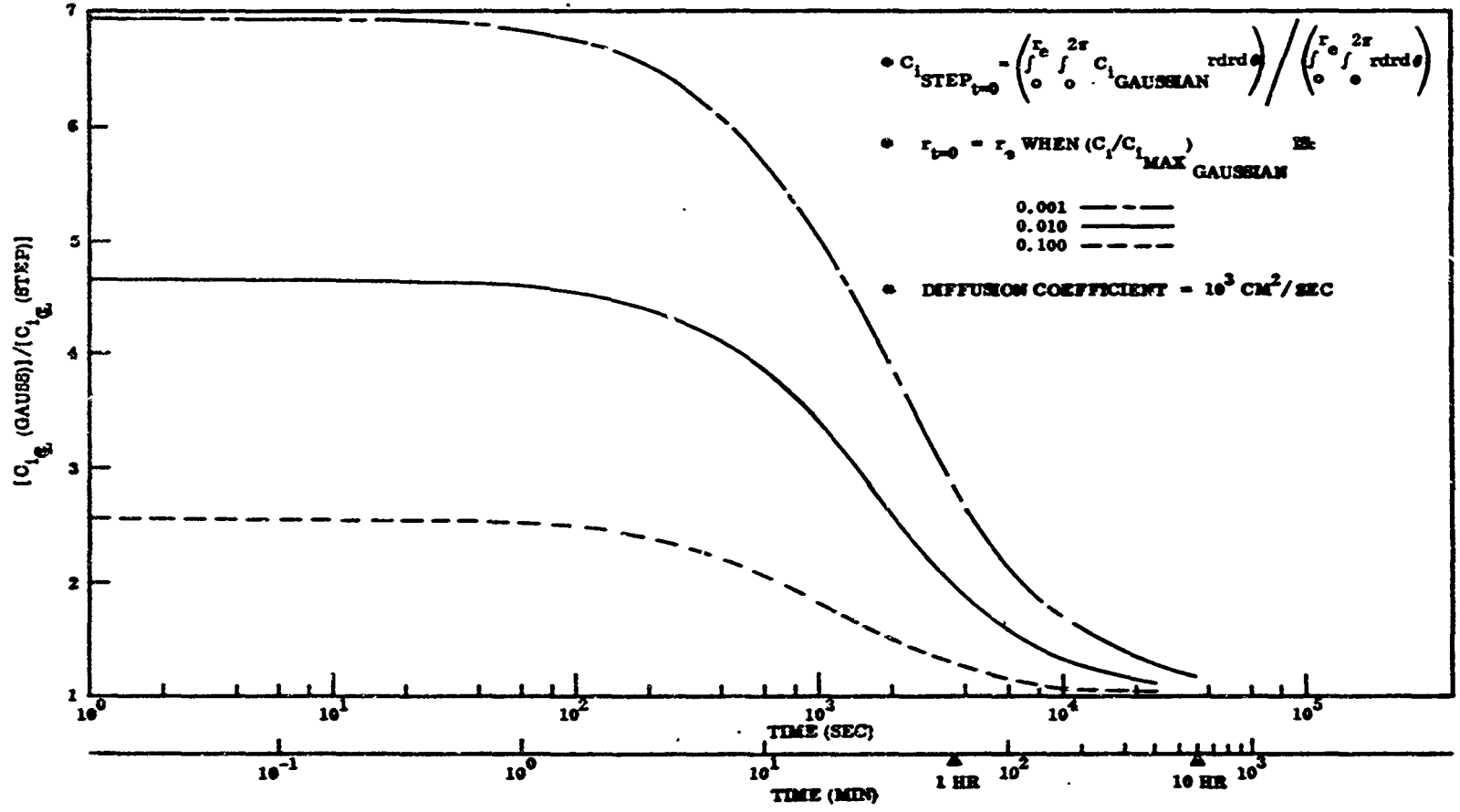

Figure 7-5 Relative Decay of Centerline Mass Fractures of Three Gaussian and Step Distributions